COLLEGE OF ENGINEERING

VIRGINIA POLYTECHNIC INSTITUTE AND STATE UNIVERSITY

BLACKSBURG, VIRGINIA

Technical Report

to

The National Aeronautics and Space Administration
Langley Research Center Grant 1-446
and
The Air Force Office of
Scientific Research Grant 84-0134

EXPERIMENTAL STUDY OF TWO SEPARATING TURBULENT BOUNDARY LAYERS

by

K.A. Nagabushana, R.L. Simpson and N.K. Agarwal

Department of Aerospace and Ocean Engineering
Virginia Polytechnic Institute and State University
Blacksburg, Virginia 24061

EXPERIMENTAL STUDY OF TWO SEPARATING TURBULENT BOUNDARY LAYERS

May 1987

K.A. Nagabushana and R.L. Simpson
N.K. Agarwal
Virginia Polytechnic Institute and State University
Aerospace and Ocean Engineering
Blacksburg, Vigrinia

SUMMARY

A detailed study of two strong adverse pressure gradient flows has been presented here. In this study mean flow and turbulent quantities along with spectral analysis are studied. Downstream of fully-developed separation, the mean backflow appears to be divided into three layers: a viscous layer nearest the wall that is dominated by the turbulent flow unsteadiness but with little Reynolds shearing stress effects; a rather flat intermediate layer that seems to act as an overlap region between the viscous wall and outer regions; and the outer backflow region that is really part of the large-scaled outer region flow. The mean velocities in the backflow are the results of time averaging the large turbulent fluctuations and are not related to the source of the turbulence. It is found in these separating adverse pressure gradient flows that

- reattachment occurs very rapidly over a very short distance, .i.e., reattachment occurs much faster than separation,

- in the backflow region there appears to be a semi-logarithmically flat region in the streamwise fluctuating velocity component, u' , which spreads over a definite range of y/δ,

- the backflow mean velocity profile scales on the maximum negative mean velocity U_N and its distance from the wall N,

- the inner flow scaling of Perry, Lim & Henbest (1985) for streamwise spectra does not hold good in the backflow region until intermittency, γ_{pu}, reaches unity in the flow and

- the flow variables $\varphi_{uu}(k_1\delta)/-\overline{uv}_{max}$ vs. $k_1\delta$ forms a unique set of scaling parameters for study of streamwise power spectra in adverse pressure gradient flows.

TABLE OF CONTENTS

LIST OF FIGURES

NOMENCLATURE

A_1	Universal constant for inverse power law in u' spectra
C_f	Skin friction co-efficient
C_p	Pressure co-efficient
F_u	Flatness factor of $u' = \overline{u^4}/(\overline{u^2})^2$
F_v	Flatness factor of $v' = \overline{v^4}/(\overline{v^2})^2$
f	frequency, Hz
H	Shape factor $= \delta^* / \theta$
κ	von Karman constant $= 0.41$
k_1	Wave number $= 2\pi f/U$
K_0	Universal constant for -5/3 power law in u' spectra
M	Distance of maximum $-\overline{uv}$ from the wall
N	Maximum mean negative velocity distance from wall
P	Pressure
Re_θ	Reynolds number based on the momentum thickness
S_u	Skewness factor of $u' = \overline{u^3}/(\overline{u^2})^{3/2}$
S_v	Skewness factor of $v' = \overline{v^3}/(\overline{v^2})^{3/2}$
$\overline{u^2}$	Mean square of longitudinal velocity fluctuation
u'	Root mean square of longitudinal velocity fluctuation, $= \sqrt{\overline{u^2}}$
u_τ	Frictional velocity
U	Longitudinal component of local mean flow velocity
U_N	Maximum negative velocity

U_w	Wall region scaling parameter for velocity
U_∞	Local free stream velocity
U^+	Non-dimensional velocity = U/u_τ
$-\overline{uv}$	Reynolds shear stress
$\overline{v^2}$	Mean square of normal velocity fluctuation
v'	Root mean square of normal velocity fluctuation, = $\sqrt{\overline{v^2}}$
V	Normal component of local mean flow velocity
$\overline{w^2}$	Mean square of transverse velocity fluctuation
w'	Root mean square of transverse velocity fluctuation, = $\sqrt{\overline{w^2}}$
W	Transverse component of local mean flow velocity
X	Streamwise distance from the leading edge
y	Normal distance from the wall
y_w	Wall region scaling parameter for distance
Y^+	a Reynolds number = yu_τ/ν
β	Flow incidence angle to the cross-wire bisector
δ	Boundary Layer thickness
δ^*	Displacement thickness
θ	Momentum thickness
γ_{pu}	Upstream-downstream intermittency
ρ	Density
$\varphi_u u$	Power spectrum of u' velocity component = $\overline{u^2}$ F(f)

1. INTRODUCTION

The analysis of the behaviour of turbulent boundary layer flows with respect to flow separation or detachment is one of the most challenging problems in fluid mechanics. The problem of flow reversal due to an adverse pressure gradient is an important factor in the design of many devices such as jet engines, rocket nozzles, missiles, airfoils and helicopter blades, and the design of fluidic logic systems. In almost all cases, the limiting performance of these devices is determined by flow separation. Without proper understanding of this phenomenon many of our fluid mechanics applications will be limited in their capabilities. Until recent years it had been difficult to get quantitative experimental information on the flow structure downstream of separation in backflow region. Much of the difficulty in treating these kind of flows was limited due to lack of proper instrumentation. The invention of directionally-sensitive laser anemometer has made it possible to study more thoroughly the flow reversal in close proximity of a wall, such as in adverse pressure gradient flows.

Many researchers have investigated adverse pressure gradient flows. One such study of adverse pressure gradient, steady, separating turbulent boundary layer flow is by Simpson, Chew & Shivaprasad (1981) using the same low speed wind tunnel test section described later. The behaviour of the pressure gradient for their flow is similar to the flow studied here. Much stronger adverse pressure gradients have been studied by Schubauer & Klebanoff (1951) which have similar features as compared to the flow under consideration, but its distribution is different from the present study.

Based on Simpson et al. (1981) we can state that incipient detachment (ID) occurs with 1% instantaneous backflow; intermittent transitory detachment (ITD) occurs with 20% instantaneous backflow or $\gamma_{pu} = 0.8$; transitory detachment (TD) occurs with 50% instantaneous backflow or $\gamma_{pu} = 0.5$; and detachment occurs where $\tau_w = 0$. The experimental results described here are concerned with two nominally two-dimensional separating turbulent boundary layers for airfoil-type flows. For these flows, the flow detaches and reattaches some distance downstream soon after detachment. Upstream of separation single and cross-wire hot-wire anemometer measurements are presented. Since a directionally-sensitive anemometer is required to provide meaningful data in the separated zone where backflow appears and the region immediately upstream, a directionally-sensitive laser anemometer technique was used in separated zone and region immediately upstream of it. Data collected using the above systems consisted of U, V, $\overline{u^2}$, $\overline{v^2}$, $-\overline{uv}$, γ_{pu} (the fraction of time that the flow moves downstream), streamwise velocity component u' power spectrum and other higher order turbulent quantities. The flow direction intermittency γ_{pu} was also measured using a thermal tuft. The data collected by these experimental techniques are presented in Appendix - I.

2. EXPERIMENTAL EQUIPMENT

2.1 Basic Wind Tunnel

The basic wind tunnel configuration used for this study is the Low Speed Boundary Layer Tunnel at the Virginia Polytechnic Institute and State University which is a blown open-circuit type. The main stream of flow is introduced into the test section after first passing through a filter, blower, a fixed-setting damper, a plenum, a section of honeycomb to remove the mean swirl of the flow, seven screens to remove much of the turbulent intensity and finally through a two-dimensional contraction nozzle to further reduce the longitudinal turbulence intensity while accelerating the flow to test speed. Figure 1 show a schematic diagram of 25 feet long and 3 feet wide test section of the wind tunnel. The upper wall is made of plexi-glass which is adjustable such that suitable free-stream velocity or pressure gradient can be obtained. The test wall is constructed with 3/4 inch thick fin-form plywood, reinforced every 11 inch with $3 \times 1\frac{1}{2} \times \frac{1}{4}$ inch cross-sectional steel channel and the side walls are made of float-glass.

The active boundary layer control system (three units, one at the beginning of the tunnel section, one at X = 2.5m and another at X = 5.0m), which is described in detail by Simpson et al. (1981), was installed on the non-test walls of the tunnel to inhibit undesirable flow three-dimensionality and to prevent flow separation on these walls. Highly two-dimensional wall jets of high-velocity air are introduced at the beginning of each of 8 feet long sections. At the latter two streamwise locations the on coming boundary layer is partially removed by a

highly two-dimensional suction system, thus maintaining two-dimensionality throughout the test section. All the data were obtained at atmospheric pressure and at 25 ± 0.5°C flow condition. It was possible to maintain steady temperature throughout the experiment by using a 5 ton air-conditioner.

The inviscid core flow is uniform within 0.05% in the spanwise direction and within 1% in the vertical direction with a turbulence intensity of 0.1% at 18.3 m/sec. The test wall boundary layer is tripped by the blunt leading edge of the plywood floor, the height of the step from the wind tunnel contraction to the test wall being ¼ inch. Smoke can be introduced uniformly into the boundary layer just upstream of this trip for use with the laser-doppler anemometer.

2.2 Laser Anemometer and Signal Processing

The laser anemometer used in these experiments is described in some detail by Simpson & Chew (1979). It is a two-velocity-component (U,V) directionally-sensitive fringe type system using backscatter measurement technique. The unshifted and 21.505 MHz Bragg-cell shifted beam lie in a horizontal plane and measure the streamwise velocity with vertical fringes. The unshifted and −15.158 MHz Bragg cell shifted beams lie in a vertical plane and measure ($-V\cos 4.4° + W\sin 4.4°$) with almost horizontal fringes. The 21.505 MHz and −15.158 MHz beams form a third fringe pattern that measures $(U + V\cos 4.4° + W\sin 4.4°)/\sqrt{2}$ around 36.663 MHz. Since $\overline{u^2}$ and $\overline{(-v'\cos 4.4° + w'\sin 4.4°)^2}$ were measured independently and $\overline{uw}$ was presumed very small, the Reynolds shearing stress $-\overline{uv}$ resulted from this

measurement. Signal processing was by fast-sweep-rate sampling spectrum analysis, as described by Simpson & Barr (1975).

Difficulties with seeding a highly turbulent flow are well known since such flows are characterized by intense mixing. This problem is even more aggravated as we move away from the wall in free-stream direction due to low smoke concentration. The smoke is generated by six adjustable Laskin nozzles, each of which blows compressed air through 4 orifices of 1 mm diameter into Dioctal Phthalate (DOP). The DOP is atomized by the shearing action of the compressed air jets and produces a mean particle diameter of 1 μm. This 1 μm DOP particles follow the highly turbulent oscillations found in separated regions. Here 0.057 cubic meters per minute of smoke at a concentration of about 4.8×10^{-3} Kg/m^3 of blown air was used. The smoke was distributed along the tunnel width just upstream of the test section by 33 evenly spaced holes in a cylinderical mainfold, which are supplied with smoke into both of its ends. A good Signal to Noise Ratio (SNR) of about 15-20 dB and a data rate of at least 400 Signals/sec., was obtained throughout the experiment.

2.3 Hot - Wire Anemometers

Miller - type (1976) integrated circuit hot-wire anemometers and linearizers, as modified by Simpson, Heizer & Nasburg (1979), are used in this study. The frequency response of these anemometers were flat up to 7.5 KHz for an overheat ratio of 0.7. This moderately high overheat ratio was used since the range of flat frequency response is improved with a high overheat ratio (Wood, 1975).

Standard TSI model 1218 - T1.5 normal wire and model 1248R - T1.5 cross-wire probes were used for boundary layer measurements. The closest to the wall that these probes could safely make measurements was about 0.002 inches and 0.035 inches, respectively. The sensing elements are 0.00015 inches in diameter and 0.05 inches in length and are made of platinum-plated tungsten wires.

The traversing mechanism used for the boundary layer velocity measurements was mounted on the supporting frame for the upper wall and provided for precise positioning of sensor probes. A cathetometer was used to accurately locate the probe sensor from the wall with an uncertainty of about ± 0.002 inch. The detailed streamwise free-stream velocity distributions were obtained using the model 1218 - T1.5 probe mounted on a mobile cart that was easily positioned along the flow. Hot-wire calibrations were made using a TSI model 1125 calibrator. Each linearized calibration had a low level dispersion from a straight line with a product moment correlation co-efficient in excess of 0.9999 with a maximum deviation of -0.008. A standard TSI model 1015C correlator was used to obtain sum and difference values of signals for the cross-wire probe.

To obtain the time-averaged results from normal and cross-wire probes a four channel Data Precision Corporation DATA 6000 model 611 universal wave form analyzer, and a true integrating voltmeter consisting of a voltage controlled oscillator and a digital counter were used. Data were sampled at 10 KHz to obtain the power spectra of streamwise fluctuating velocity component using the

DATA 6000 and averaged over 100 records to have total record-time in excess of 20 seconds.

2.4 Thermal Tuft

In practice, τ_w has been extensively used as a parameter to locate flow detachment as τ_w approaches zero. As is well known, its measurement in the near detachment region is difficult. Due to this, the location of flow detachment based on τ_w alone is relatively uncertain. Flow direction intermittency, γ_{pu}, the fraction of the time that the flow moves downstream, provides more precise information in locating flow separation from the surface.

Using hot-wire sensors to detect the wake of a central heater wire, the thermal tuft is a simple and inexpensive technique of measuring γ_{pu} , flow direction intermittency. A simple electronic circuit produces a high or low output voltage depending on whether the flow is moving downstream or upstream. Even though the LDV is a more versatile technique for such a measurement compared to the thermal tuft, it is more laborious and time consuming. Thermal tuft γ_{pu} results are very repeatable within 3-4% uncertainty. The thermal tuft used in this study is essentially based on the principles demonstrated by Rubesin, Okuno, Mateer & Brosh (1975) which was further improved by Eaton, Jeans, Ashjaee & Johnston (1979).

3. DESCRIPTION OF TEST FLOWS

In this study two strong adverse pressure gradient steady free-stream flows are studied. In one flow the free-stream velocity at the throat of the tunnel at X = 1.62 m is 33 m/sec, which produces a Re_θ of about 27000 at detachment (Flow C). For the second flow, a leading edge single rectangular cross-section roughness element of 12.5 mm high and 10.3 mm wide was placed across the two-dimensional flow, 51 mm downstream of the blunt leading edge of the plywood floor (Flow D). The free-stream velocity at the throat of the tunnel for this flow is 22 m/sec. which produces a Re_θ of about 19000 at detachment. For these flows, the flow detaches and reattaches some distance downstream soon after detachment.

Figures 2 and 3 show the free-stream velocity and non-dimensional pressure gradient dC_p/dx distributions obtained along the tunnel centerline of the bottom test wall using the single-wire probe for both the flows. The mean velocity measurements were repeatable well within the uncertainty of hot-wire anemometer ($\pm 2.4\%$ for measuring the mean velocity). The C_p was calculated using the relation

$$C_p \equiv \frac{2(P - P_i)}{\rho U_{\infty i}^2} = 1 - \left(\frac{U_\infty}{U_{\infty i}}\right)^2 \qquad (1)$$

where i denotes free-stream entrance condition at a distance of 0.153m along the tunnel. To determine the derivative of C_p, a five point local least-square curve fit of C_p data was used at each streamwise location. From figures 2 and 3 we can observe that the static pressure gradient has very similar behaviour. Also, in both

these cases the slope of static pressure gradient changes its sign at X-location of 2.5m approximately, where second wall jet boundary layer control unit is located. Thus, the pressure gradient relaxation begins upstream of intermittent detachment near the wall jet control in these flows and continues until the location of detachment.

4. EXPERIMENTAL RESULTS AND DISCUSSION

4.1 Mean Velocity Profiles

Mean velocity profiles for both the flows are presented in figures 4 and 5. Upstream of intermittent backflow these composite plots represent hot-wire measurements. Downstream of intermittent backflow laser measurements along with valid hot-wire measurement are presented. To check the validity of hot-wire measurements from the region of flow reversal (where γ_{pu} is less than unity), the following approximations were used as a rough check. In case of single-wire data it was considered that if the Gaussian velocity probability distribution is less than 0.3 then the measurements are valid. i.e.,

$$\frac{\sqrt{\overline{u}^2}}{U} < 0.3 \tag{2}$$

This approximation for single-wire measurements is based on Simpson (1976), argument of Gaussian probability distribution in the adverse pressure gradient flows.

In the case of cross-wire data, if the magnitude of the flow incidence angle to the cross-wire bisector is less than or equal to 30° then the data are considered valid. i.e.,

$$\beta = \tan^{-1}\left|\frac{(V + 2v')}{(U - 2u')}\right| \leq 30° \tag{3}$$

By the above approximations the cross-wire and single-wire data validity decrease in the streamwise direction as the backflow region is approached.

With these approximations the valid hot-wire data for mean velocity show good agreement with laser measurements with an overlap region, thus demonstrating the reliability of these measurements by different techniques. The maximum discrepancy among these measurements are about 2-3% in the mean velocity measurement. Based on the above analysis we can summarise that the data obtained using hot-wire anemometer probes is valid in the unseparated upstream boundary layer region and the outer part of the separated flow region. The laser-anemometer results obtained on different days at the same location indicated a high level of data repeatability. The uncertainities in laser-anemometer measurements are as follows: in mean velocity (U) ± 0.1 m/sec; in $\overline{u^2}$

$\pm 3\%$ of maximum profile value; in γ_{pu} ± 0.02; in $-\overline{uv}$ $\pm 5\%$ of maximum profile value; in third order turbulent quantities $\pm 10\%$ of the maximum profile value and in fourth order turbulent quantities $\pm 14\%$ of the maximum profile value.

In the inner region where the backflow exists, the law of the wall does not hold good. Figures 6 & 7 represents the law of the wall plots for both the flows in the upstream of intermittent backflow region. It can be noted that the extent of the logarithmic region decreases continuously after the beginning of intermittent flow-reversal. Simpson et al. (1981) have also reported similar findings in their adverse pressure gradient flow studies. Both these flows exhibit profile similarity in the backflow region as can be noted from the mean flow profiles (figures 4 and 5). To get a better understanding of this similarity in the backflow region U and y are normalized with maximum negative velocity $|U_N|$ and its distance N from the wall respectively. Figure 8 show one such correlation

of U and y with $|U_N|$ and N. The solid line in this figures is an empirical relation given by Simpson (1983) for $0.02 < y/N < 1.0$ as follows:

$$\frac{U}{|U_N|} = A\left(\frac{y}{N} - \ln\left(\frac{y}{N}\right) - 1\right) - 1 \qquad (4)$$

(for the semilogarithmic overlap region between the viscous wall layer and the large-scaled outer region). Clearly the above equation with $A = 0.3$ describes the $U/|U_N|$ vs. y/N profile for $0.02 < y/N < 1.0$ in the present study. This correlation of negative velocity agree with many other researchers observation (free-stream data of Simpson et al. 1981; Westphal,1982; and Hastings & Moreton,1982) with $A = 0.3$. Dianat & Castro (1986) have also studied similar kind of correlation in their separating boundary layer study and claims that $A = 0.235$ gives a better fit than $A = 0.3$. Even though there is some scatter in the present data and Simpson et al. (1981) data, it is clearly evident that equation 4 with $A = 0.3$ gives better fit than that with $A = 0.235$. However, it can be concluded that there exists a 'universal law' for negative velocity correlation given by equation 4 (except for a unique value of constant A). In these flows both U_N and N increases with streamwise direction. The U^+ vs. Y^+ law of the wall velocity profile is not consistent with this correlation since the law of the wall length scale ν/u_τ varies inversely with its velocity scale u_τ unlike U_N and N which increase along streamwise direction.

In another correlation with backflow velocity the maximum negative velocity is studied with respect to shape factor given in figure 9 ($|U_N|/U_\infty$ vs. 1/H). The solid line in this figure is given by the following equation (Simpson & Shivaprasad, 1983)

$$\frac{|U_N|}{U_\infty} = 0.807\left(1-\frac{1}{H}\right)-0.577 \qquad (5)$$

It shows that in the present study no data fall below the solid line given by above equation. The above correlation of negative velocity is also studied by Simpson et al. (1981) and Simpson & Shivaprasad for both steady and unsteady flow data showing that no data fall below the solid line given by the above equation. As the solid line is a fit for steady flow data, it appears that these flows tend to depart from steady flow characteristic. This may be due to strong adverse pressure gradient of the flow.

4.2 Skin-Friction Results

Figures 6 and 7 gives law of the wall plots for both the flows along the streamwise direction. The mean wall shear stress values were obtained by adopting Coles & Hirst (1969) method which requires that for a given u_τ, $U^+ = 16.23$ at $Y^+ = 100$. The logarithmic law of the wall equation

$$U^+ = \frac{1}{\kappa}\ln Y^+ + 5.0 \qquad (6)$$

where κ is 0.41 is shown in Figures 6 and 7 (solid line). Skin friction co-efficient values obtained by this method are presented in tables 1 and 2 for both the flows. As can be expected for these adverse pressure gradient flows the skin friction values decrease in the streamwise direction until the reattachment process begins. The skin friction co-efficient was also calculated using the Ludwieg-Tillman (1950) relation which is valid in the attached flow region:

$$C_f = 0.246 \times 10^{-0.678H} \times Re_\theta^{-0.268} \quad (7)$$

The skin friction co-efficients obtained by these two methods show good agreement in the attached flow region. Close to detachment the values obtained by the Coles & Hirst method are 6% lower compared to the values obtained by Ludwieg-Tillman relationship. This difference reduces to as little as 1.2% upstream of intermittent backflow.

4.3 Upstream-Downstream Intermittency

Figures 10 and 11 show the fraction of time that the flow is in the downstream direction γ_{pu} vs. y obtained by LDV measurements. A similar measurement of γ_{pu} vs. X measured at 1.2 mm from the wall in the streamwise direction by thermal tuft is presented in figures 12 and 13 for both flows along with γ_{pu} obtained by LDV at same location (X and y). The tuft data were obtained in two different orientations at each X location. In the first orientation one of the sensor wires senses forward flow and other sensor wire senses backward flow. In the second orientation the sensing position of these wires are interchanged by rotating the tuft by 180° in the flow. Two sets of data were obtained using the thermal tuft in each orientation. All these measurements show a good agreement with maximum discrepancy of 7%.

In the flow C without the roughness element (throat velocity of 33 m/sec.), ID occurs at 3.05m, ITD occurs at 3.46m and TD occurs at 3.71m from from the leading edge. This flow reattaches at γ_{pu} = 0.5 (at 1.2mm from the wall) which is approximately at 4.7m from the leading edge. In the flow D with roughness

element (throat velocity of 22 m/sec.), ID occurs at 3.05m, ITD occurs at 3.36m and TD occurs at 3.71m from the leading edge. Sandborn & Kline (1961) have defined region of intermittent separation and fully-developed separation based on mean velocity profile information, i.e., shape factor H and $\delta^*/\delta_{0.99}$ (which can be shown using boundary layer parameters from table 1 & 2). The intermittent and fully-developed separation locations (based on the mean velocity profile information) in both the flows found to agree with ITD and TD (based on γ_{pu}) respectively. Estimating the locations of intermittent transitory detachment and transitory detachment from the mean velocity profile information is more laborious and time consuming. Thermal tuft measurements are very simple and data can be obtained in a relatively easy manner. At the same time, the data obtained using thermal tuft can be considered very reliable.

From γ_{pu} vs. y/δ observation it can be noted that the maximum mean negative velocity (i.e., backflow velocity) is reached at a point slightly away from the wall. This is also been reported by Simpson et al. (1981) in their separating turbulent boundary layer flow studies. γ_{pu} distributions near the wall are trough-shaped in the region downstream of intermittent separation and show some similarity.

In another parameter cross-plot, the γ_{pu} distribution is tested for $(\gamma_{pu} - \gamma_{pu\,min})/(1 - \gamma_{pu\,min})$ vs. y/M similarity, where M is the distance from the wall of the maximum u' or v' or $-\overline{uv}$ value. Figure 14 show one such correlation where M has been chosen as distance of maximum $-\overline{uv}$ distribution. It can be noted that all the data for $\gamma_{pu} < 0.8$ at 1.2mm from the wall correlates together and all the data for $0.8 < \gamma_{pu} < 1.0$ at 1.2mm from the wall correlate together.

These observations are consistent with the Simpson et al. (1981) studies in detached flow region where γ_{pu} is less than 0.8.

The displacement thickness (given in tables 1 and 2) of the boundary layer, which increases rapidly just downstream of incipient detachment. The behaviour of intermittency, γ_{pu}, and boundary layer parameters such as C_f, θ, δ and δ^* show that both the flows reattaches approximately at X location of 4.70m. In case of flow D with the roughness element the mean velocity measurements were not conducted beyond 4.5m. In these two flows, the flow without the roughness element (flow C) show separated characteristics further upstream than the flow with the roughness element (flow D). At 4.7m in the flow with the roughness element the intermittency factor still is decreasing.

4.4 Second Order Turbulent Quantities

$\sqrt{\overline{u^2}}/U_\infty$, $\sqrt{\overline{v^2}}/U_\infty$ and $-\overline{uv}/U_\infty^2$ vs. y/δ plots are shown in figures 15-20. To minimize the uncertainty in cross-wire probe data, measurements were performed with the probe oriented perpendicular to test wall in attached flow region and parallel to top wall of the tunnel in separated region. After the measurements, all the data were reduced to a laboratory co-ordinate system. This minimized the uncertainty in turbulent quantities measured by cross-wire probe. Measurements of second order turbulent quantities measured by cross-wire show good agreement with single-wire (in $\overline{u^2}$ only) and laser measurement techniques with greater overlap within the uncertainty limit of these quantities.

Near the wall $\overline{u}^2$ is greater than $\overline{v}^2$ at all the locations. It was observed that this difference is very significant in separated flow region. From the intermittent backflow region (which is approximately 3.05m from the leading edge for both the flows) and downstream, the slope of $\sqrt{\overline{u^2}}/U_\infty$ first increases with y /δ and then decreases to a constant value over a short region before increasing again until reaching a maximum value in the flow. This semi-logarithmic constant slope region was observed to spread between approximately y 0.01 to 0.1 y/δ (figures 15 and 16). Shiloh, Shivaprasad & Simpson (1981) in their work on adverse pressure gradient flows have also reported a semi-logarithmic constant slope region and they recognize this region as infliction point region. Even in their study this region is noticed to be between 0.01 to 0.1 y/δ (Refer figure 4 of Shiloh et al.). This infliction region for these flows are as shown in figures 15 and 16 where "A" marks the beginning of this region and "B" shows the end of this region. It appears that the flow is controlled by the turbulence in this region.

This semi-logarithmic region in u' distribution may be due to two different sets of scaling parameters dominating the inner and outer region of the flow. In inner region the turbulent motion for u' may be represented as

$$\frac{\sqrt{\overline{u}^2}}{U_w} = f\left(\frac{y}{y_w}\right) \tag{8}$$

where U_w and y_w are wall region scaling parameters. Here y_w has to be some function of viscosity. In outer region the scaling parameters can be U_∞ and δ such that

$$\frac{\sqrt{\overline{u^2}}}{U_\infty} = g\left(\frac{y}{\delta}\right) \tag{9}$$

If so, then the overlapping region should satisfy these two relations simultaneously. The function that matches two different scaling is logarithmic (based on Millikan, 1938 type of argument). Here it can be written as

$$A \ln \left|\frac{y}{y_w}\right| + B \ln \left|\frac{y_w}{\delta}\right| = constant \tag{10}$$

It appears that the semi-logarithmic region observed in $\sqrt{\overline{u^2}}$ distribution may be due to this reason. (However, the slopes of these flat regions in each profile is found to be different in the present study and also in Shiloh et al. study.)

The maximum value of $\overline{u^2}$ along streamwise direction was noted to be increasing until the flow reattaches after separation. Once the flow is reattached the maximum value of $\overline{u^2}$ decreases. Contrary to the behaviour of the maximum $\overline{u^2}$, the normal and Reynolds shear stress components $\overline{v^2}$ and $-\overline{uv}$ maximum values were noted to be increasing even after the flow reattachment. All these three second order turbulent quantities show some profile similarity and low levels of Reynolds shearing stress in the wall region after detachment. All these observations are consistent with Simpson et al. (1981) steady flow data for similar pressure gradient flows. (Their study was limited to upstream of reattachment).

4.5 Turbulent Correlations

Figures 21 and 22 show distribution of shear stress correlation co-efficient $-\overline{uv}/\sqrt{\overline{u^2}}\sqrt{\overline{v^2}}$, upstream of separation which is a measure of the extent of correlation between u' and v' fluctuations. Near the outer edge the values are large since $-\overline{uv}$, u' and v' approaches zero.

Upstream of separation along the streamwise direction of flow, the correlation co-efficient falls until the beginning of intermittent backflow. This is consistent with the Schubauer & Klebanoff shear stress correlation co-efficient distribution in their strong adverse pressure gradient boundary layer flow, even though the adverse-pressure gradient distributions are different. Upstream of separation all these profiles show a nearly constant value of correlation co-efficient at each streamwise locations. This constant value was about 0.42 at X = 2.2m and monotonically decreases to as low as 0.3 in the vicinity of the beginning of intermittent backflow.

Unlike the distribution far upstream the shear stress correlation co-efficient does not exhibit a constant value over a large part of the outer layer once the backflow starts to appear. As one moves downstream, the peaks of the distribution seem to be gradually moving towards the outer edge of the boundary layer with maximum correlation co-efficient of 0.3. Once the flow starts reattaching, correlation co-efficient shows attaining higher maximum value of 0.4 again as shown in figures 23 and 24.

All these observations are in agreement with those of Simpson et al. (1981) for similar adverse pressure gradient distribution study. Upstream of intermittent backflow the constant value for shear stress correlation co-efficient noted by them was as high as 0.5 and decreases monotonically until the beginning of intermittent backflow. In the backflow region the maximum correlation coefficient of 0.3 was observed (refer figure 13 of Simpson et al. ,1981).

4.6 Spectral Measurement

Spectra describe the energy distribution amongst different sizes of eddies i.e., largest eddies to smallest eddies where they dissipate to heat. Based on dimensional analysis Perry, Lim & Henbest (1985) have proposed new scaling for power spectrum in a turbulent wall region (defined as $yu_\tau/\nu >> 1$ and $y/\delta < 1$). For turbulent flows they define three types of scaling such as inner, outer and Kolmogoroff flow scale. Many researchers have used this inner flow scaling, showing good agreement in zero and favourable pressure gradient flows (Ahn, 1986, zero and favourable pressure gradient flows; Erm, Smits & Joubert, 1985 zero pressure gradient flow). However, none of these studies shows the effectiveness of this model for adverse pressure gradient flow conditions. In this study an attempt has been made to check the validity of Perry et al. (1985) inner flow scaling for adverse pressure gradient conditions. It is known that in the separated flow region u_τ is nearly zero and using this quantity as scaling parameter will not lead to any meaningful results. Thus, in adopting Perry et al. (1985) scaling for the present study, the maximum Reynolds shear stress is used as a scaling parameter instead of u_τ in the backflow region. However, upstream of intermittent flow detachment region the maximum Reynolds shearing stress is

also the wall shear stress. These data are also compared with the model equations proposed by Perry et al. (1985) in terms of inner flow scaling as follows:

For K_1^{-1} region,

$$\frac{\varphi_{uu}(k_1 y)}{-\overline{uv}_{max}} = \frac{A_1}{k_1 y} \tag{11}$$

For $K_1^{-5/3}$ region,

$$\frac{\varphi_{uu}(k_1 y)}{-\overline{uv}_{max}} = \frac{K_0}{\kappa^{2/3}(k_1 y)^{5/3}} \tag{12}$$

For K_1^{-7} region,

$$\frac{\varphi_{uu}(k_1 y)}{-\overline{uv}_{max}} = \frac{1}{126}\frac{y^{+4}}{(k_1 y)^7} \tag{13}$$

Here $A_1 = 0.833$ and $K_0 = 0.49$, which are universal constants and the maximum Reynolds shear stress has been used instead of u_τ.

In each flow studied, u' power spectra were taken at five different streamwise locations (three locations in each flow is presented here). Using the Perry et al. (1985) inner flow scaling definition and the maximum shear stress the spectral data are normalized for these adverse pressure gradient flows (figure 25-30). Figure 25 and 26 represent u' power spectra for both the flows at X = 1.63m where the maximum shear stress is also the wall shear stress. In this region

spectral measurements show excellent agreement with the model equation (11) with features of K_1^{-1} law region. Further from the wall and downstream before the beginning of intermittent backflow a $K_1^{-5/3}$ law region starts dominating the higher wave number energy structure. Until intermittent backflow an envelope in spectral distribution was observed (figures 25-28). This kind of envelope was also reported by Perry, Henbest & Chong (1986) and Ahn in their zero and favourable pressure gradient flows. Since the flow is attached in this region the spectral scaling exhibit the wall-bounded flow behaviour even in the adverse pressure gradient conditions. Spectra have higher energy closer to the wall and decrease as one approaches the boundary layer edge. Thus near the wall the contribution to the turbulent energy in the low wave number range made by larger eddies decreases while the contribution of smaller eddies increases.

Figure 29 represent spectral data at X = 5.40m which is downstream of reattachment. Figure 30 represent spectral data at X = 3.5m with intermittent backflow. In the backflow region the model equation using inner flow scaling fails to show full agreement. Also, in this region no such significant envelope in spectral distribution was observed as seen in upstream of backflow. It was also noticed that where the intermittency, γ_{pu}, reaches unity in the flow u' spectra starts showing some agreement. In these (X,y) locations hot-wire data are no good where intermittent backflow is present. The data in the $K_1^{-5/3}$ region show higher values and almost dominate the entire flow in the backflow region. (At the X-locations of figures 29 and 30, γ_{pu} does not reach unity until y/δ of 0.17 and 0.25 for flow with and without roughness element respectively.)

Regarding the validity of these type of scaling Erms et al. concludes that for u' power spectra the agreement was good only up to $Re_\theta = 5010$. Also, for the broad band turbulence measurements, the spectra have a Reynolds number dependence and an apparent dependence on the tripping device. In these adverse pressure gradient flows considered, the Perry et al. (1985) model for inner flow scaling shows good agreement up to $Re_\theta = 5000$, as noted by Erms et al. Here, even though Re_θ is greater than 5000 there was a moderate agreement with inner flow scaling before the backflow appearance. The disparity of this type of scaling in the negative velocity region can be attributed to the directional-insensitivity of the hot-wire sensor as discussed earlier.

From the above observation of Perry et al., inner flow scaling it can be noted that this type of scaling does not show good correlation in streamwise spectral data for adverse pressure gradient flows in the intermittent backflow region. In this region even after intermittency, γ_{pu}, reaching unity the inner flow scaling fails to show good correlation in power spectra. In order to get a better correlation of u power spectra several other scaling parameters have been tried. One correlation using the outer flow variable such as $\delta_{0.99}$ instead of inner flow variable y shows a good correlation at all streamwise locations irrespective of the flow behaviour (attached or separation). The inverse power law and $-5/3$ law with $\delta_{0.99}$ as scaling parameter can be modified as follows:

for K_1^{-1} region,

$$\frac{\varphi_{uu}(k_1\delta)}{-\overline{uv}_{\max}} = \frac{A_1}{k_1\delta} \tag{14}$$

for $K_1^{-5/3}$ region,

$$\frac{\varphi_{uu}(k_1\delta)}{-\overline{uv}_{max}} = \frac{K_0}{\kappa^{2/3}(k_1\delta)^{5/3}} \tag{15}$$

Figures 31 - 40 represents u' power spectra using the outer flow variable $\delta_{0.99}$ as scaling parameter (from throat to separation) region for both the flows with and without roughness element. Upstream of intermittent backflow (attached flow region) figures 31 - 34 show a good correlation of spectral data that agrees with the model equation (14) representing the inverse power law. However, the outer flow scaling does not show any envelope in the spectral distribution as observed with the inner flow scaling. In this type of scaling, the constant A_1 of the model equation (14) is still 0.833 (which is the universal constant). Thus, the type of scaling using either inner or outer flow parameter does not have any significant effect on the spectral distribution in unseparated flows.

As the intermittent backflow region is approached the $K^{-5/3}$ law starts dominating the spectral distribution. In backflow region (figures 37 - 40) the inverse power law looses its significance and a dominant $-5/3$ power region with good correlation can be noted when outer flow variable is used. The constant K_0 of the model equation (15) for $-5/3$ region has higher value for outer flow scaling than universal constant which is 0.49. The -5/3 law with K_0 = 11.5 presents a best fit to this type of scaling for the adverse pressure gradient flows.

From figures 31-41 it can be observed that at lower wave number (specially in K^{-1} law region) u' power spectra peels off. The spectral peel off is

in order of increasing Reynolds number and increasing y/δ at the low wave number end. At higher wave number all spectra show good collapse showing good spatial resolution in $\sqrt{\overline{u^2}}$ causing a greater inertial subrange. Figure 33 - 41 indicates that the data match quite well with the -5/3 line associated with higher value of constant K_0 ($\cong$ 11.5) in the inertial subrange. However, once the flow shows reattaching characteristics the spectral data (figure 39) for outer flow scaling does not quite match with -5/3 line associated with K_0 = 11.5. The deviation may be due to low Reynolds number effects.

For outer flow scaling, the inverse power law region appears in the wave number range of $k_1\delta \cong 10^0 \sim 4\times10^1$ with its value $\varphi_{uu}(k_1\delta)/-\overline{uv}_{max}$ ranging from $4\times10^{-2} \sim 5\times10^{-1}$. The inertial subrange has almost same wave number range of $k_1\delta \cong 4\times10^1 \sim 10^3$ with its value ranging from $10^{-4} \sim 5\times10^{-1}$. In the inverse power law region the presence of roughness element in the flow does not show any effect. However, in the inertial subrange the roughness element in the flow show some effect on energy content. In this region the spectral distribution is shifted to higher wave number range ($10^2 \sim 4\times10^3$) compared to spectral distribution for flow without roughness element.

The present data with the outer flow scaling is compared with Simpson, Strickland & Barr (1974) spectral data in adverse pressure gradient separated flows and Bradshaw (1967) data of equilibrium boundary layer study in separating flows. In each flow (C & D) under consideration two sets of data at two different locations (in the separated flow region) has been selected for comparison. The selection of these sets of data was arbitrary. Figure 41 presents one such comparison where a "universal" behaviour in the streamwise power

spectra can be observed. Thus it appears that the spectral distribution for streamwise power spectra using flow variables $\varphi_{uu}(k_1\delta)/-\overline{uv}_{max}$ vs. $k_1\delta$ as scaling parameter correlates the spectral data and forms a unique set of parameters for streamwise power spectral study in adverse pressure gradient flows.

4.7 Higher Order Turbulent Quantities

In this section the effect of separation on higher-order structure functions has been studied. The third and fourth moments are given by

$$\overline{u^n} = \int_{-\infty}^{+\infty}(\mathbf{U} - U)^n P(\mathbf{U})d\mathbf{U} \qquad (14)$$

with n = 3,4 were calculated from each **U** and **V** laser anemometer velocity histogram P(**U**) and P(**V**). Simpson & Chew showed that the skewness factors, $S_u = (\overline{u^3})/(\overline{u^2})^{3/2}$ and $S_v = (\overline{v^3})/(\overline{v^2})^{3/2}$, and flatness factors, $F_u = (\overline{u^4})/(\overline{u^2})^2$ and $F_v = (\overline{v^4})/(\overline{v^2})^2$, were about ± 0.1 and ± 0.2 uncertain (for skewness and flatness respectively). The instantaneous value of odd moments can have either positive or negative sign and very slight off-sets can adversely affect the behaviour of their measurements. Some scatter in the data can be noted compared to Simpson, Chew & Shivaprasad (1981,b) data. In the present study all the data have been presented irrespective of its uncertainity without setting any arbitrary uncertainty limit (which is 25% for Simpson et al. ,1981,b).

Figures 42 - 45 present flatness factor F_u and F_v for the two adverse pressure gradient flows under consideration. The flatness of Gaussian noise and a sine wave are 3 and 1.5 respectively. The former is completely random where as the latter is well organized. Comparison of figures 42 - 45 show that F_u and

F_v have flatness factor above that of Gaussian noise. It also indicates that separation does not have much effect on F_u and F_v over the shear layer. Comparison of the data for both flows suggest that the roughness element also does not have any significant effect on F_u and F_v over the shear layer. The results are compatible with that of Simpson et al. (1981,b) observations for these higher order turbulent quantities in their earlier adverse pressure gradient flow. When this quantity was studied using Y^+ co-ordinate instead of y/δ co-ordinate, the flatness factor (both F_u and F_v) show some effect of pressure gradient close to the wall. This behaviour in flatness has also been reported by Simpson et al. (1981,b), Ueda & Hinze (1975) and Sandborn (1959). The flatness factor of above 3 in adverse pressure gradient has been also reported by Simpson et al. (1981,b) which is above the Gaussian probability distribution. This is possible because the inrush phase of the bursting cycle which brings in high-velocity fluid from the outer region results in large-amplitude positive u' fluctuations and consequently produces a large skirt in the velocity probability distribution. Similarly, near the outer edge of the boundary layer, intermittent large-amplitude negative u' fluctuations occur as a result of the large eddies driving the fluid from the low velocity regions outwards, which tends to increase the flatness factor. Sandborn's data for F_u in an adverse pressure gradient boundary layer flow also show similar behaviour as seen in the present data.

Very close to the wall the data for skewness factor S_u and S_v presented in figures 46 and 47 increase with increasing distance from the wall. They reach maximum values in the region of 0.07 to 0.2 y/δ. Thereafter, they decrease with increasing y/δ and continues to fall. Their sign changes at approximately $y/\delta \cong 0.65$. This kind of increasing and then decreasing behaviour in the skewness

or has been reported by Ueda & Hinze in a flat-plate boundary layer, Ueda lizushina (1977) in a fully-developed pipe flow, Arora & Azad (1980) in a ar diffuser with 8° divergence angle and Simpson et al. (1981,b) in their rse pressure gradient flow. However, only Simpson et al. (1981,b) has n sign change in skewness factor away from the wall. All other authors have rted skewness factor reaching a constant value of nearly 0.35 at $Y^+ \geq 100$. estingly, this sign change location corresponds to the region where the olds shearing stress and the second order turbulent intensities reach their imum value. This may be due to the intense momentum exchange in this n resulting in the lack of occasionally very high or very low fluctuations in gion. As a result probability distribution does not have much skewness in region.

Also downstream of detachment the skewness of u', S_u, is reduced to tive values in the negative velocity region close to wall as shown in figure 46. negative skewness value close to wall in S_u was limited to the flow region re $\gamma_{pu} < 0.5$ at 1.2mm from the wall. Thus, skewness factor in the separated show a sign change twice, once closer to the wall and once away from the . In between it reaches a maximum value. As one moves closer to the wall, intermittent large amplitude positive u' fluctuation makes the probability ibutions more positively skewed and *vice versa* when one moves away from wall.

The maximum value of S in these experiments range from 0.32 to 0.85. ny researchers have reported a constant value of S which is in the range of to 0.5. However very few of these studies belong to adverse pressure gradient

or separating flows. Two such studies are of Simpson et al. (1981,b), Arora & Azad where they have reported skewness factor as high as 1.0 in adverse pressure gradient flows.

The distribution of $\overline{v}^3$ for both the flows are shown in figures 48 and 49. The behaviour of this higher order fluctuating velocity component agree with the results of Wygnanski & Fiedler (1970) in two-dimensional incompressible mixing layer flow and Smits, Eaton & Bradshaw (1979) study of cylinder-flare model in 20° bend blower rig. Near the wall region this velocity component has very small value nearly equal to zero. Away from the wall it reaches a maximum in the flow and then continuously decreases attaining negative value before $y = \delta$. This maximum was observed to be increasing in the streamwise direction. Flow separation and reattachment do not show any influence on this higher order turbulent quantity. The maximum values observed in this study is less than that of Wyganaski & Fiedler mixing-layer data.

Triple products of velocity fluctuations of $\overline{q^2u}$, $\overline{q^2v}$, $\overline{u^2v}$ and $\overline{uv^2}$ appear in the turbulent-transport terms of the transport equations for turbulent kinetic energy and shear stress. These are believed to be the footprints of the large eddies. Two such triples product are presented here as $-\overline{u^2v}+\overline{uv^2}$ (figures 50 and 51). This third-order cross product was estimated from $\overline{(u-v)^3}$, $\overline{v}^3$ and $\overline{u}^3$ LDV measurements. Even though some scatter is present in the data, the general behaviour of this triple product can be followed (shown in solid line). It appears that until reattachment the cross product show increasing trend in streamwise direction and after reattachement it show decreasing trend. It appears to be

showing sign change at two locations, one very close to wall and once away from the wall.

5. CONCLUSIONS

In conclusion we can summarize that in these separating turbulent boundary layer flows due to adverse pressure gradient

- the reattachment occurs very rapidly over a very short distance compared to flow separation,

- in the backflow there appears to be a semi-logarithmic constant slope region in the streamwise velocity fluctuation, u', which spreads over a definite range of y/δ,

- the backflow mean velocity profile scales on the maximum negative mean velocity U_N and its distance from the wall N,

- it indicates that a 'universal law' exists for negative velocity correlation except for unique value of constant (A of equation 4),

- the correlations of Sandborn & Kline for the locations of intermittent separation and fully-developed separation based on mean velocity profile information agree with ITD and TD based on γ_{pu} alone,

- spectral measurements compared with Perry et al. (1985) inner flow scaling show good agreement up to Re_θ = 5000. Even though, Re_θ is greater than 5000 it shows good agreement if negative velocity is not present in that region,

- in the intermittent backflow region inner flow scaling for streamwise spectra fails until flow intermittency, γ_{pu}, reaches unity,

- the flow variables $\varphi_{uu}(k_1\delta)/-\overline{uv}_{max}$ vs. $k_1\delta$ forms a unique set of scaling parameters for study of streamwise power spectra in adverse pressure gradient flows,

- compare to inner flow scaling, the effect of tripping device is more significant with outer flow scaling,

- upstream of intermittent backflow, near the wall region, the production of turbulence predominates and the spectral law for the non-viscous subrange is K_1^{-1}. However, away from the wall the inertial transfer among the eddies predominates and the spectral law for inertial subrange is $K_1^{-5/3}$,

- flatness factors both F_u and F_v have greater values than gaussian probability distribution values in the adverse pressure gradient flow,

- in separated flow region the flow is negatively skewed closer to the wall. Far away from the wall it reaches positive maximum before changing sign again. This change in sign location far away from the wall corresponds to the region where the Reynolds shearing stress and other turbulent intensities show maximum value.

6. ACKNOWLEDGEMENT

This study was supported by NASA-Langley Research Center under Grant 1-446 and by Air Force Office of Scientific Research under Grant 84-0134.

References

1. Ahn, S., "Some Unsteady Features of Turbulent Boundary Layers," *MS Thesis, Aerospace and Ocean Eng., Virginia Polytechnic Institute and State University*, 1986.

2. Arora, S.C. and Azad, R.S., "Applicability of the Isotropic Vorticity Theory to an Adverse Pressure Gradient Flow," *Journal of Fluid Mechanics*, vol.97, part 2, pp.385-404, 1980.

3. Bradshaw, P.,"The Turbulence Structure of Equilibrium Boundary Layers", *Journal of Fluid Mechanics*, vol.29, part 4, pp.625-645, 1967.

4. Coles, D. and Hirst, E.A., "Analysis of Turbulent Boundary Layers," *1968 AFOSR-IFP-Stanford Conference,* Stanford University Press, Stanford, California, 1969.

5. Dianat, M. and Castro, I.P., "Measurements in Separating Boundary Layers," *International Congress on Aerospace Sciences*, London, September 1986.

6. Eaton, J.K., Jeans, A.H., Ashjaee, J. and Johnston, J.P., "A Wall-Flow-Direction Probe for Use in Separating and Reattaching Flows," *Journal of Fluids Engineering*, vol.101, pp.364-366, 1979.

7. Erm, L.P., Smits, A.J. and Joubert, P.N., "Low Reynolds Number Turbulent Boundary Layers on a Smooth Flat Surface in a Zero Pressure Gradient", *5th Symposium on Turbulent Shear Flows*, Ithaca, New York, 1985.

8. Hastings, R.C. and Moreton, K.G., "An Investigation of a Separated Equilibrium Turbulent Boundary Layer," *International Symposium On Applied L.D.A. to Fluid Mechanics*, pp.11.1, 1982.

9. Ludwieg, H. and Tillmann, W., "Investigation of the Wall-Shearing Stress in Turbulent Boundary Layers," *NACA-TM-1285,* 1950.

10. Miller, J.A., "Simple Linearized Hot-Wire Anemometer," *Journal of Fluids Engineering*, vol.98, pp.550-557, 1976.

11. Millikan, C.B., *Proceedings of 5th International Congress on Applied Mechanics,* Cambridge, Mass., pp.386, 1938.

12. Perry, A.E., Henbest, S.M. and Chong, M.S., "A Theoretical and Experimental Study of Wall Turbulence," *Journal of Fluid Mechanics,* vol.165, pp.163-199, 1986.

13. Perry, A.E., Lim, K.L. and Henbest, S.M., "A Spectral Analysis of Smooth Flat-Plate Boundary Layers," *5th Symposium on Turbulent Shear Flows,* Ithaca, New York, 1985.

14. Rubesin, M.W., Okuno, A.F., Mateer, G.G. and Brosh, A., "A Hot-Wire Surface Gage for Skin Friction and Separation Detection Measurements," *NASA TM X-62, 465,* 1975.

15. Sandborn, V.A.,"Measurements of Intermittency of Turbulent Motion in a Boundary Layer," *Journal of Fluid Mechanics,* vol.6, pp.221-240, 1959.

16. Sandborn, V.A. and Kline, S.J., "Flow Models in Boundary-Layer Stall Inception," *Journal of Basic Engineering,* vol.83, pp.317-327, 1961.

17. Schubauer, G.B. and Klebanoff, P.S.,"Investigation of Separation of the Turbulent Boundary Layer," *NACA Report 1030,* 1951.

18. Shiloh, K., Shivaprasad, B.G. and Simpson, R.L., "Feature of a Separating Turbulent Boundary Layer. Part 3, Transverse Velocity Measurements," *Journal of Fluid Mechanics,* vol.113, pp.75-90, 1981.

19. Smits, A.J., Eaton, J.A. and Bradshaw, P., "The Response of a Turbulent Boundary Layer to Lateral Divergence," *Journal of Fluid Mechanics,* vol.94,part2, pp.243-268, 1979.

20. Simpson, R.L., "Interpreting Laser and Hot-film Anemometer Signals in a Separating Boundary Layer," *AIAA Journal,* Vol.14, pp.124-126, 1976.

21. Simpson, R.L., "A Model for the Backflow Mean Velocity Profile," *AIAA Journal,* Vol.21, No.1, pp.142-143, 1983.

22. Simpson, R.L. and Barr, P.W., "Laser Doppler Velocimeter Signal Processing Using Sampling Spectrum Analysis," *Rev. Sc. Instrum.,* vol.46, pp.835-837, 1975.

23. Simpson, R.L. and Chew, Y.T., "Measurements in Steady and Unsteady Separating Turbulent Boundary Layers. Laser Velocimetry and Particle Sizing," *Thompson and Stevenson, ed.,* Hemisphere, NewYork, 1979.

24. Simpson, R.L., Chew, Y.T. and Shivaprasad, B.G., "The Structure of a Separating Turbulent Boundary Layer. Part 1. Mean flow and Reynolds stresses," *Journal of Fluid Mechanics,* vol.113, pp.23-51, 1981.

25. Simpson, R.L., Chew, Y.T. and Shivaprasad, B.G., "The Structure of a Separating Turbulent Boundary Layer. Part 2. Higher-Order Turbulence results," *Journal of Fluid Mechanics*, vol.113, pp.53-73, 1981(b).

26. Simpson, R.L., Heizer, K.W. and Nasburg, R.E.,"Performance Characteristics of a Simple Linarized Hot-Wire Anemometer," *Journal of Fluids Engineering*, vol.101, pp.381-382, 1979.

27. Simpson, R.L. and Shivaprasad, B.G., "The Structure of a Separating Turbulent Boundary Layer. Part 5. Frequency effects on unsteady free-stream flows," *Journal of Fluid Mechanics*, vol.131, pp.319-339, 1983.

28. Simpson, R.L., Strickland, J.H. and Barr, P.W.,"Laser and Hot-film Anemometer Measurements in a Separating Turbulent Boundary Layer," *NTIS report*, AD-A001115, 1974.

29. Ueda, H. and Hinze, J.O.,"Fine-Structure Turbulence in the Wall Region of a Turbulent Boundary Layer," *Journal of Fluid Mechanics*, vol.67, part 1, pp.125-143, 1975.

30. Ueda, H. and Mizushina, T.,"Turbulence Structure in the Inner Part of the Wall Region in a Fully Developed Turbulent Tube Flow," *5th Biennial Symposium on Turbulence, University of Missouri,* Rolla, pp.357-366, 1977.

31. Westpal, R.V., *Ph.D. Dissertation*, Dept. of Mechanical Engineering, Thermo-sciences Division, Stanford University, 1982.

32. Wood, N.B., "A Method for Determination and Control of the Frequency Response of the Constant-Temperature Hot-Wire Anemometer," *Journal of Fluid Mechanics*, vol.67, pp.769-786, 1975.

33. Wyganaski, I. and Fiedler, H.E., "The Two-Dimensional Mixing Region," *Journal of Fluid Mechanics*, vol.41, part 2, pp.327-361, 1970.

Tables

Table 1. Parameters of the mean flow development for flow without roughness element.

x (m)	U_∞ (m/s)	dU_∞/dx (s^{-1})	$\delta_{0.99}$ (cm)	δ^* (cm)	Re_θ	H_{12}	$10^3 \times C_f$
1.63	31.47	-1.624	2.2064	0.2549	3958.8	1.2965	3.1708
2.21	29.30	-5.533	3.5666	0.4433	5724.7	1.4459	2.4814
2.85	24.49	-9.203	5.0800	1.2025	11641.7	1.6250	1.3795
3.46	21.23	-2.890	16.3223	5.1079	27587.9	2.5145	0.1161
3.96	19.80	-1.724	20.8585	10.6095	36293.1	3.7118	-
4.47	19.59	-1.556	31.9532	17.0502	40883.0	5.6861	-
4.88	18.07	-1.551	40.1551	22.3519	43862.8	5.8935	-
5.77	14.24	-0.588	38.8595	13.5157	54421.5	2.2700	0.1907

Table 2. Parameters of the mean flow development for flow with roughness element.

x (m)	U_∞ (m/s)	dU_∞/dx (s^{-1})	$\delta_{0.99}$ (cm)	δ^* (cm)	Re_θ	H_{12}	$10^3 \times C_f$
1.63	21.45	-0.881	2.4600	0.1897	2052.1	1.2619	3.8143
2.21	20.33	-5.325	9.4102	0.7428	7808.0	1.2396	2.7956
2.85	16.11	-6.041	15.2400	1.6997	11600.2	1.5070	1.4328
3.20	14.07	-3.168	16.9370	2.8512	13110.2	1.8895	0.5417
3.46	13.60	-2.146	21.4503	6.6817	24351.6	2.4401	0.2071
3.96	13.04	-1.594	32.1005	13.1089	29105.7	3.7614	-
4.47	12.09	-1.221	37.8746	21.7251	31268.8	7.1653	-

Figure 1 . Sectional Schematic Diagram of the wind tunnel test section.

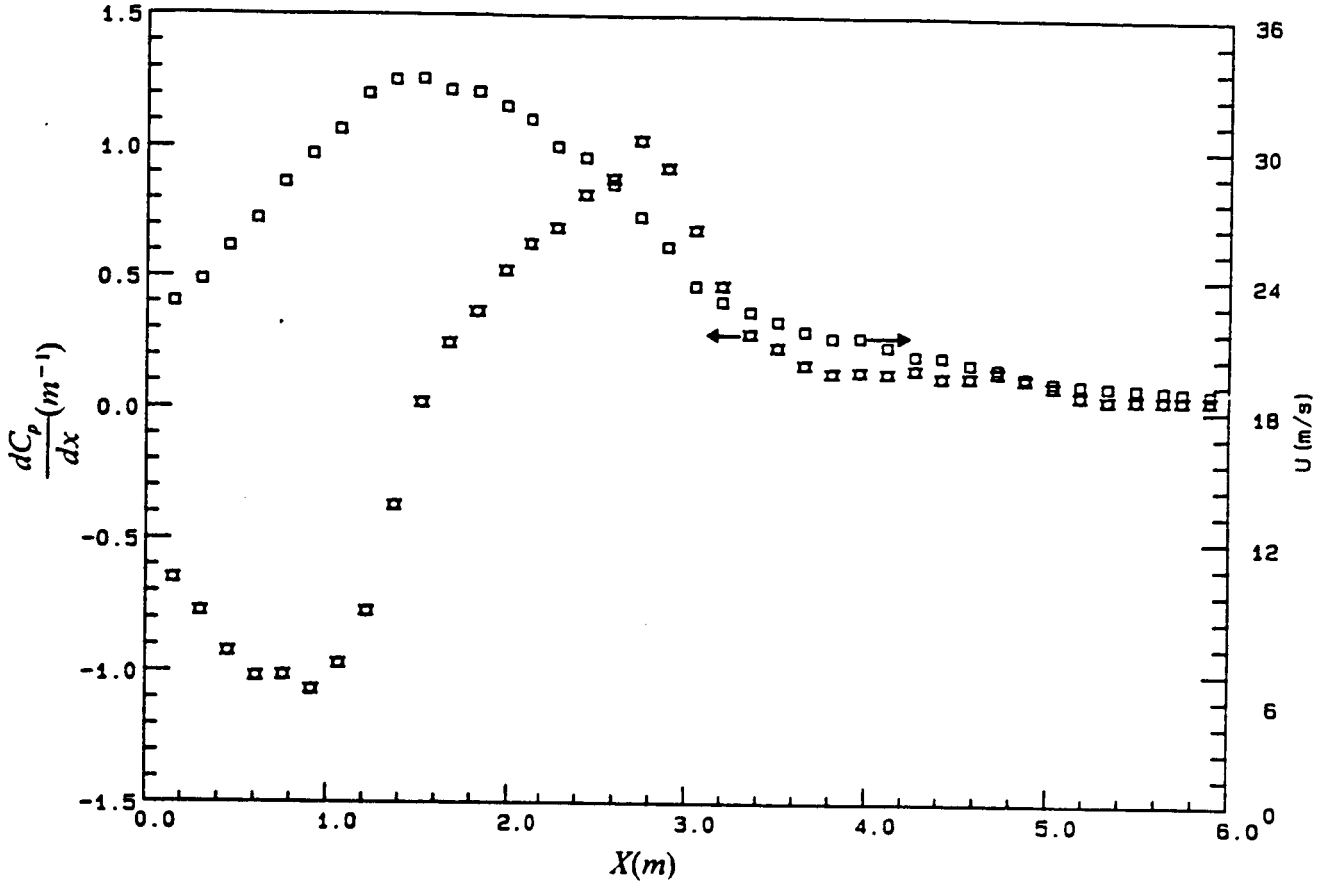

Figure 2 . Pressure gradient distribution and Free-stream velocity along the tunnel center-line for flow without roughness element (Flow C).

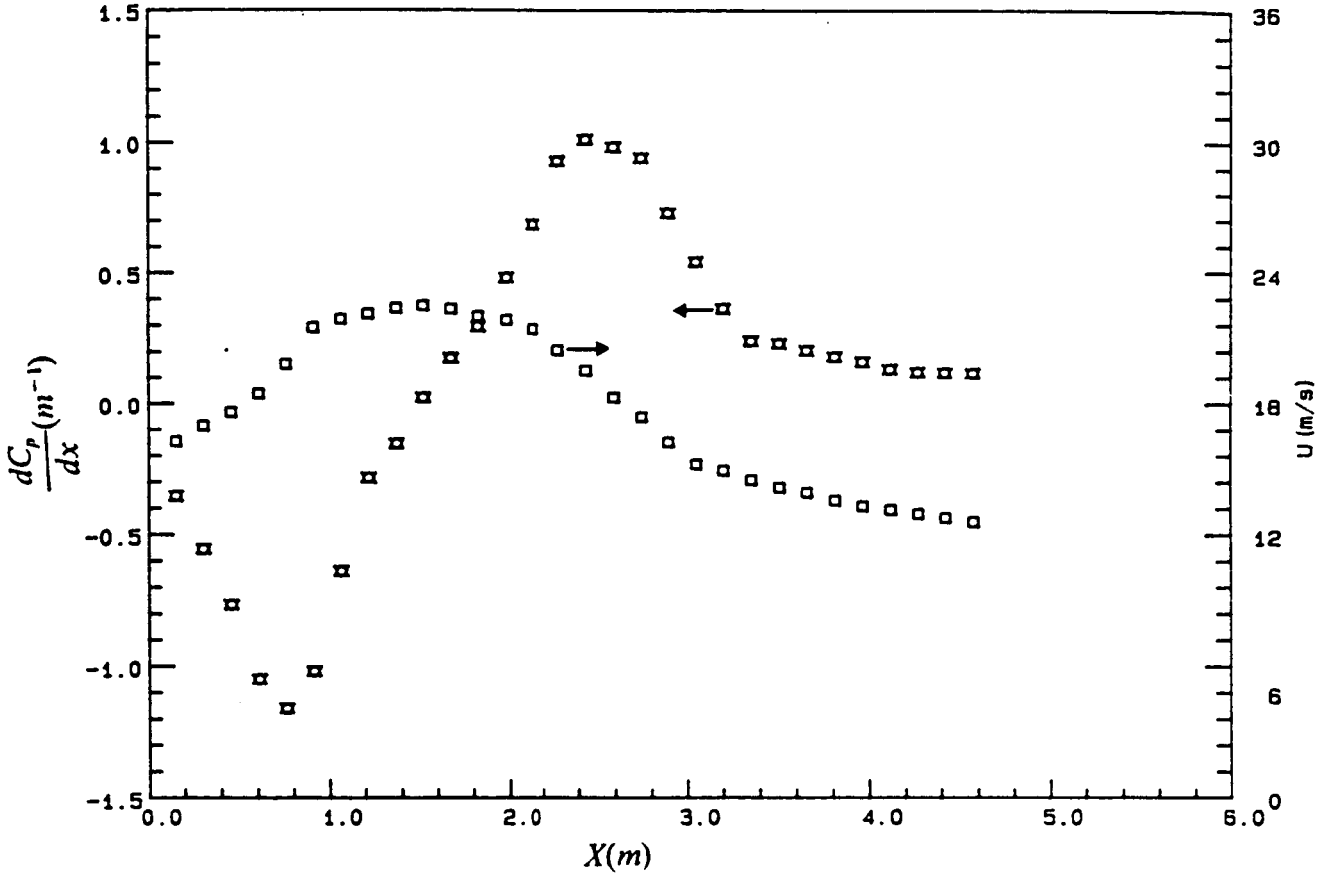

Figure 3 . Pressure gradient distribution and Free-stream velocity along the tunnel center-line for flow with roughness element (Flow D).

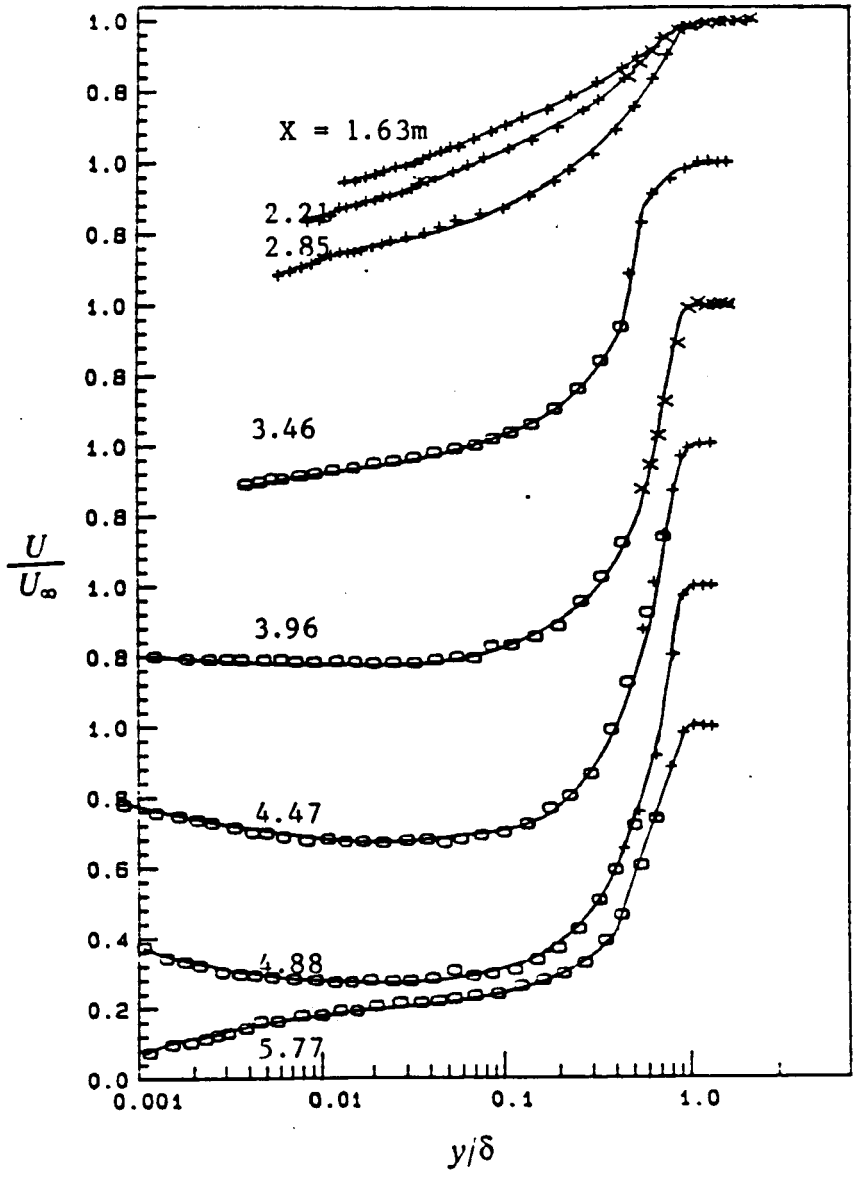

Figure 4 . Non-dimensional composite mean-velocity profile from the laser anemometer and hot-wire anemometers for flow C without roughness element. Note the displaced ordinate for X > 2.85m. Solid lines are for visual aid only. " o " Laser; " × " Cross-wire; " + " Single-wire.

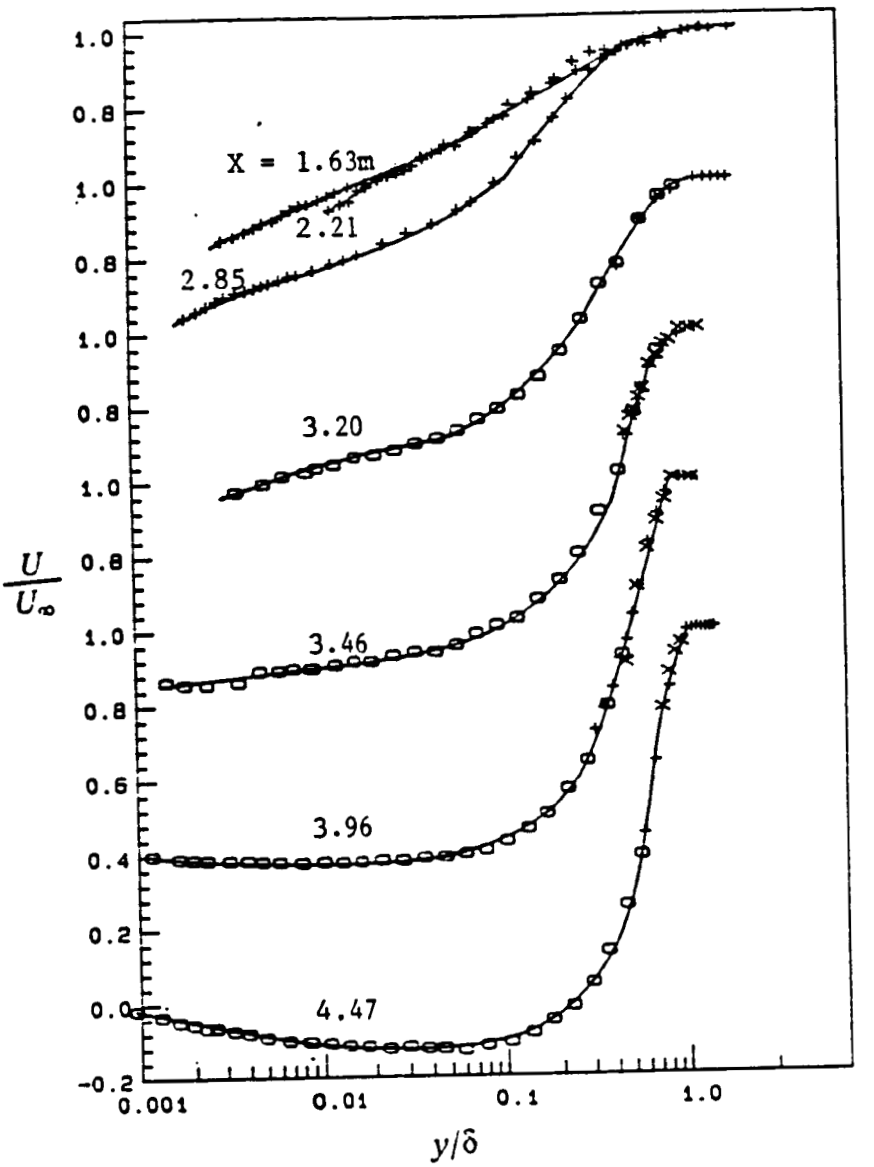

Figure 5 . Non-dimensional composite mean-velocity profile from the laser anemometer and hot-wire anemometers for flow D with roughness element. Note the displaced ordinate for X > 2.85m. Solid lines are for visual aid only. " o " Laser; " × " Cross-wire; " + " Single-wire.

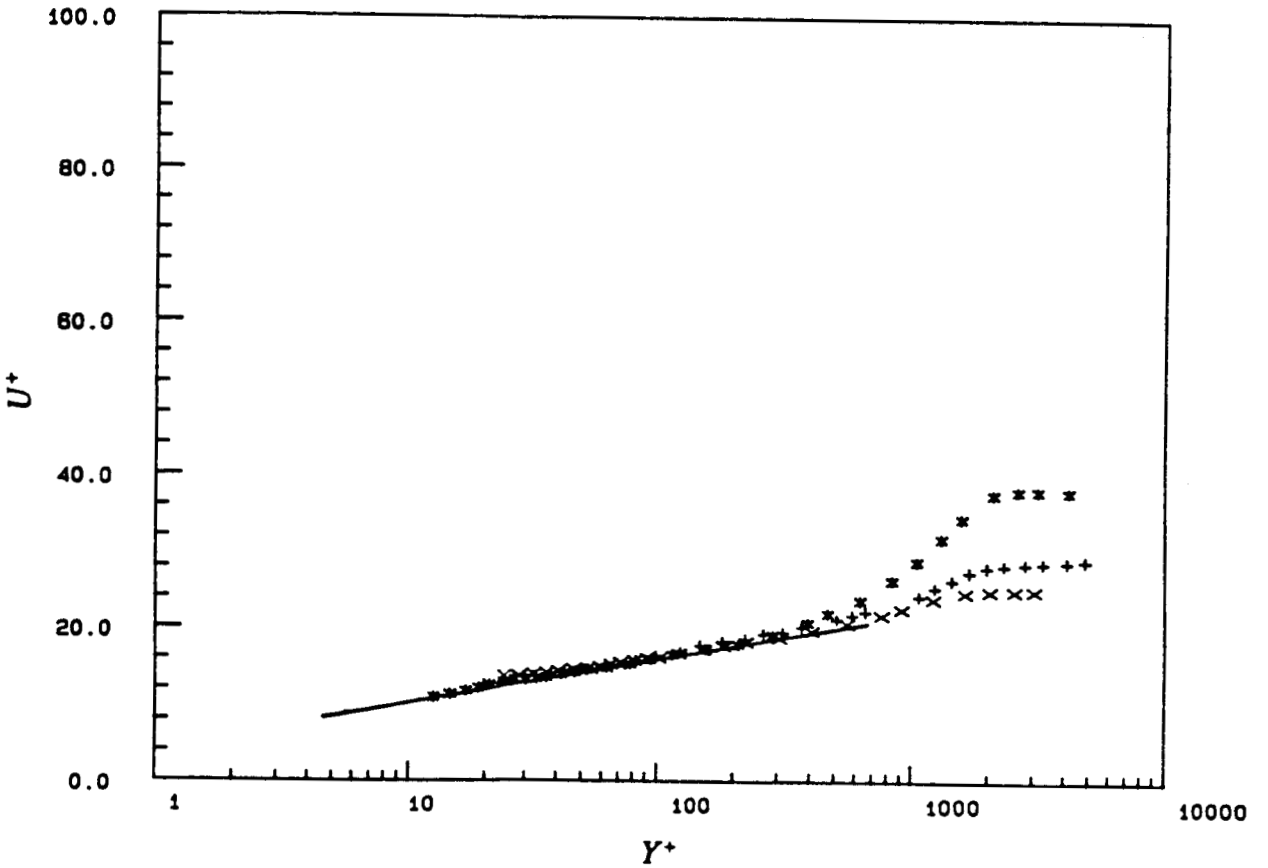

Figure 6 . Universal wall law plot for flow C without roughness element upstream of intermittent backflow region. Solid line represent equation 6. " ✕ " 1.62m; " + " 2.20m; " ✱ " 2.85m.

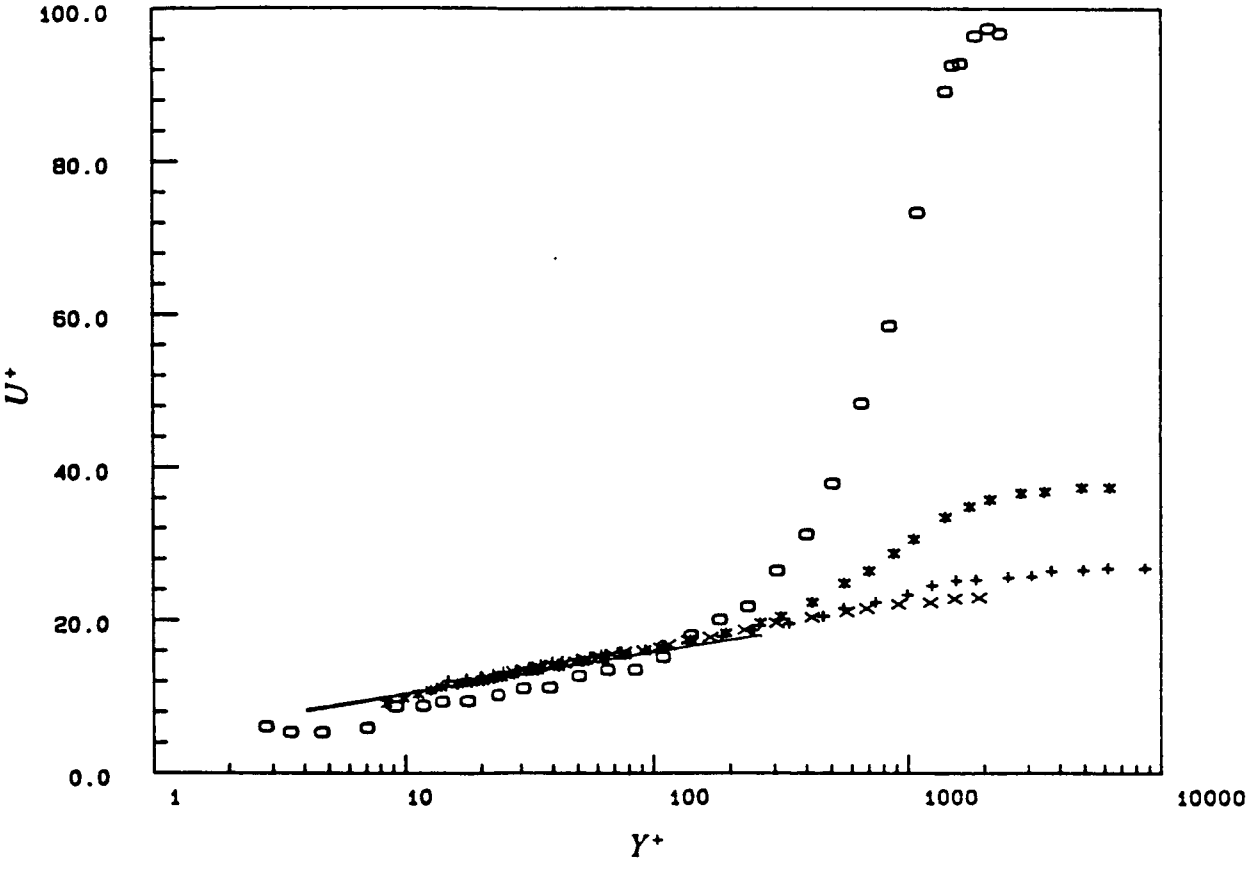

Figure 7 . Universal wall law plot for flow D with roughness element upstream of intermittent backflow region. Solid line represent equation 6. " × " 1.62m; " + " 2.20m; " * " 2.85m; " O " 3.20m.

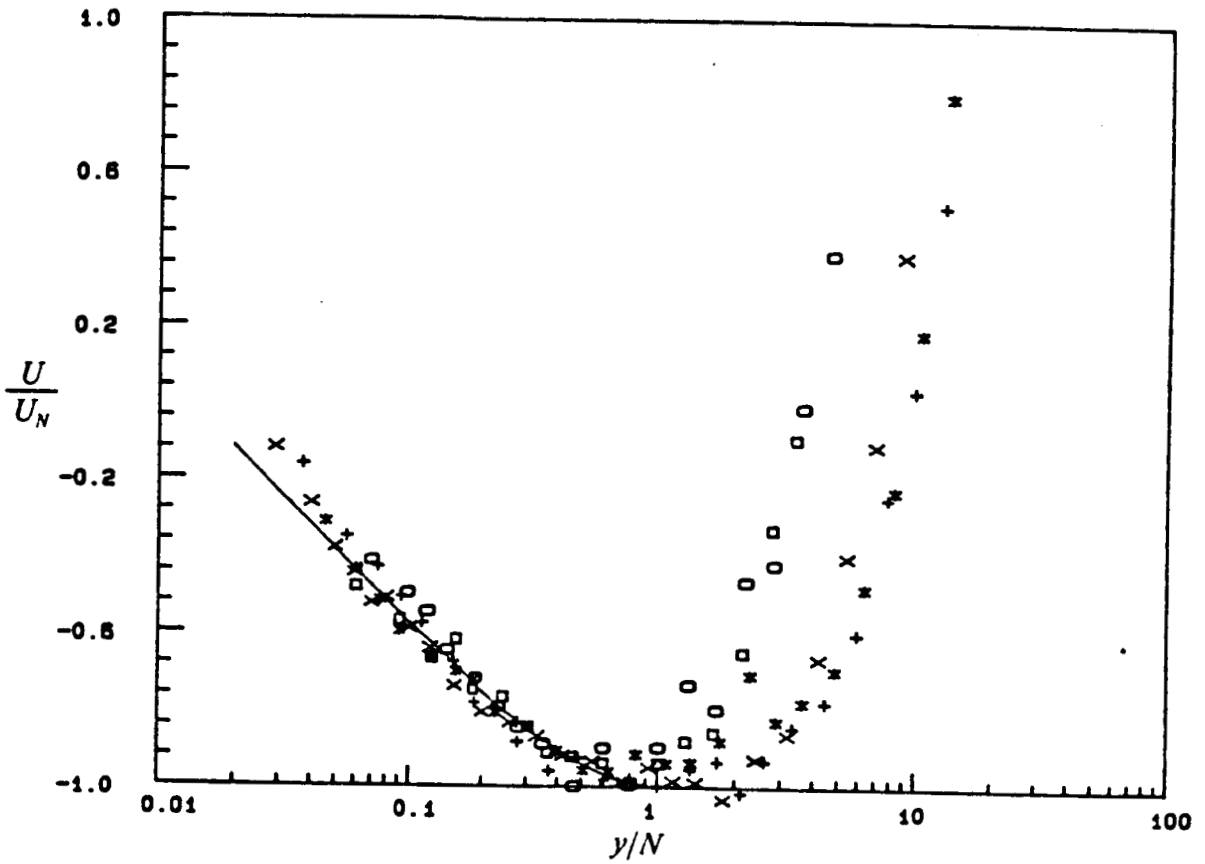

Figure 8 . Normalized backflow mean velocity profiles: U/U_N vs y/N Flow C without roughness element " □ " 3.96m; " + " 4.47m; " ✱ " 4.88m. Flow D with roughness element " ○ " 3.96m; " ✕ " 4.47m. Solid line represents equation 4.

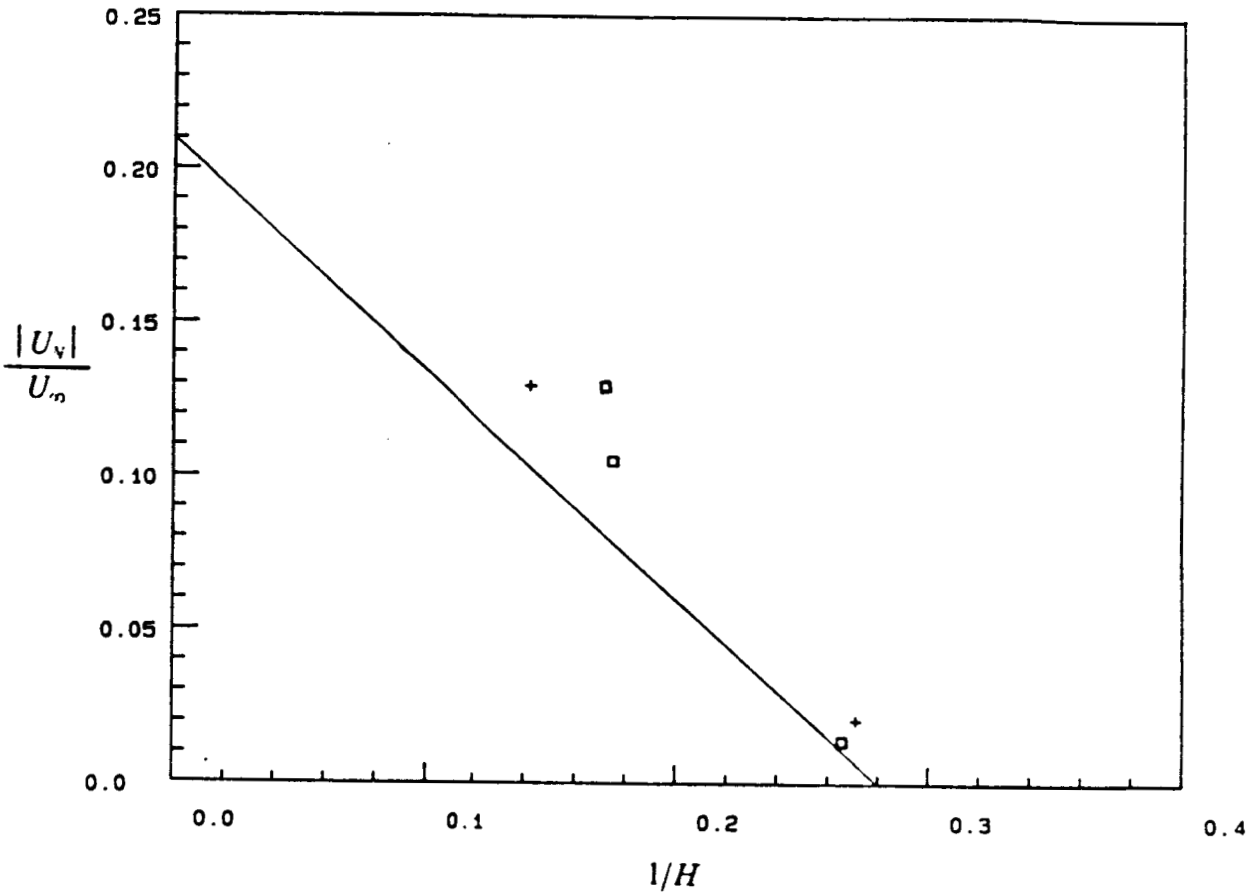

Figure 9 . $|U_N|/U_\infty$ vs 1/H " □ " and " + " for flow without and with roughness element respectively. Solid line represents equation 5.

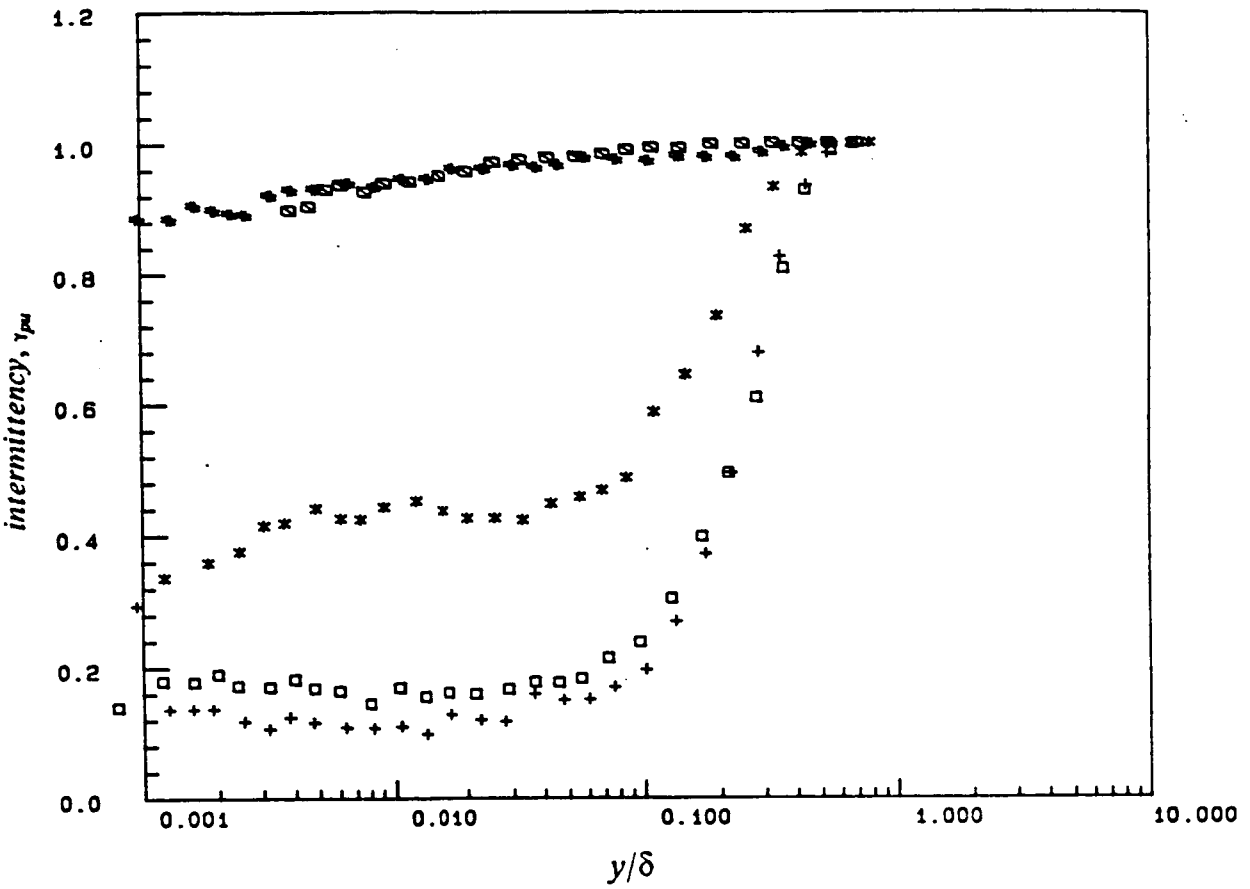

Figure 10 . LDV measurements of the γ_{pu} fraction of time that the flow is in downstream direction for flow C without roughness element. " ◙ " 3.45m; " ✱ " 3.96m; " □ " 4.47m; " + " 4.88m; " # " 5.77m.

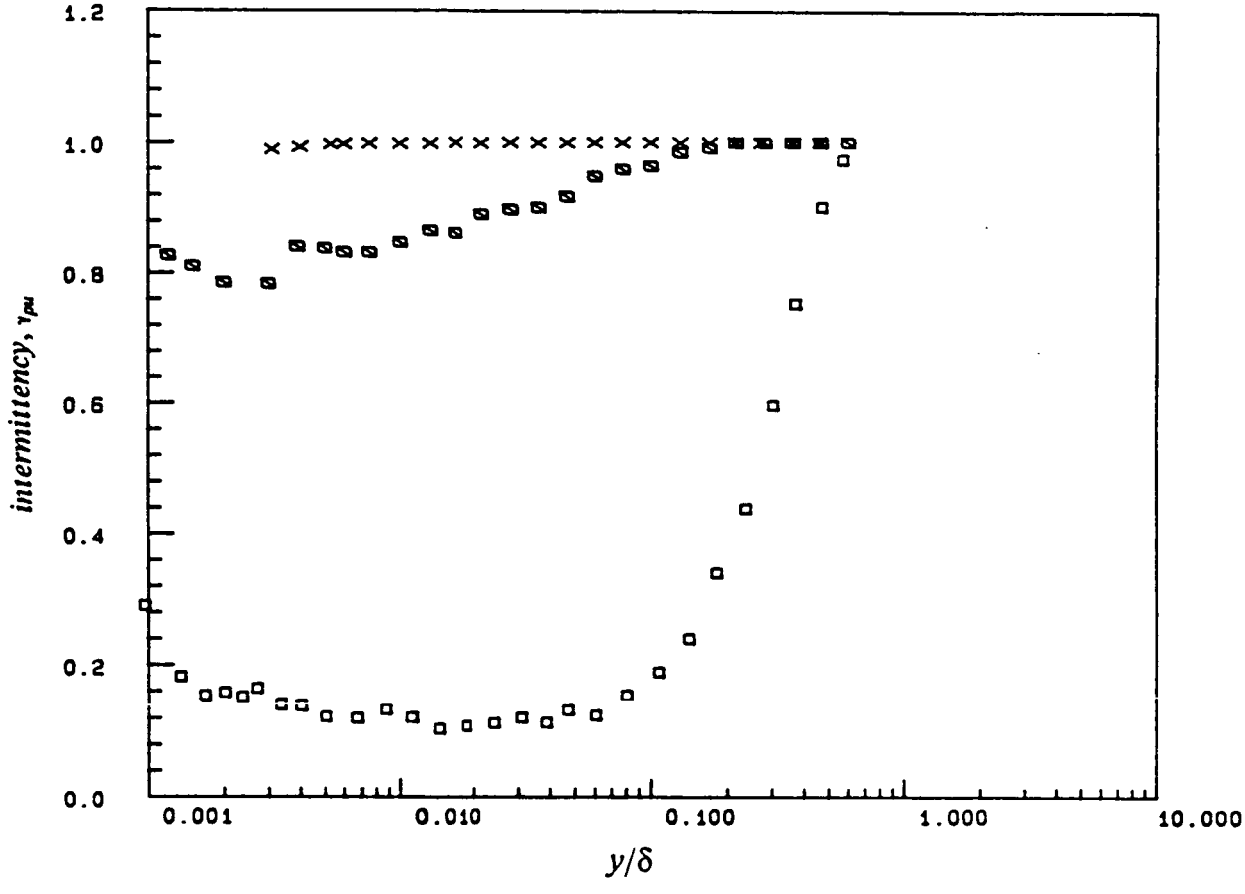

Figure 11 . LDV measurements of the γ_{pu} fraction of time that the flow is in downstream direction for flow D with roughness element. " × " 3.20m; " ◙ " 3.96m; " □ " 4.47m.

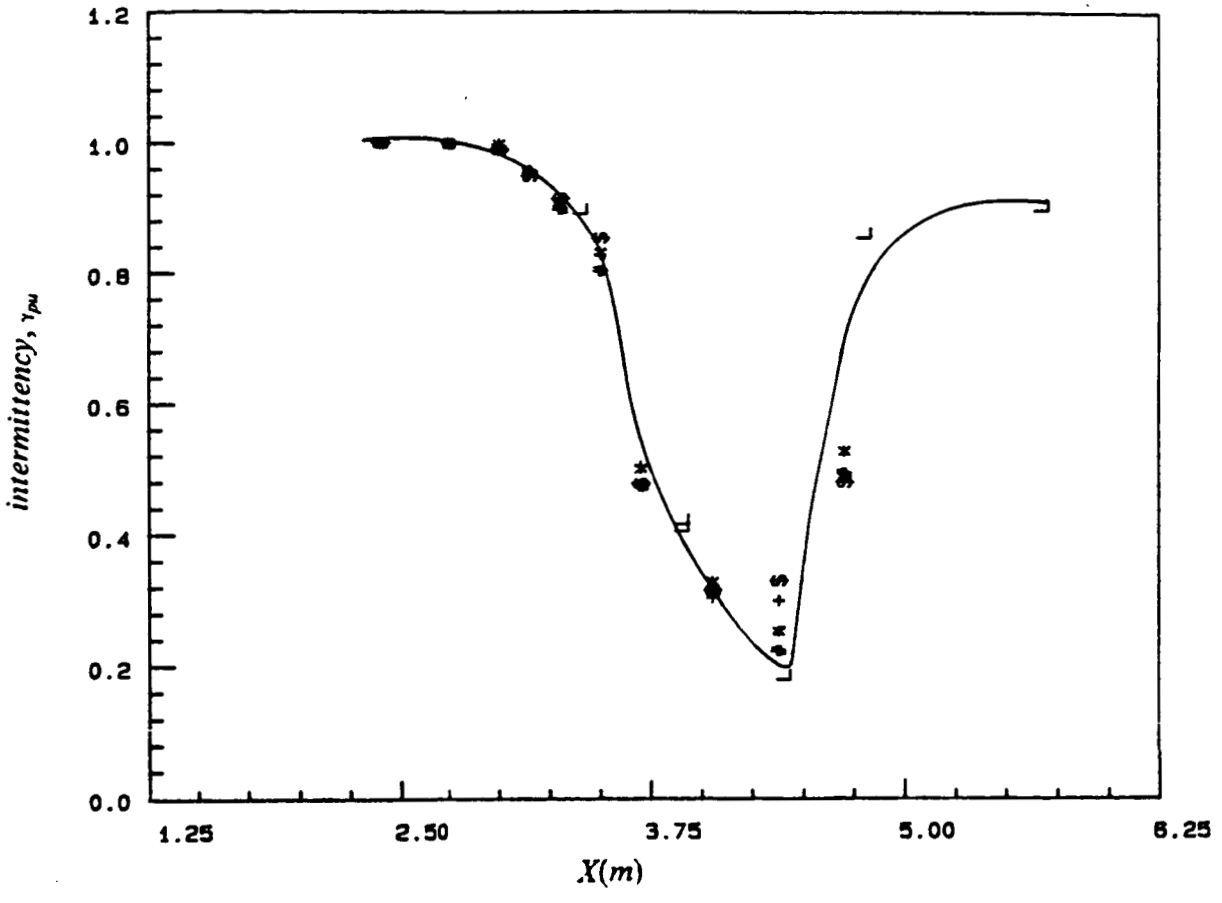

Figure 12 . γ_{pu} fraction of time that the flow is in downstream direction at 1.2mm from the wall vs. X for flow C without roughness element. Solid lines are for visual aid only. " L " Laser; " #, S, *, + ".Thermal tuft for two orientation.

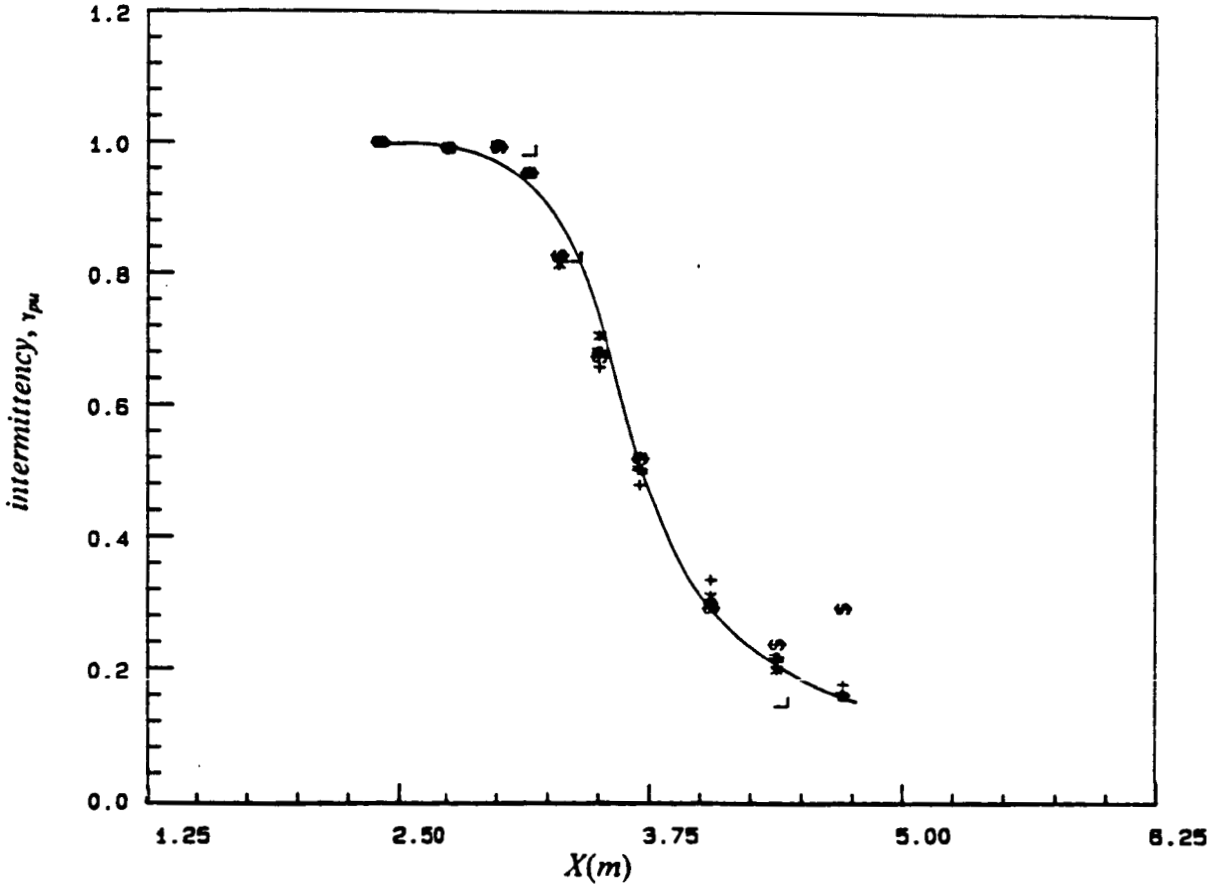

Figure 13 . γ_{pu} fraction of time that the flow is in downstream direction at 1.2mm from the wall vs. X for flow D with roughness element. Solid lines are for visual aid only. " L " Laser; " #, S, *, + " Thermal tuft for two orientation.

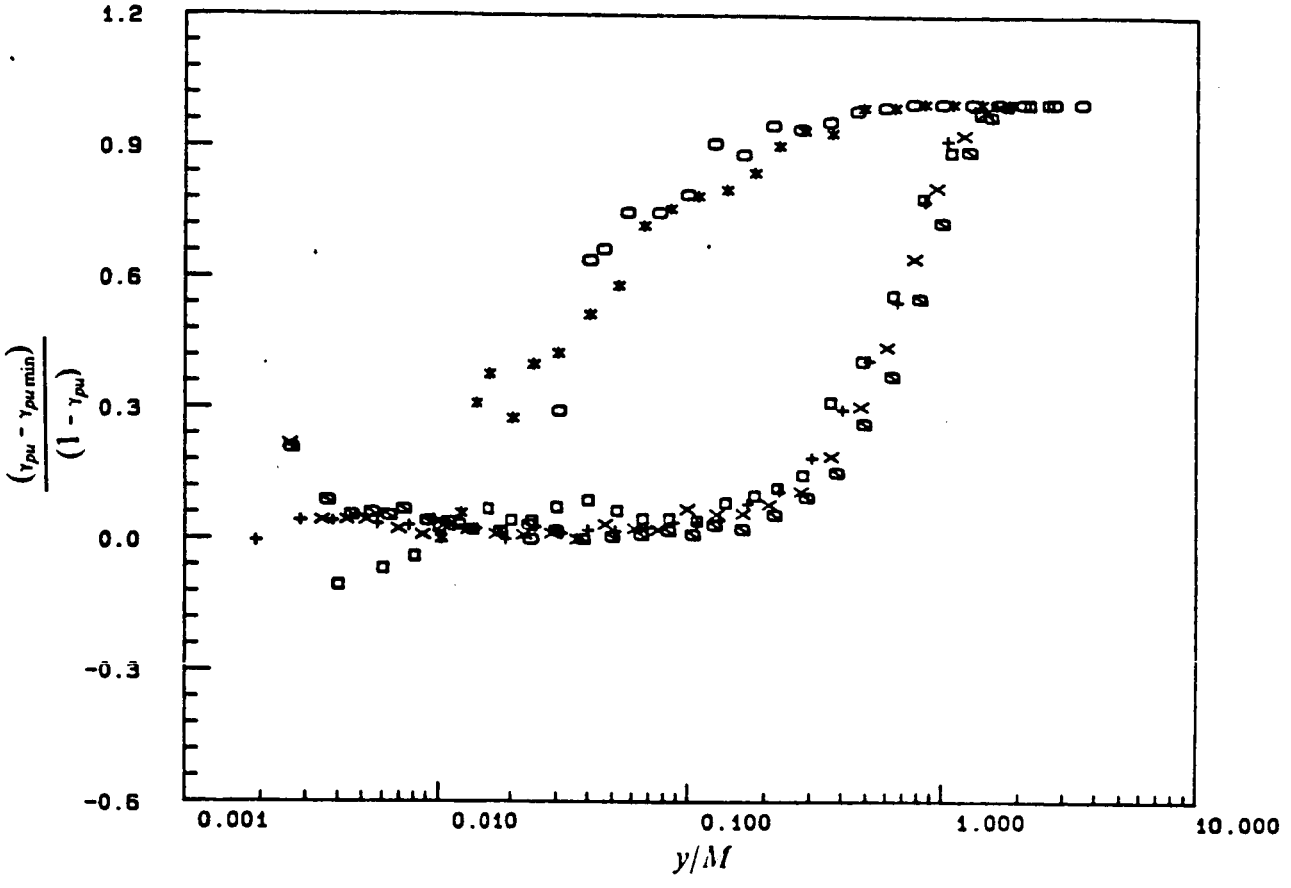

Figure 14 . $(\gamma_{pu} - \gamma_{pu\,min})/(1 - \gamma_{pu\,min})$ vs. y/M, where M is the distance of the maximum $-\overline{uv}$ from wall. Flow C without roughness element " □" 3.45m; " + " 3.96m; " ✱ " 4.47m; " ✕ " 4.88m. Flow D with roughness element " ○" 3.20m; " ⊠ " 4.47m.

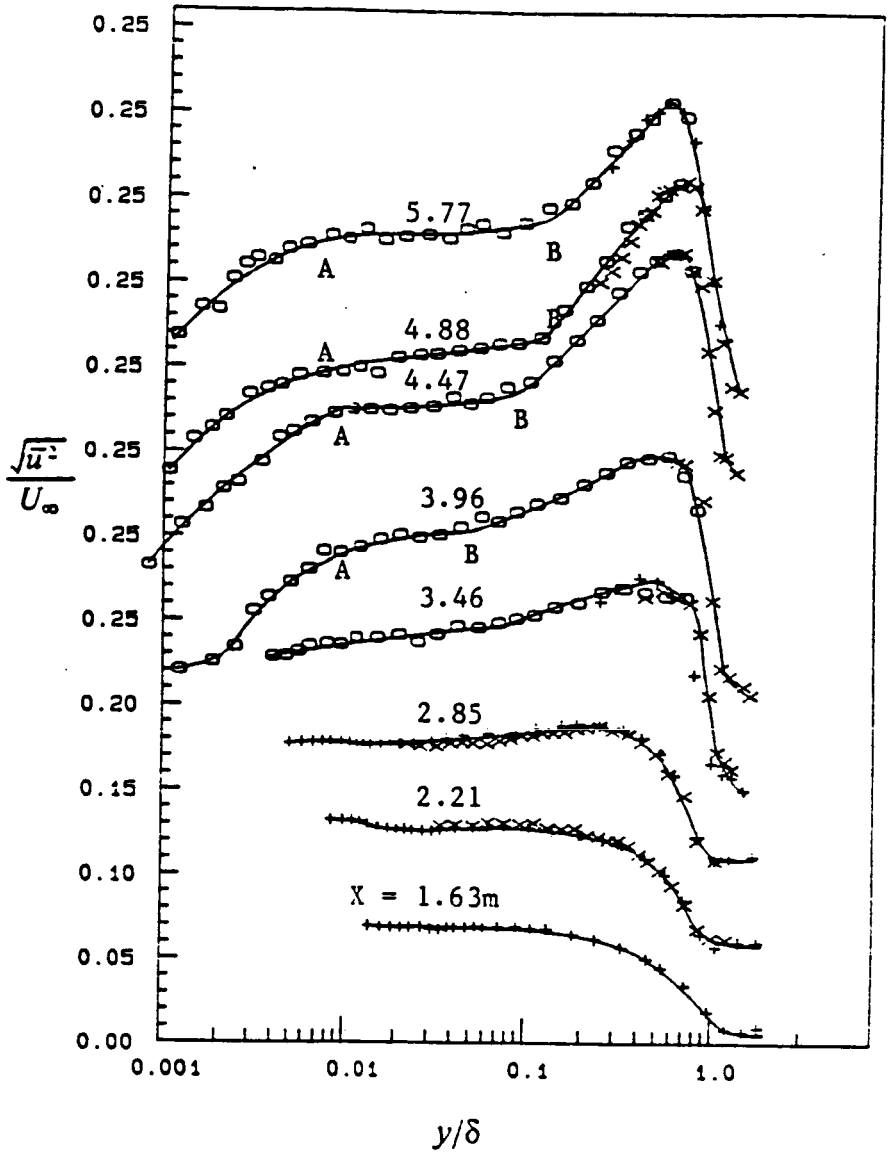

Figure 15 . Axial turbulence intensity profiles, $\sqrt{\overline{u^2}}/U_\infty$ vs y/δ for flow C without roughness element. Note the displaced ordinate. Solid lines are for visual aid only. "O" Laser; " × " Cross-wire; " + " Single-wire.

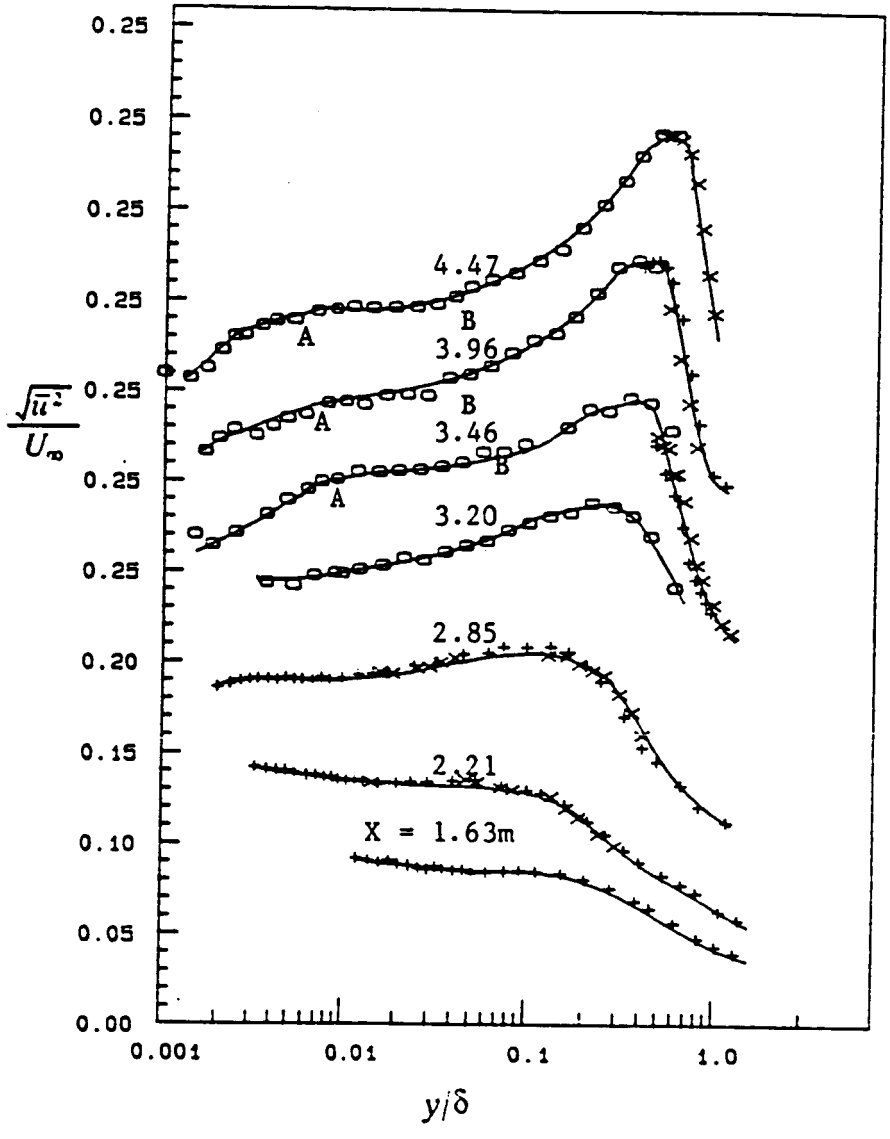

Figure 16 . Axial turbulence intensity profiles, $\sqrt{\overline{u^2}}/U_\infty$ vs y/δ for flow D with roughness element. Note the displaced ordinate. Solid lines are for visual aid only. " O " Laser; " × " Cross-wire; " + " Single-wire.

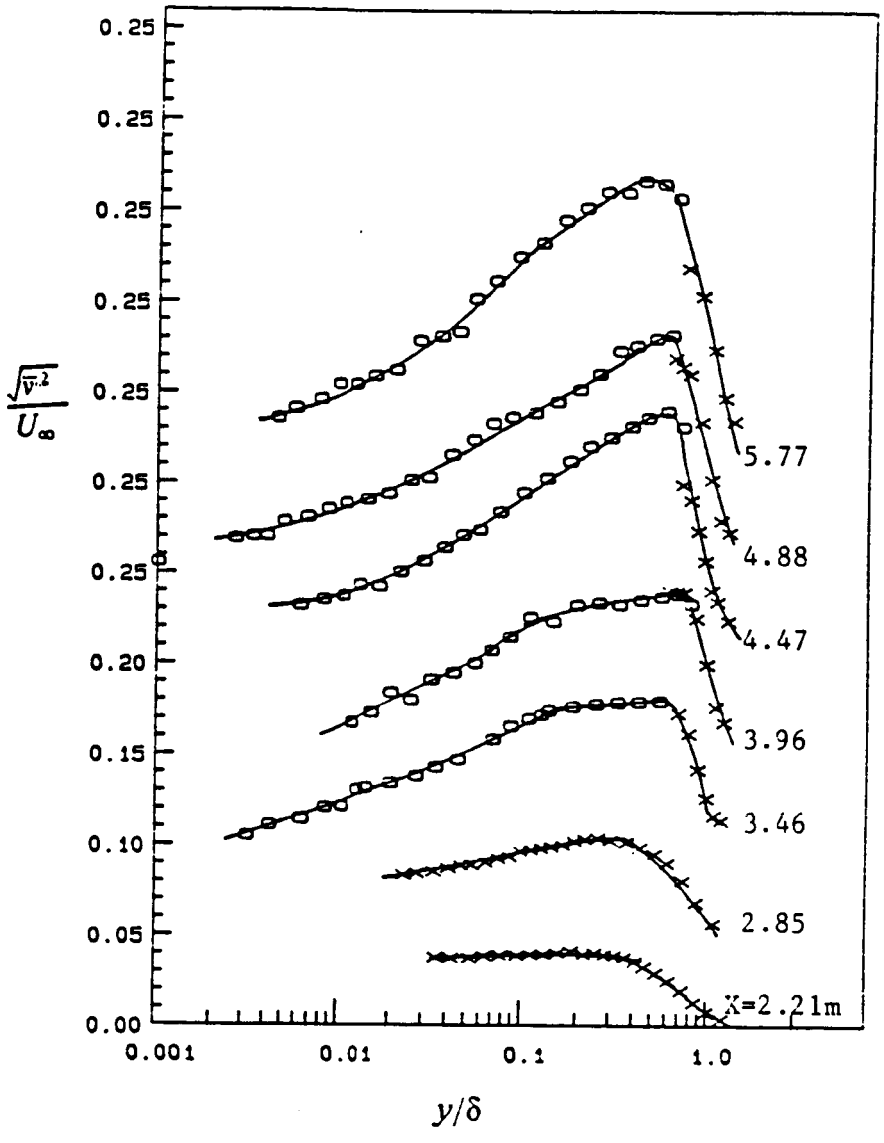

Figure 17. Normal turbulence intensity profiles, $\sqrt{\overline{v^2}}/U_\infty$ vs y/δ for flow C without roughness element. Note the displaced ordinate. Solid lines are for visual aid only. "O" Laser; "×" Cross-wire.

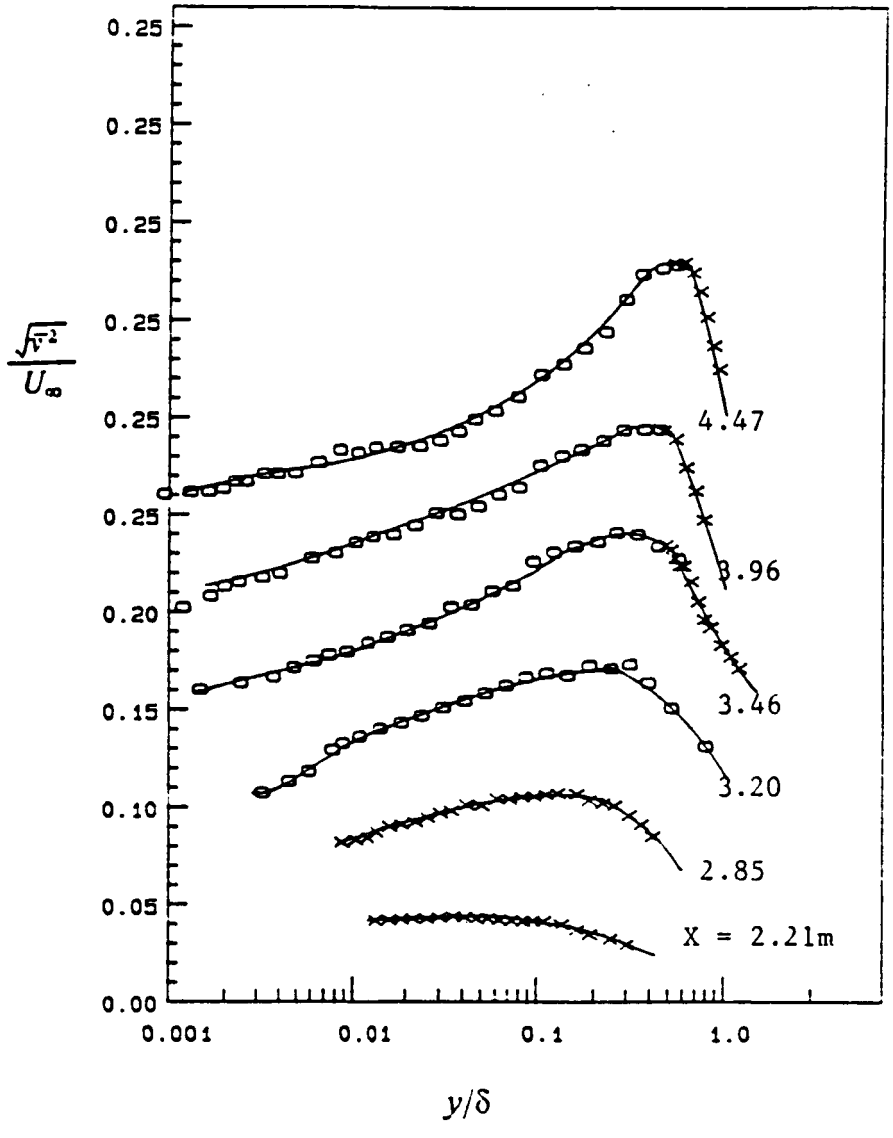

Figure 18 . Normal turbulence intensity profiles, $\sqrt{\overline{v^2}}/U_\infty$ vs y/δ for flow D with roughness element. Note the displaced ordinate. Solid lines are for visual aid only. "O" Laser; "×" Cross-wire.

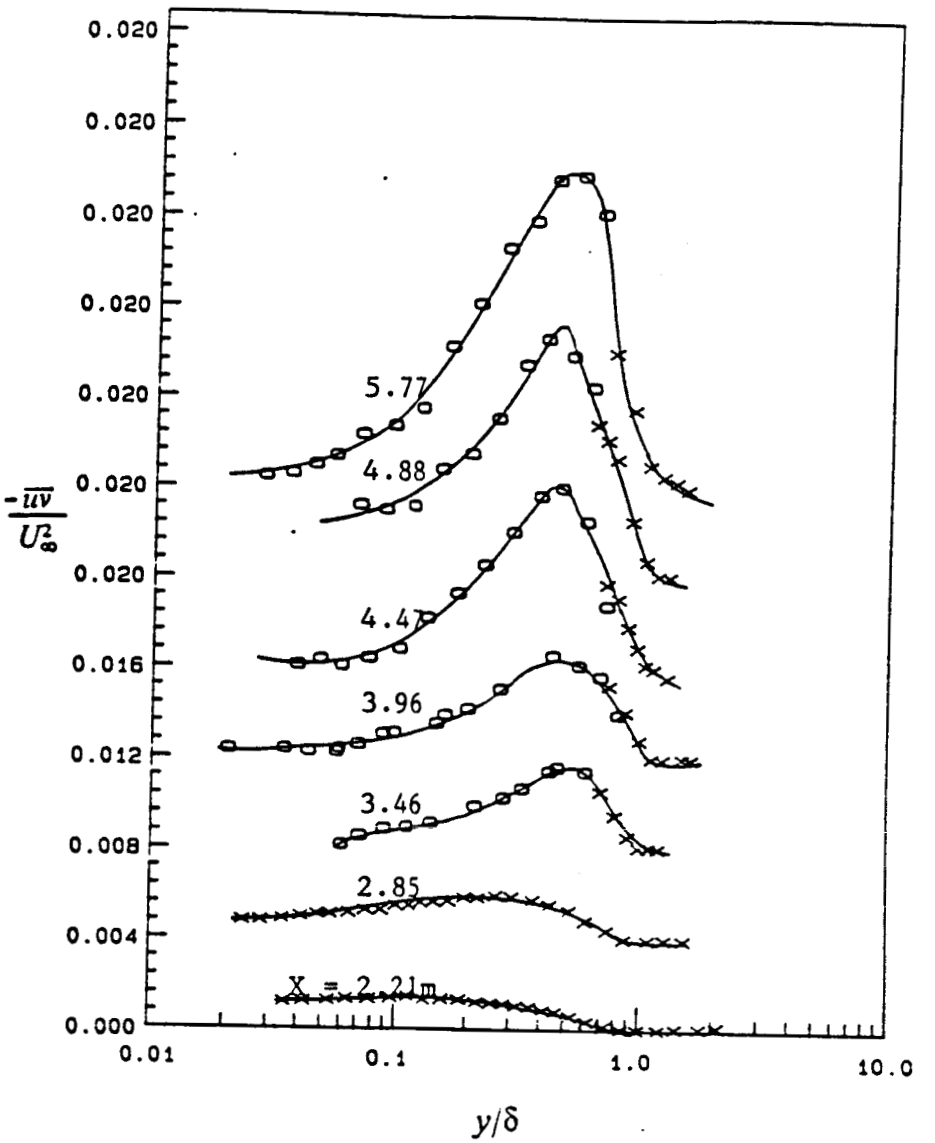

Figure 19 . Reynolds shear stress profiles, $-\overline{uv}/U_\infty^2$ for flow C without roughness element. Note the displaced ordinate. Solid lines are for visual aid only. "o" Laser; "×" Cross-wire.

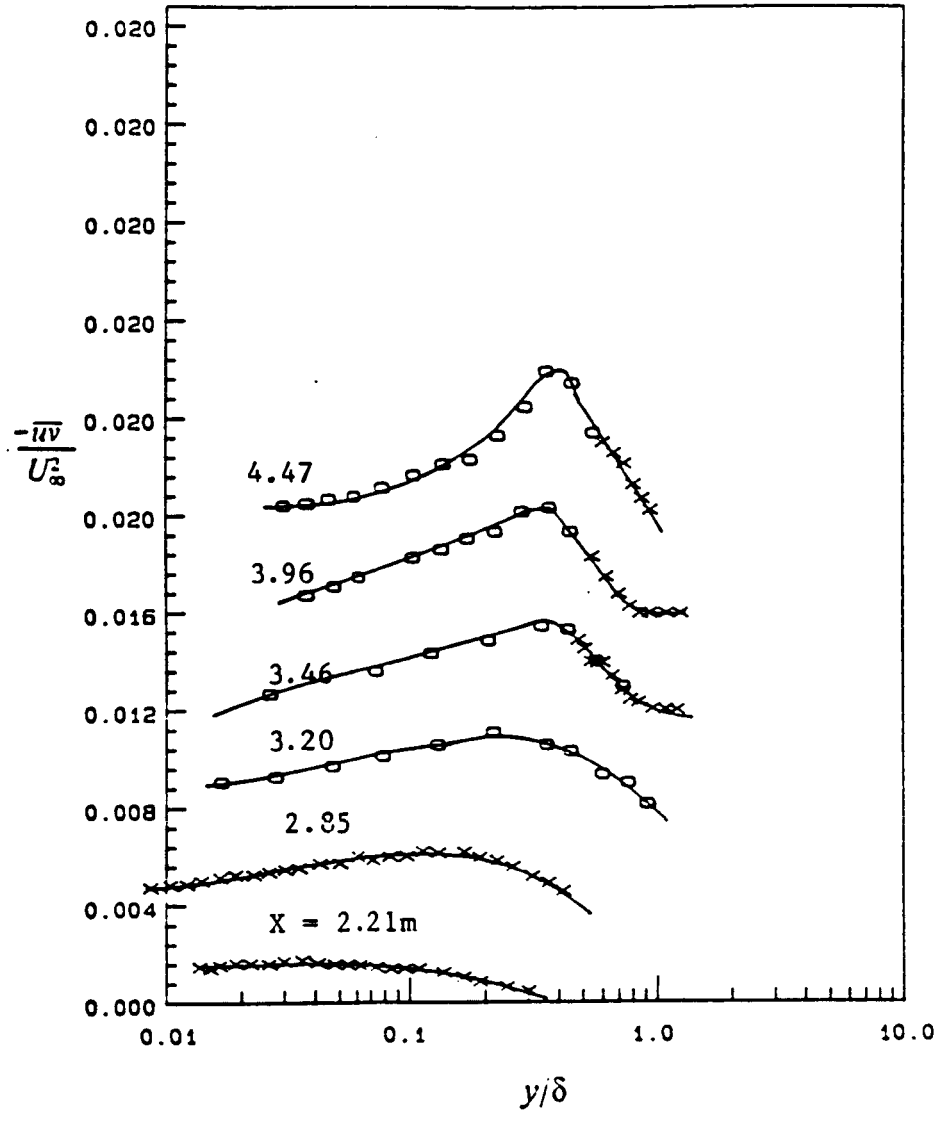

Figure 20 . Reynolds shear stress profiles, $-\overline{uv}/U_\infty^2$ for flow D with roughness element. Note the displaced ordinate. Solid lines are for visual aid only. "O" Laser; "×" Cross-wire.

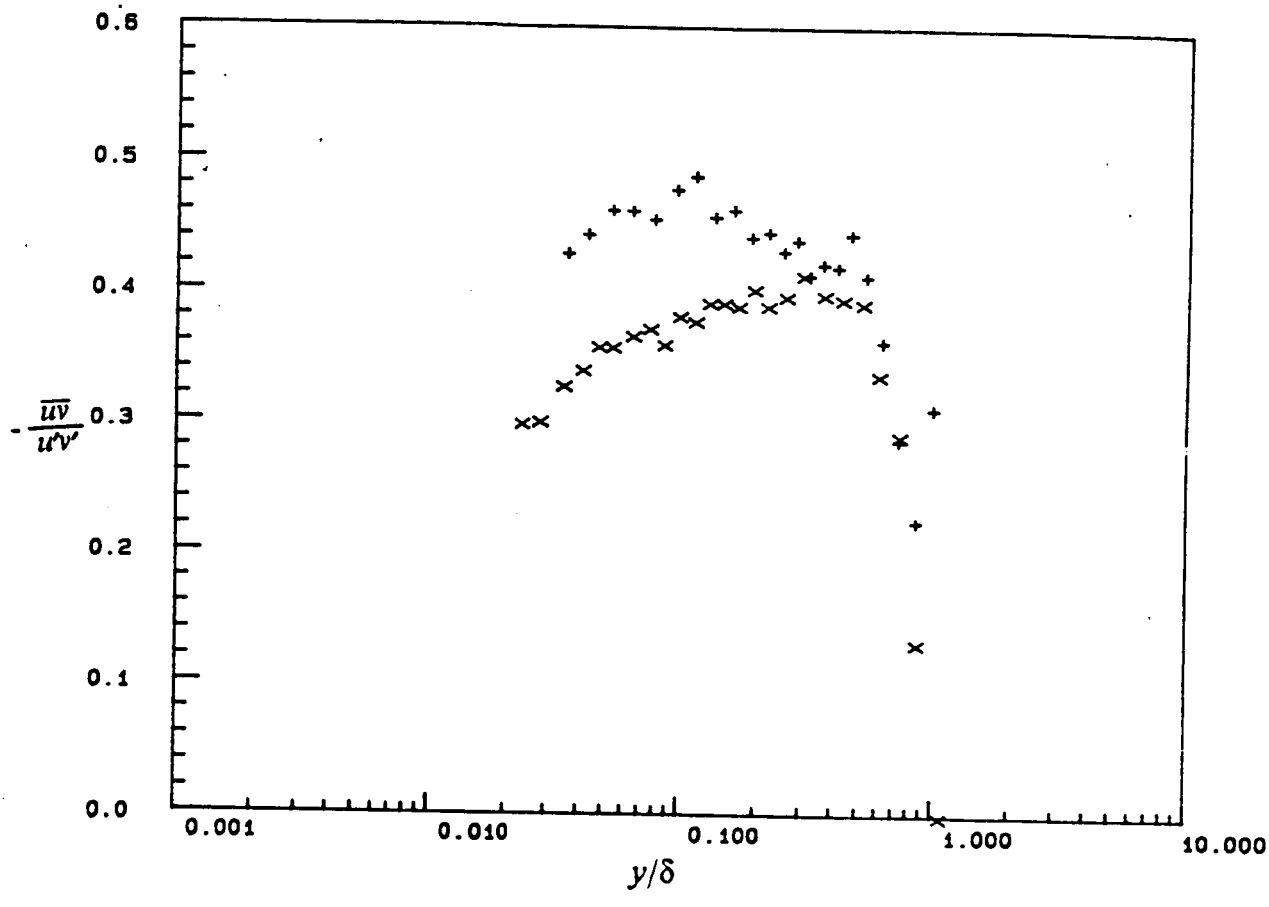

Figure 21 . Distribution of shear stress correlation co-efficient, $-\overline{uv}/u'v'$ vs y/δ (from cross-wire measurement) for flow C without roughness element in unseparated region. " + " 2.20m; " × " 2.85m.

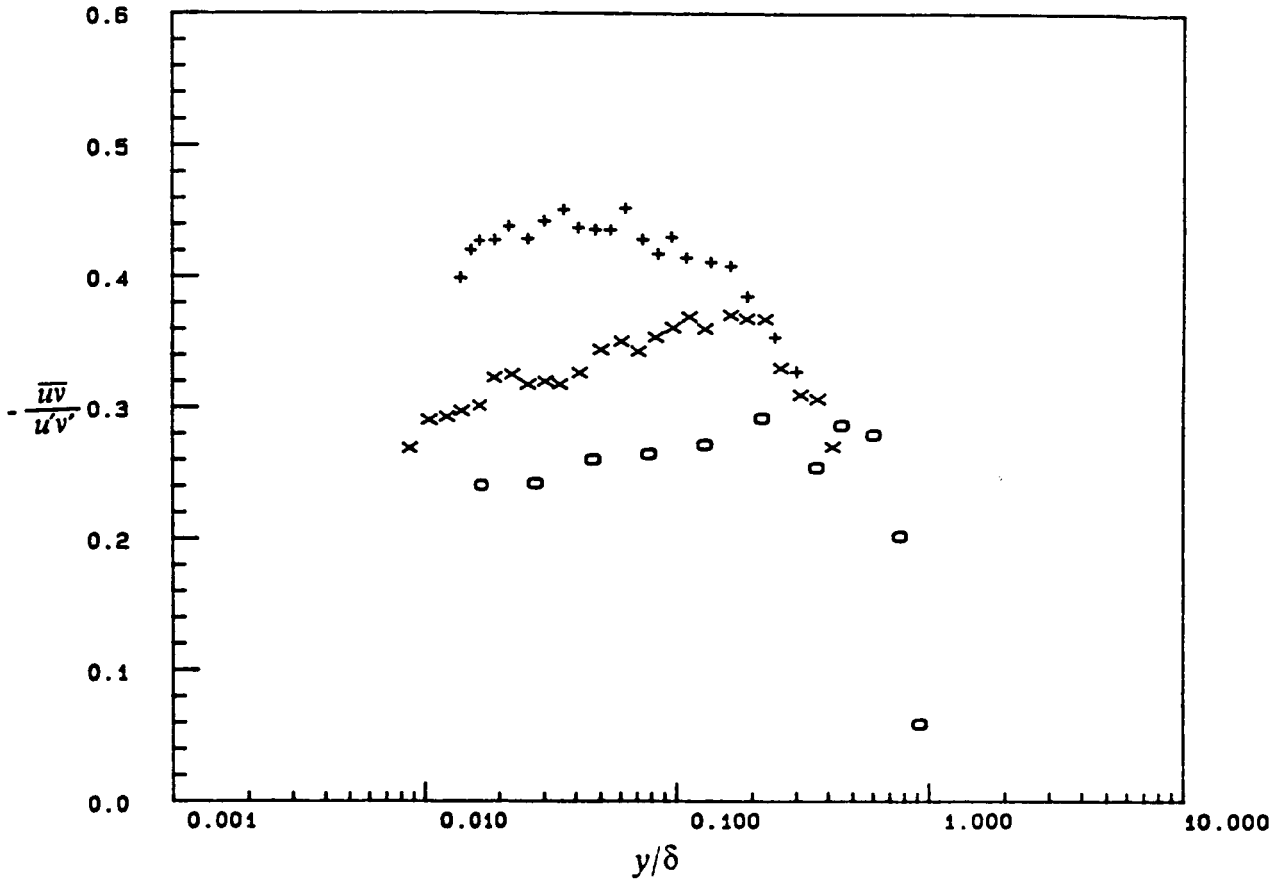

Figure 22 . Distribution of shear stress correlation co-efficient, $-\overline{uv}/u'v'$ vs y/δ (from cross-wire measurement) for flow D with roughness element in unseparated region. " + " 2.20m; " × " 2.85m; " o " 3.20m.

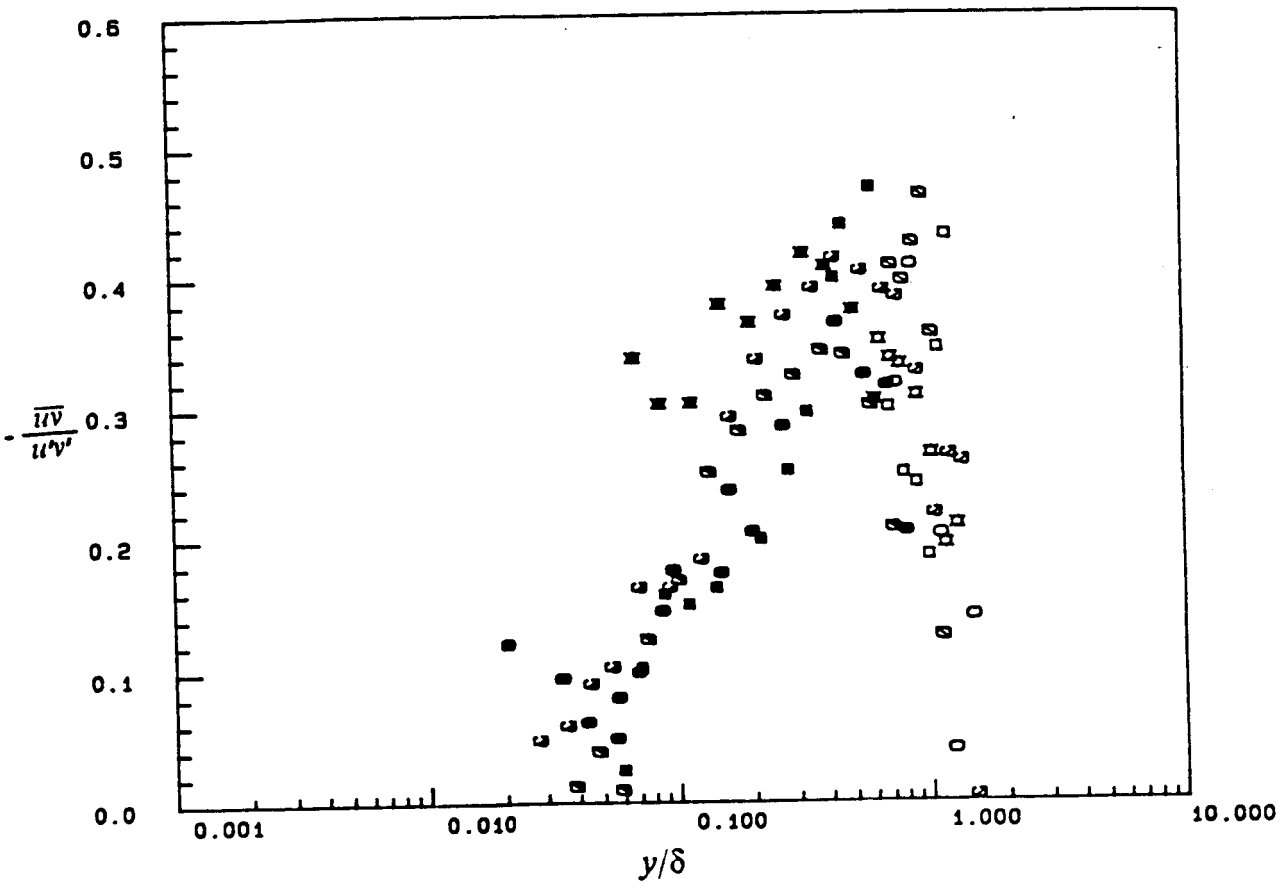

Figure 23 . Distribution of shear stress correlation co-efficient, $-\overline{uv}/u'v'$ vs y/δ for flow C without roughness Solid symbols for laser and open symbols for cross-wire data. " □ " 3.45m; " ○ " 3.96m; " ◙ " 4.47m; " ▣ " 4.88m; " ◉ " 5.77m.

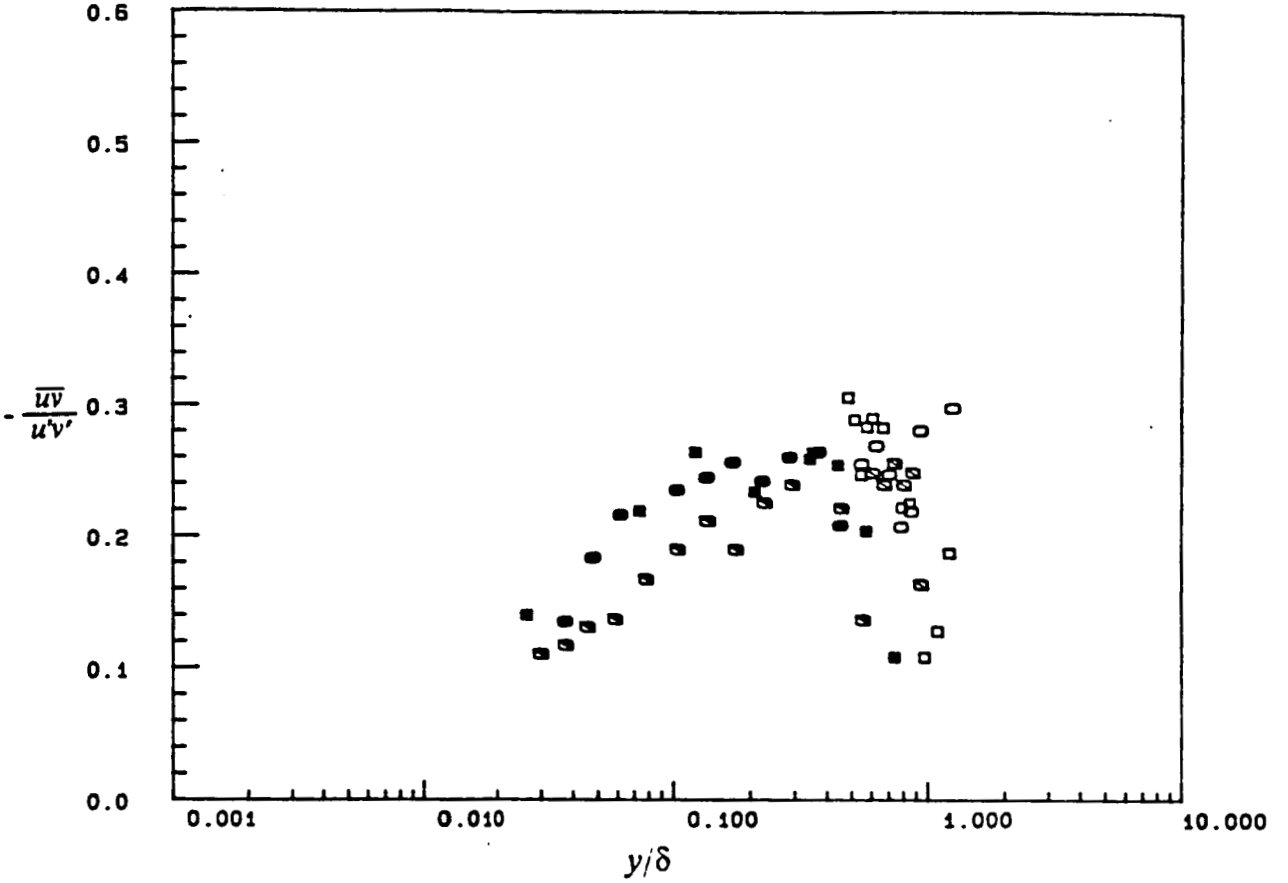

Figure 24 . Distribution of shear stress correlation co-efficient, $-\overline{uv}/u'v'$ vs y/δ for flow D with roughness element downstream of intermittent detachment (ID). Solid symbols for laser and open symbols for cross-wire data. " ◘ " 3.45m; " ○ " 3.96m; " ◙ " 4.47m.

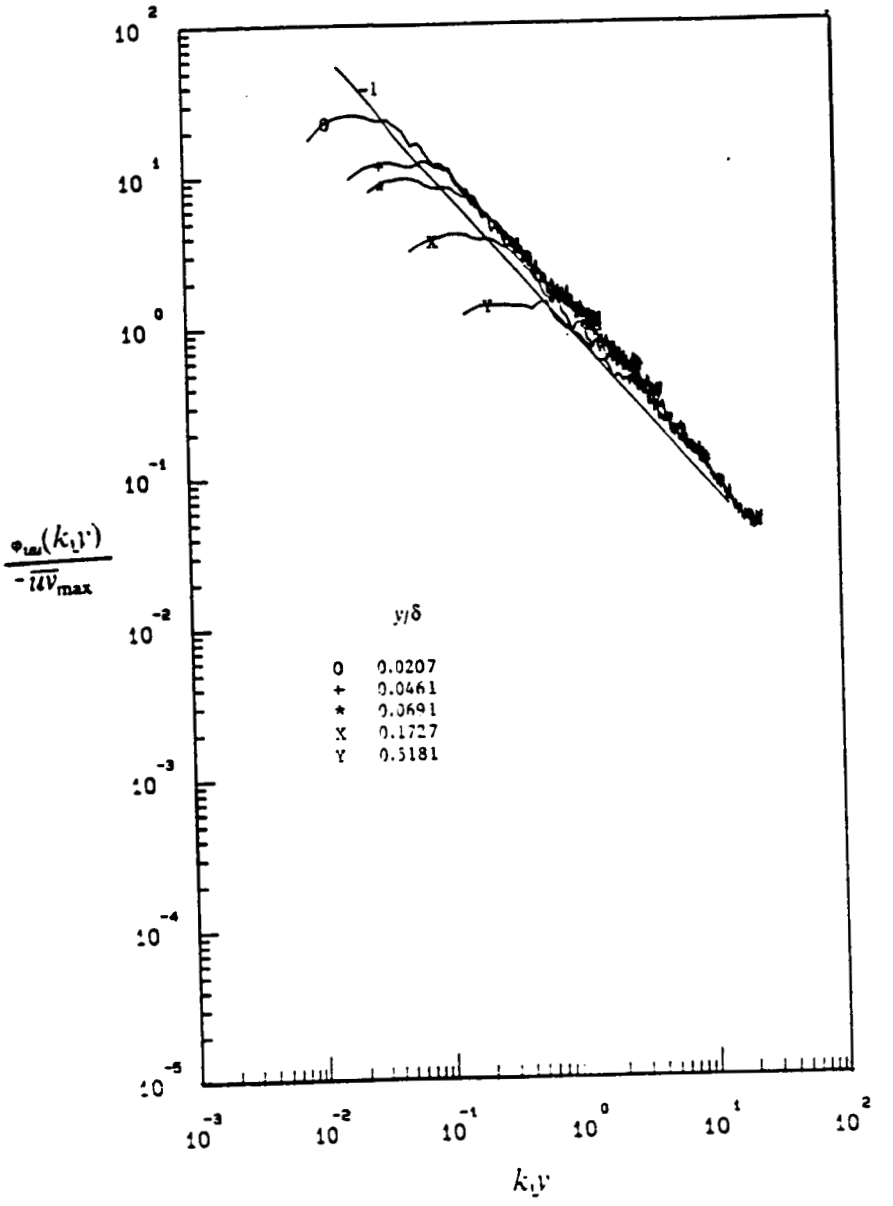

Figure 25 . Normalized *u'* power spectral distribution from single wire measurements at throat (X = 1.63m) for flow C without roughness element. Solid line represents equation 11.

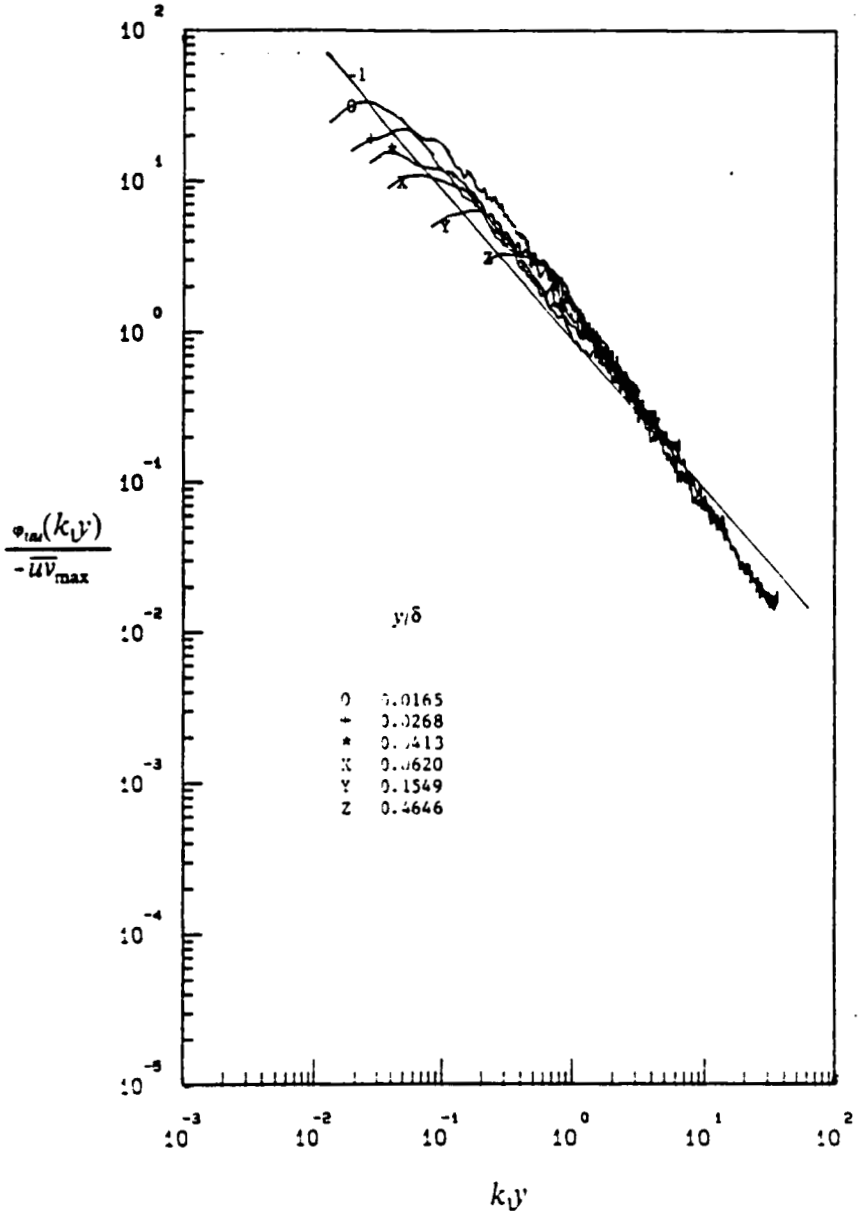

Figure 26 . Normalized *u'*power spectral distribution from single wire measurements at throat (X = 1.63m) for flow D with roughness element. Solid line represents equation 11.

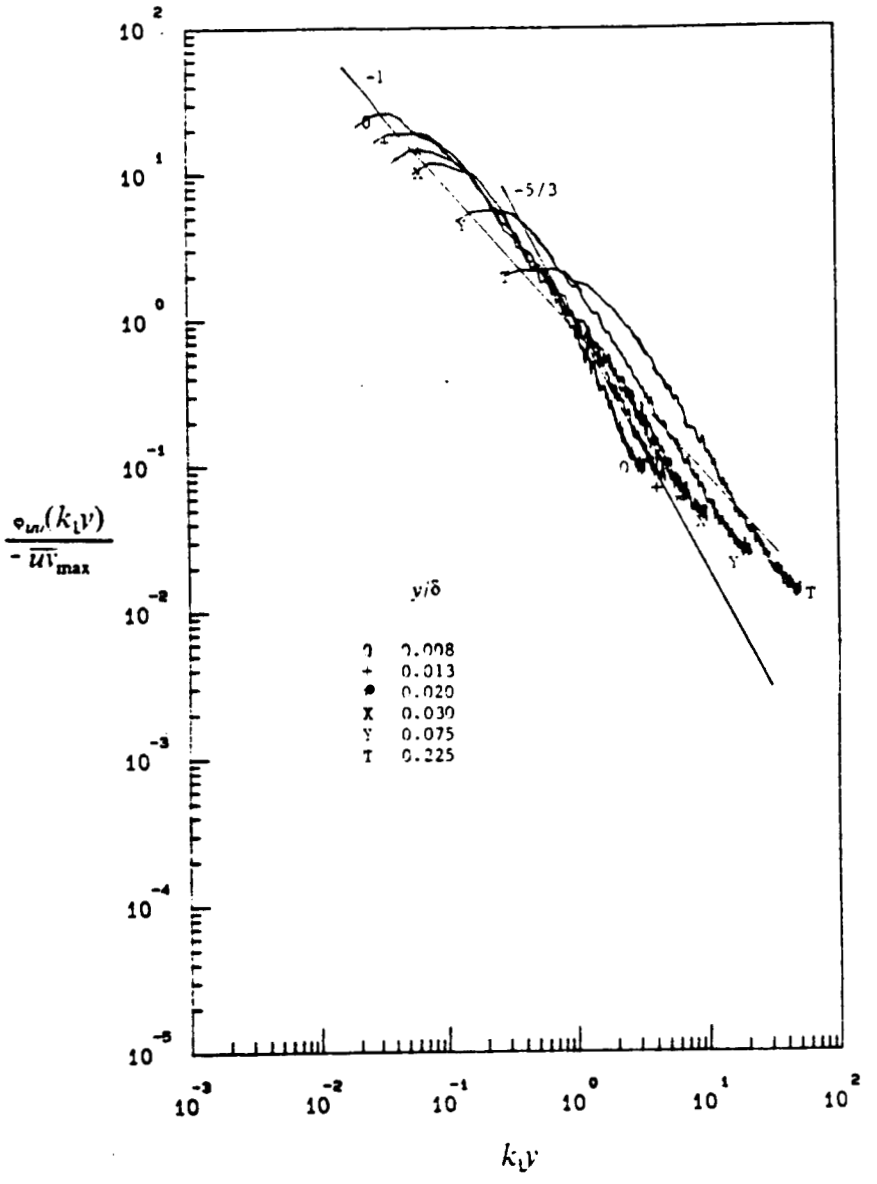

Figure 27. Normalized u' power spectral distribution at X = 2.85m (between throat and intermittent backflow region) for flow C without roughness element. Solid line represents equation 11 and 12.

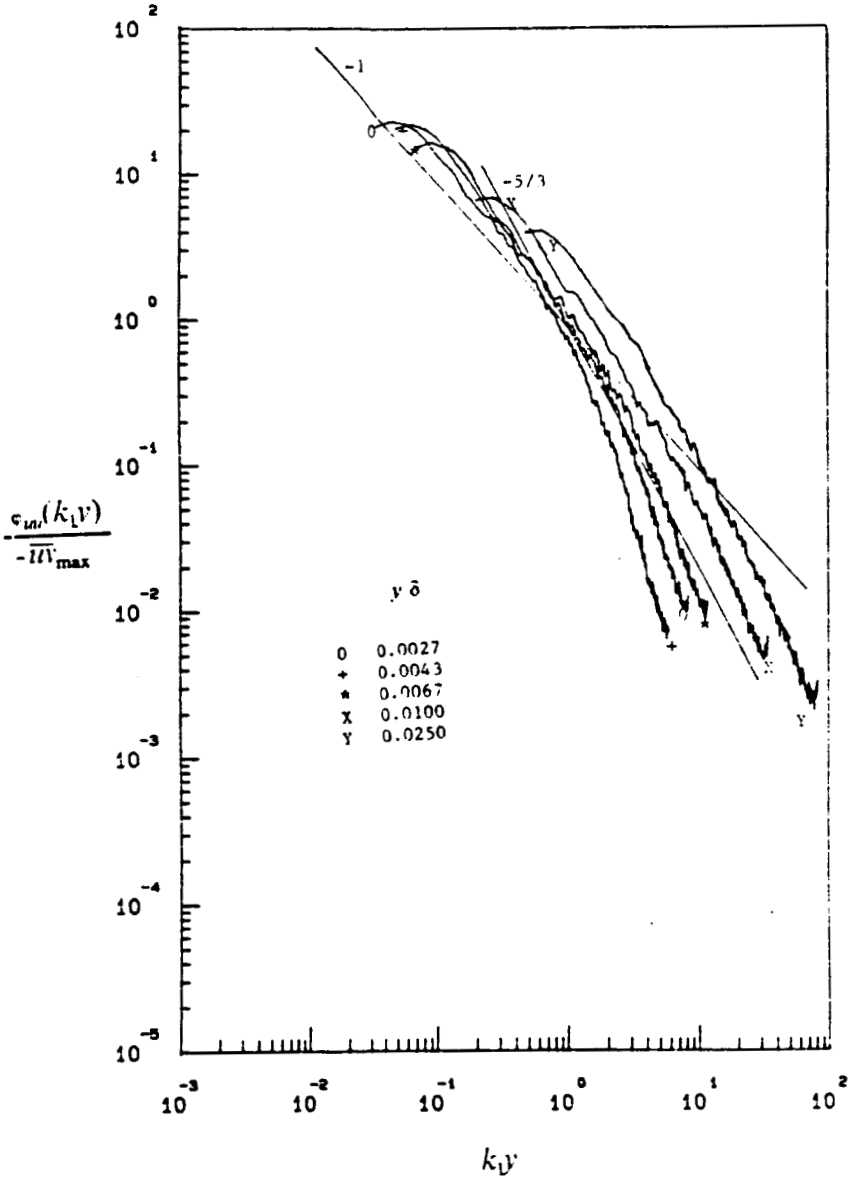

Figure 28. Normalized *u'* power spectral distribution at X = 2.85m (between throat and intermittent backflow region) for flow D with roughness element. Solid line represents equation 11 and 12.

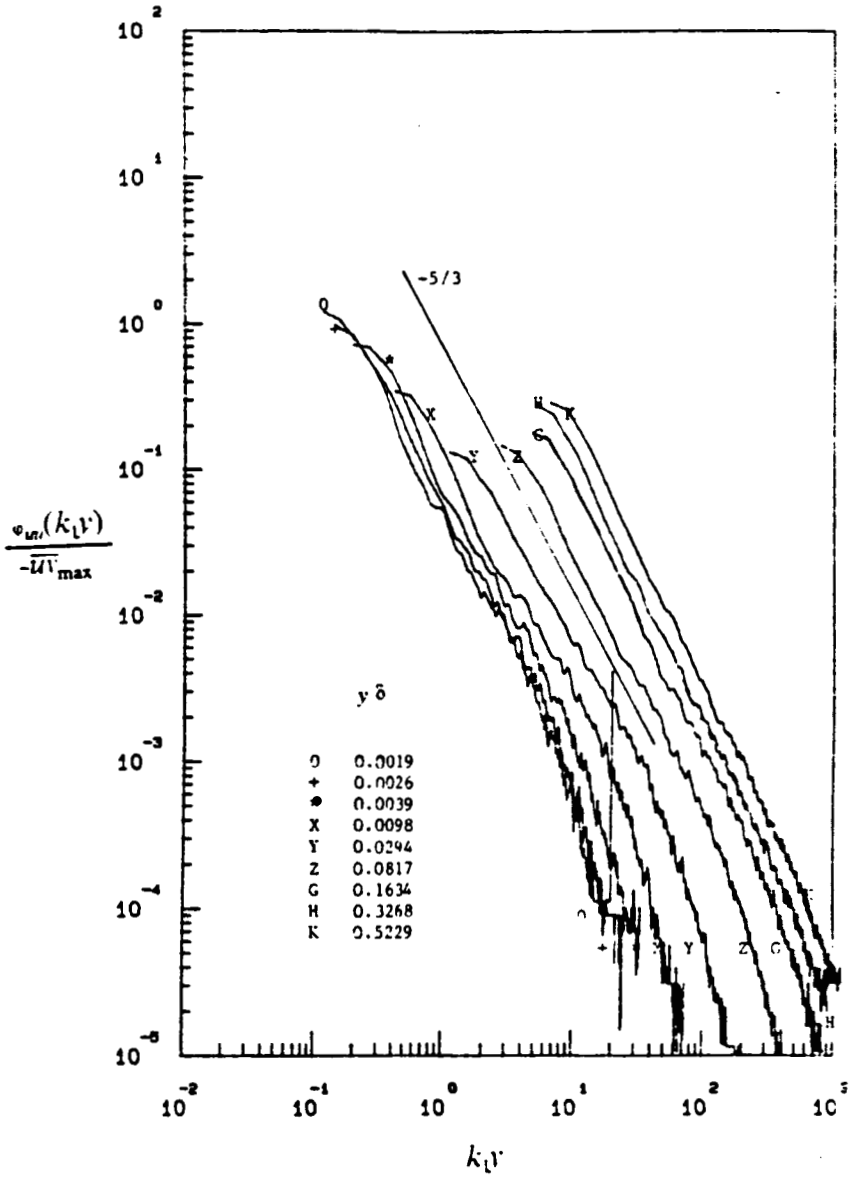

Figure 29. Normalized u' power spectral distribution at X = 5.4m (downstream of reattachment) for flow C without roughness element. Solid line represents equation 12.

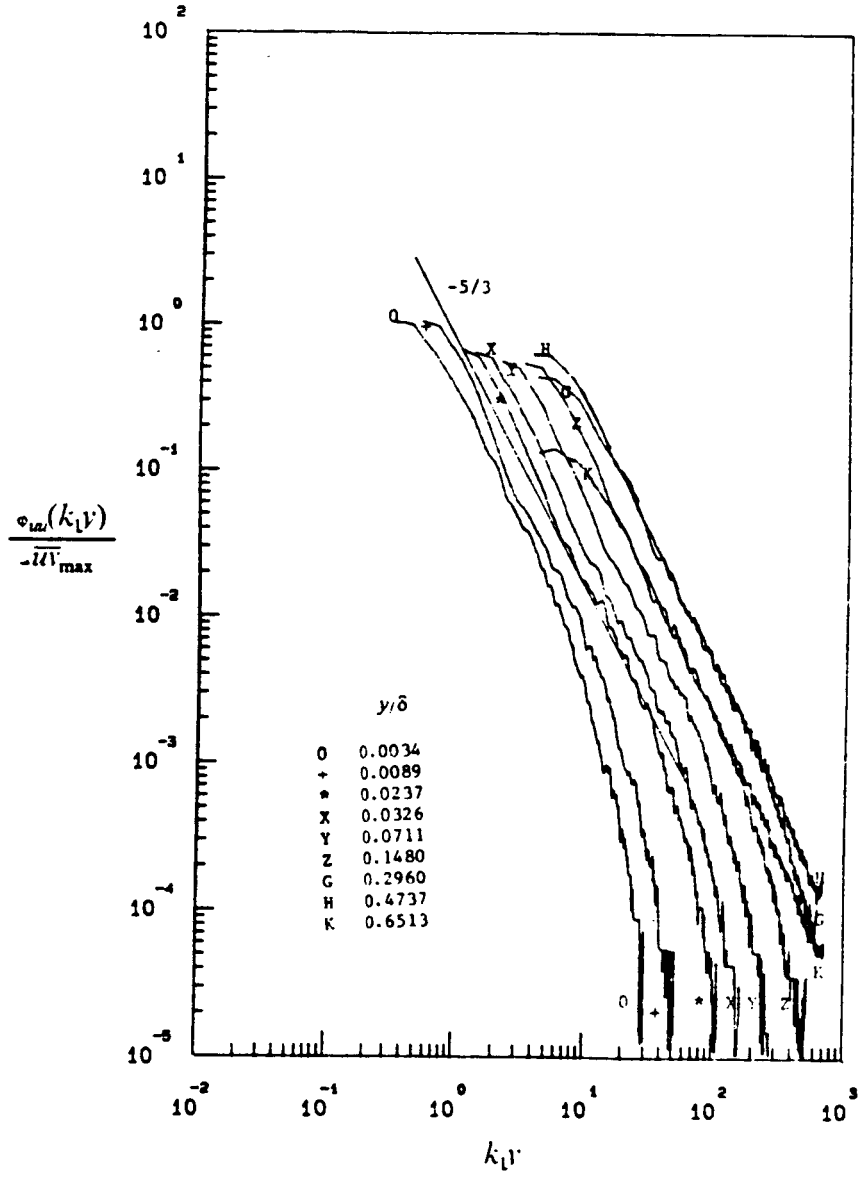

Figure 30 . Normalized *u'* power spectral distribution at X = 3.5m (in the intermittent backflow region) for flow D with roughness element. Solid line represents equation 12.

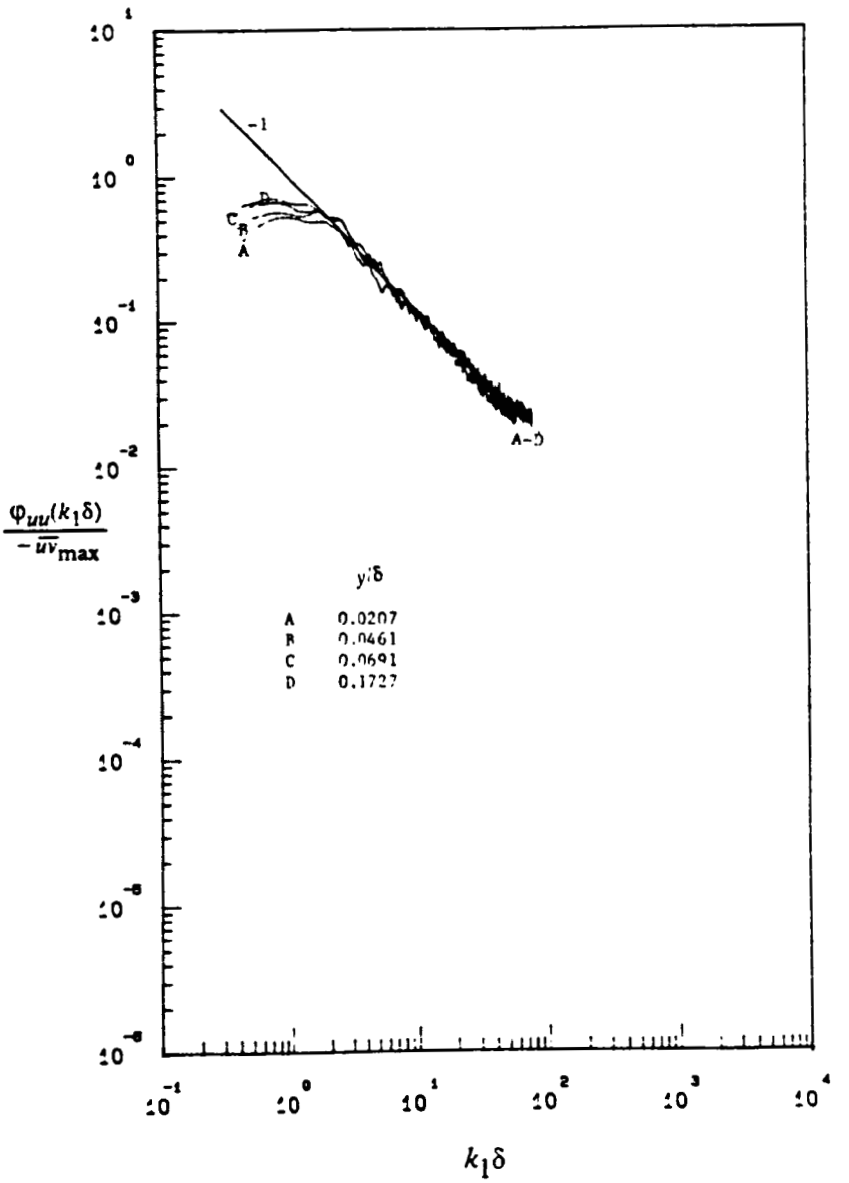

Figure 31 . Normalized u'power spectral distribution from single wire measurements at throat (X = 1.63m) for flow C without roughness element. Solid line represents equation (14).

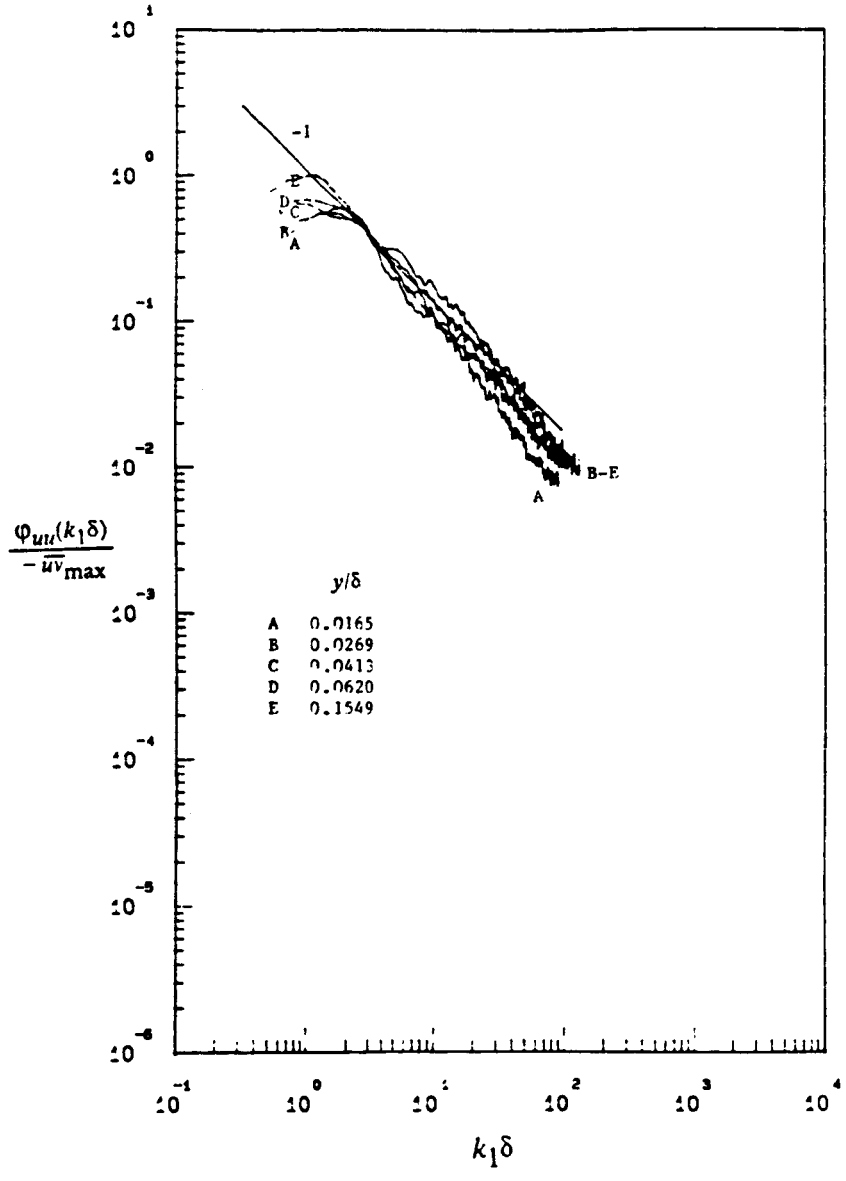

Figure 32 . Normalized u'power spectral distribution from single wire measurements at throat (X = 1.63m) for flow D with roughness element. Solid line represents equation (14).

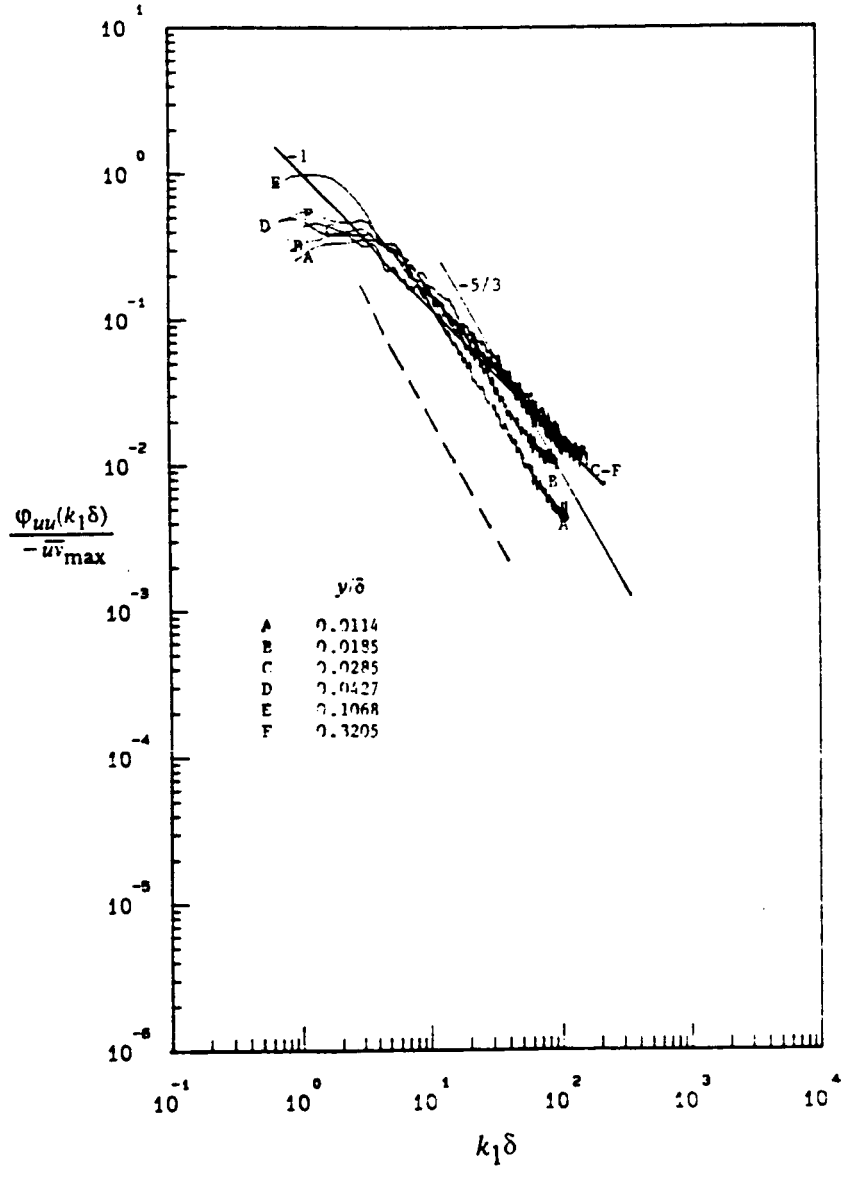

Figure 33 . Normalized u' power spectral distribution at X = 2.21m (between throat and intermittent backflow region) for flow C without roughness element. Solid lines represents equation (14) and (15). Dash line represents equation (15) with K_0 = 0.49.

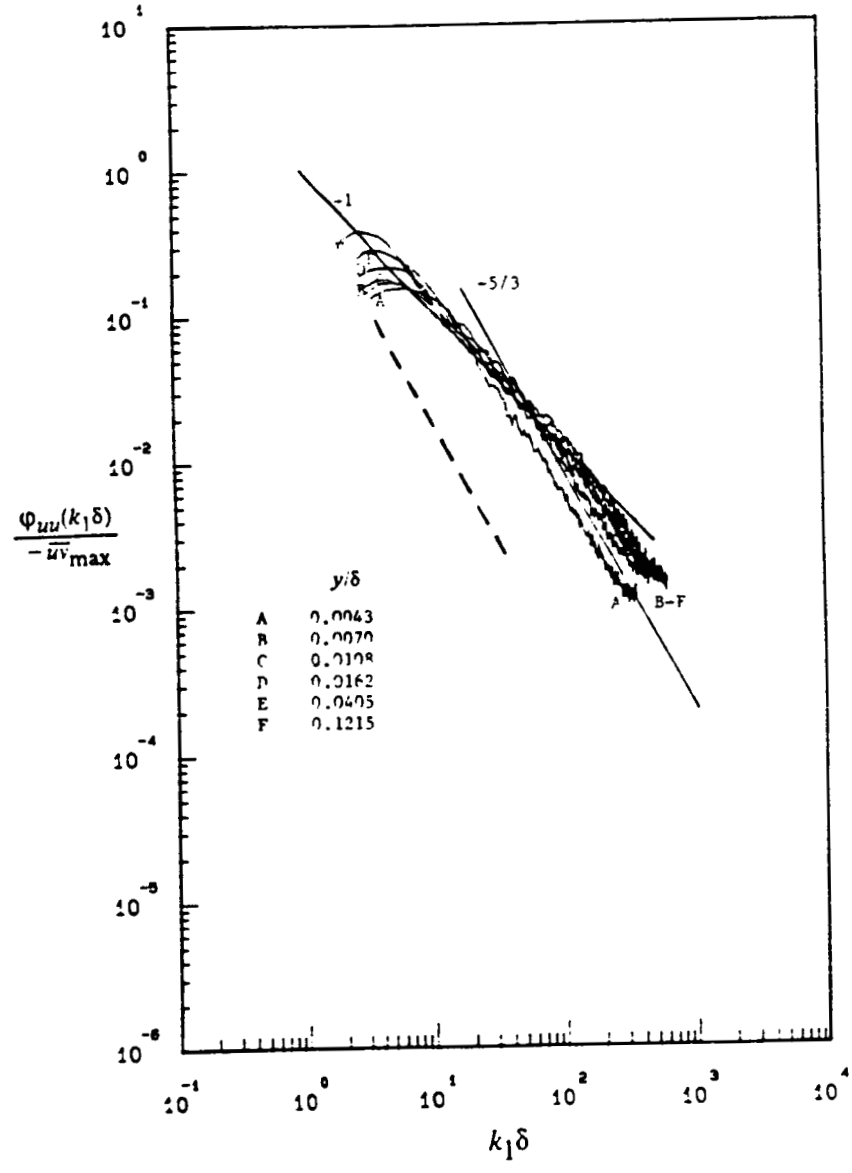

Figure 34 . Normalized u' power spectral distribution at X = 2.21m (between throat and intermittent backflow region) for flow D with roughness element. Solid lines represents equation (14) and (15). Dash line represents equation (15) with K_0 = 0.49.

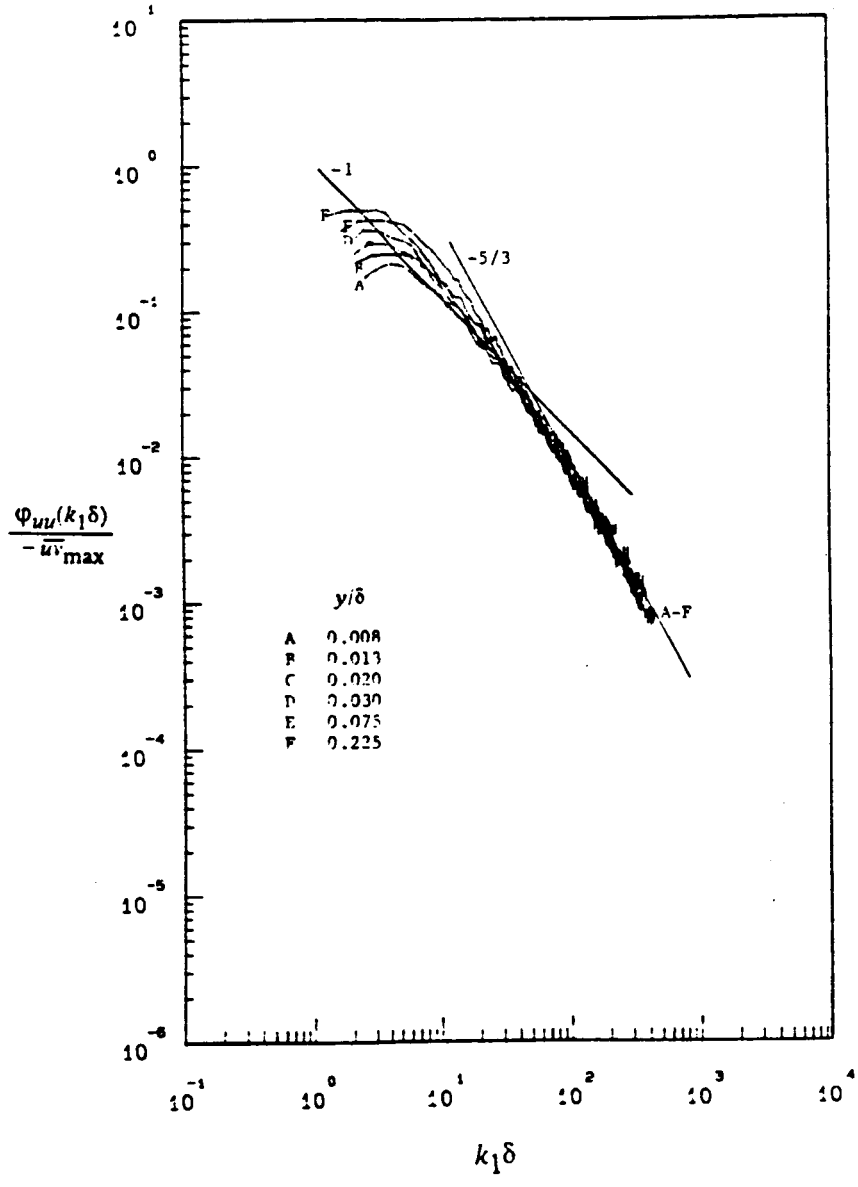

Figure 35. Normalized u' power spectral distribution at X = 2.85m (between throat and intermittent backflow region) for flow C without roughness element. Solid lines represents equation (14) and (15).

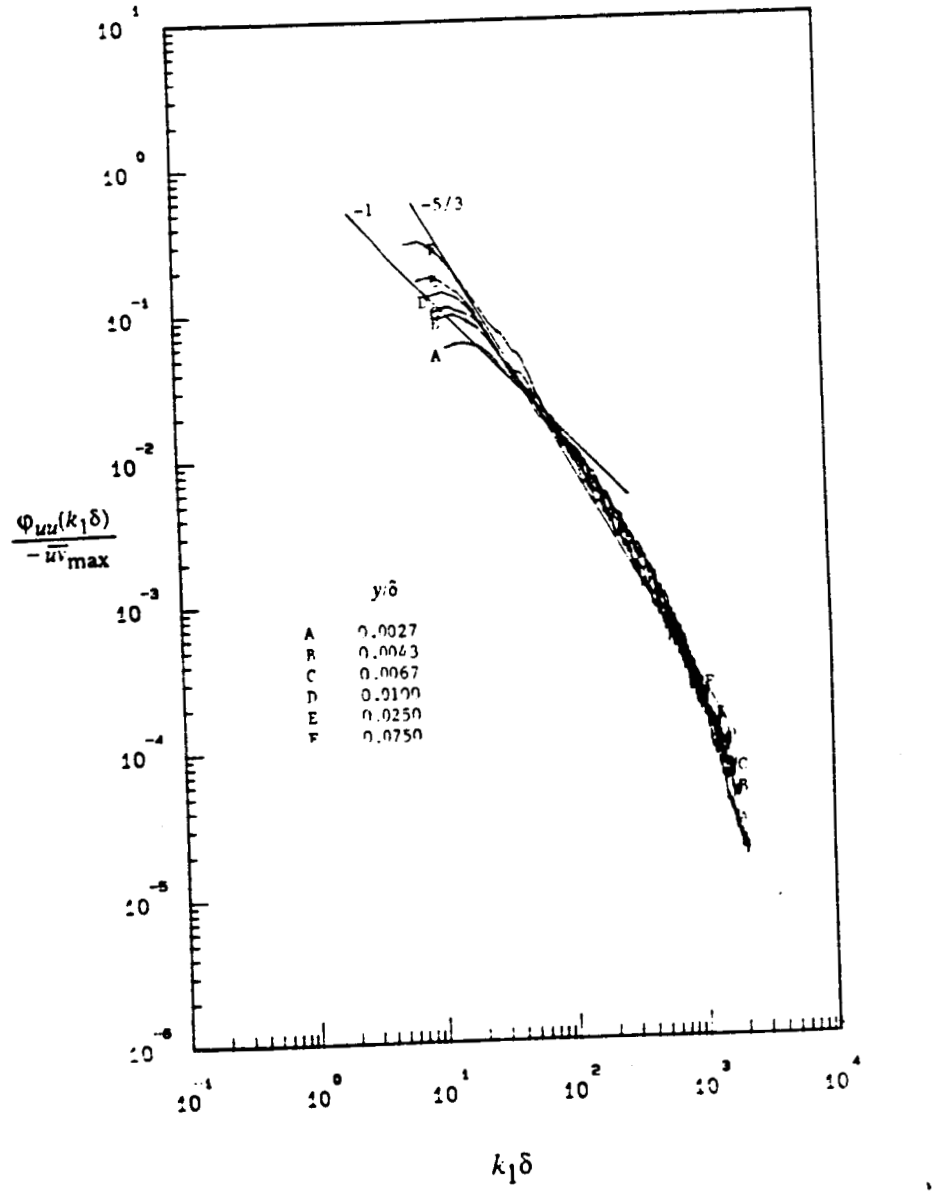

Figure 36 . Normalized u' power spectral distribution at X = 2.85m (between throat and intermittent backflow region) for flow D with roughness element. Solid lines represents equation (14) and (15).

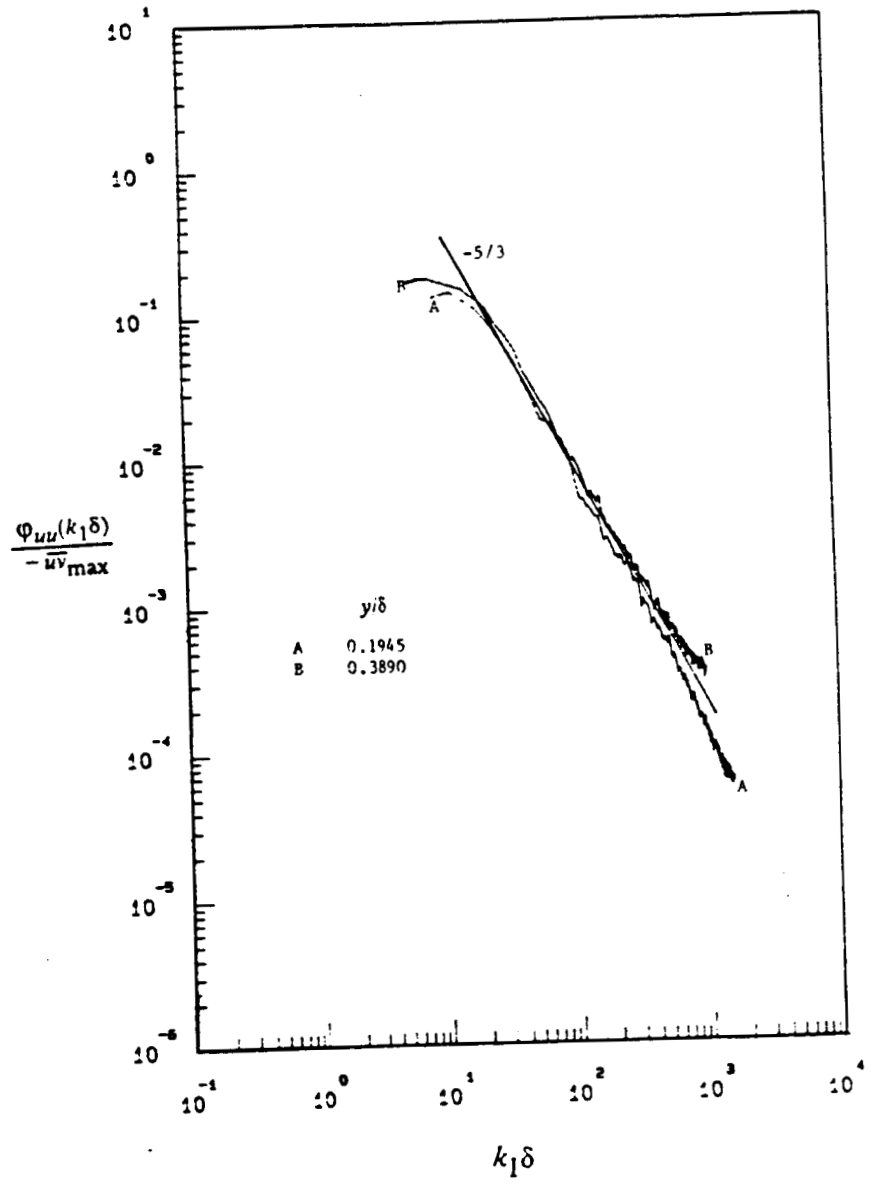

Figure 37. Normalized u' power spectral distribution at X = 3.46m (at the viscinity of intermittent backflow region) for flow C without roughness element. Solid line represents equation (15).

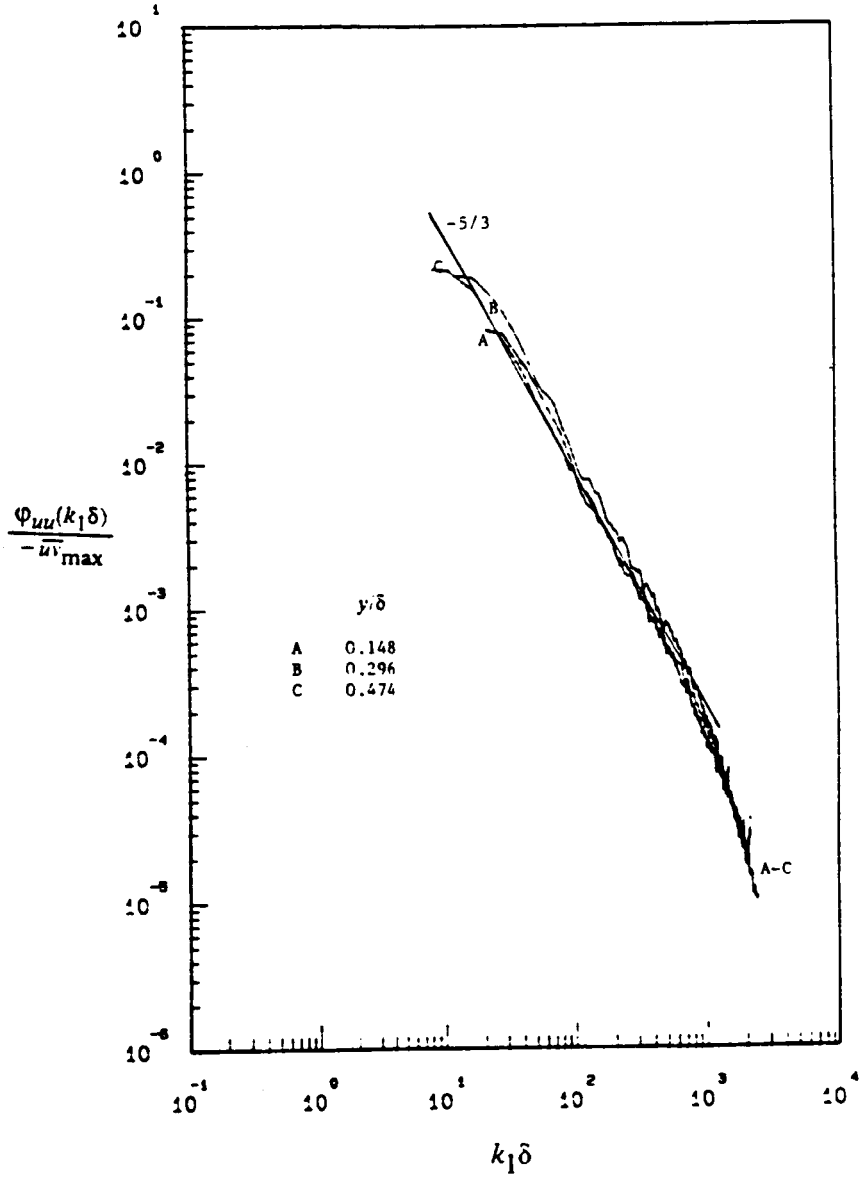

Figure 38 . Normalized u' power spectral distribution at X = 3.46m (at the viscinity of intermittent backflow region) for flow D with roughness element. Solid line represents equation (15).

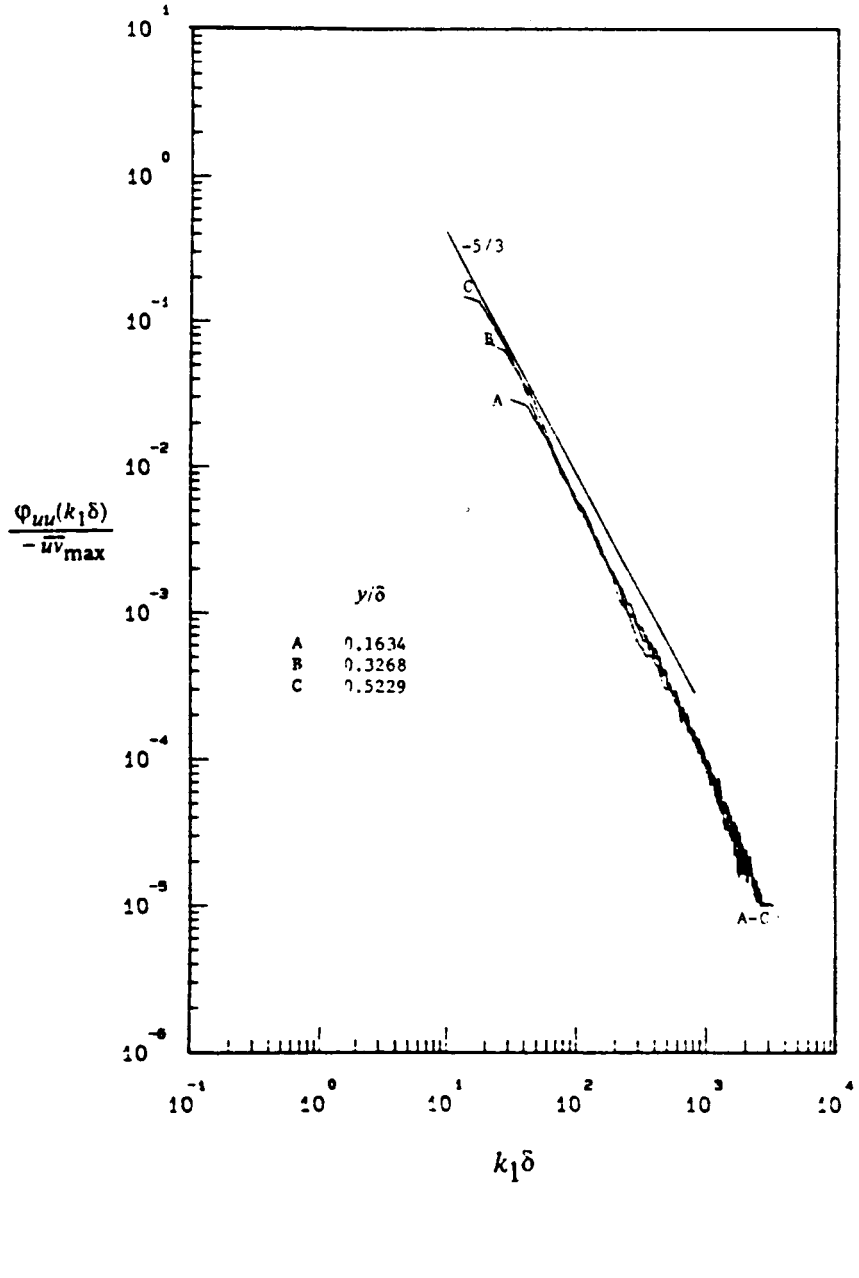

Figure 39. Normalized u' power spectral distribution at X = 5.4m (downstream of reattachment) for flow C without roughness element. Solid line represents equation (15).

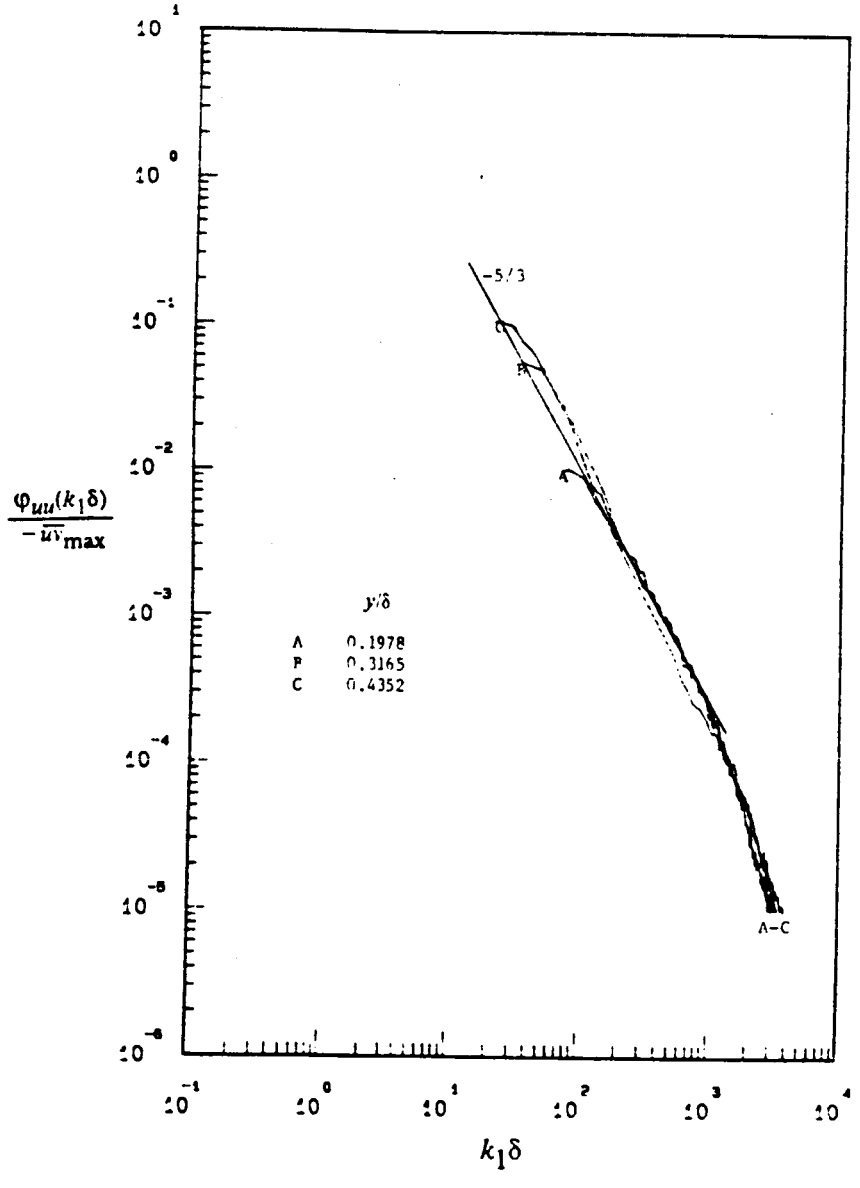

Figure 40. Normalized u' power spectral distribution at X = 3.96m (in the intermittent backflow region) for flow D with roughness element. Solid line represents equation (15).

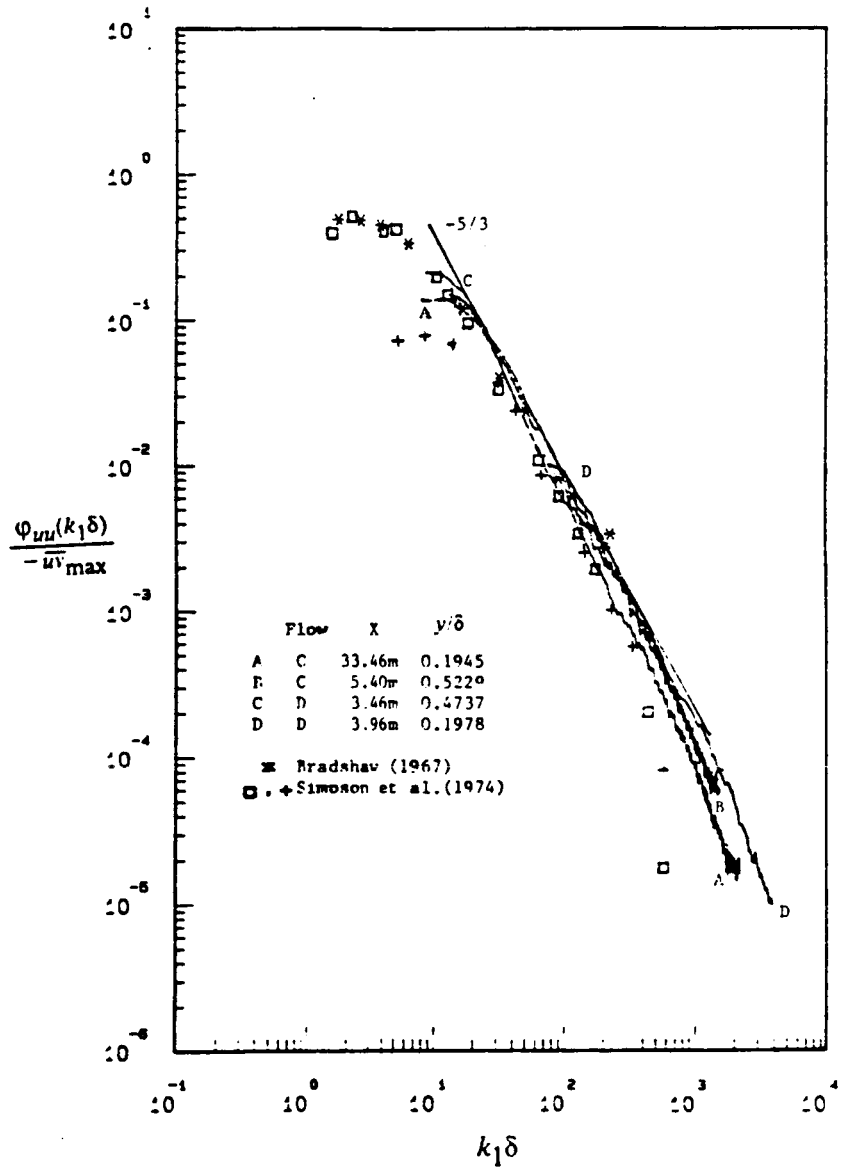

Figure 41 . Comparision of normalized *u'*power spectra distribution with other studies. Solid line represents equation (15).

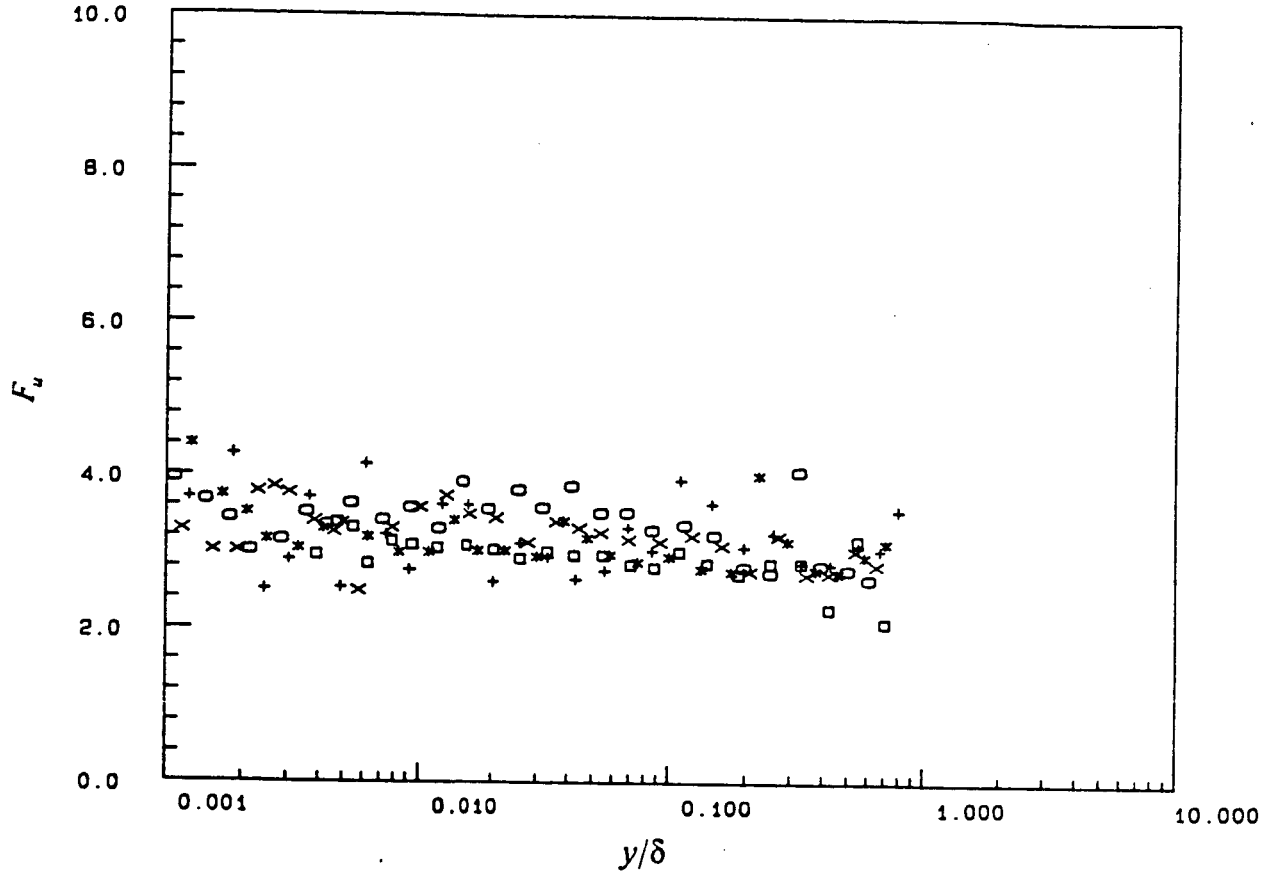

Figure 42 . Flatness factor, F_u for flow C without roughness element. " □ " 3.45m; " + " 3.96m; " ✱ " 4.47m; " ○ " 4.88m; " × " 5.77m.

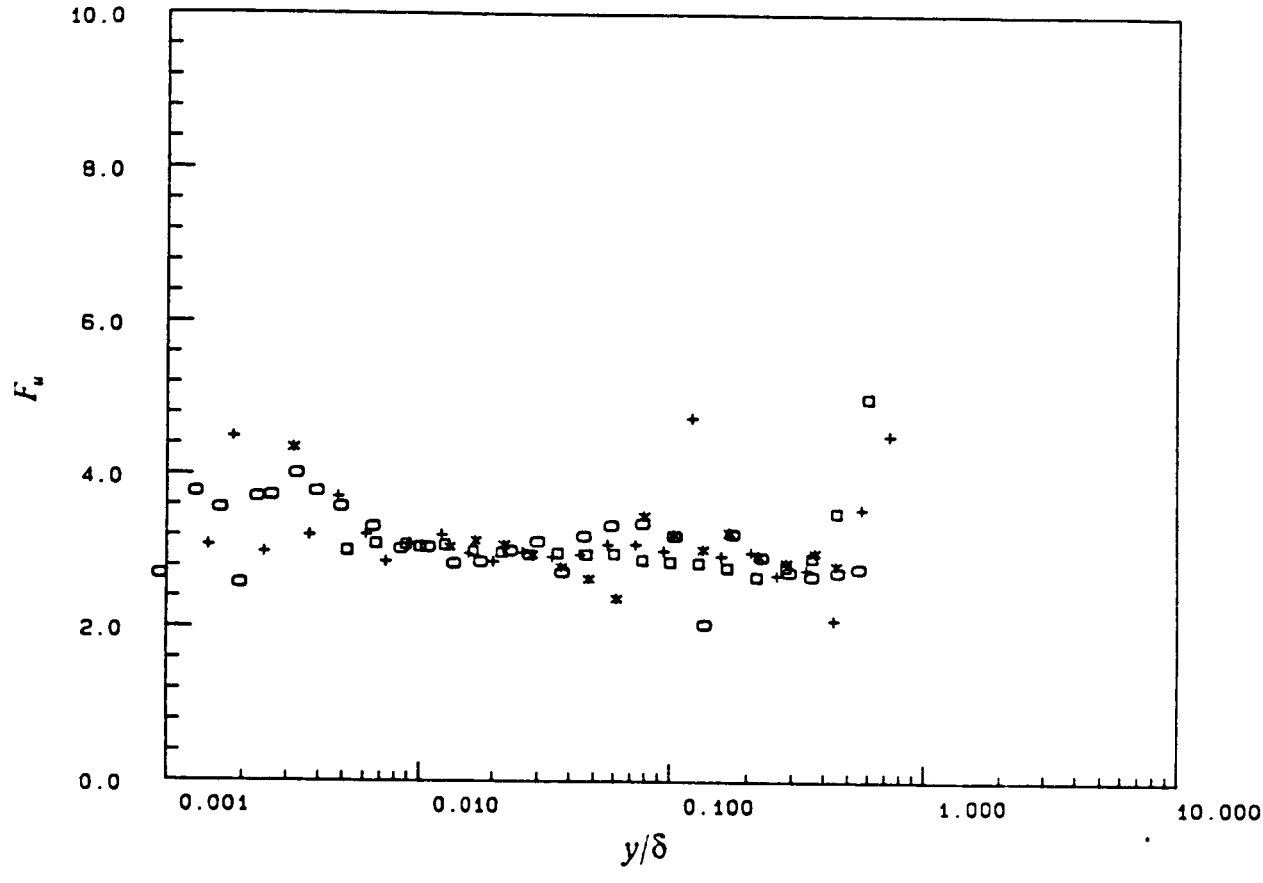

Figure 43 . Flatness factor, F_u for flow D with roughness element. " □ " 3.20m; " + " 3.45m; " ✱ " 3.96m; " O " 4.47m.

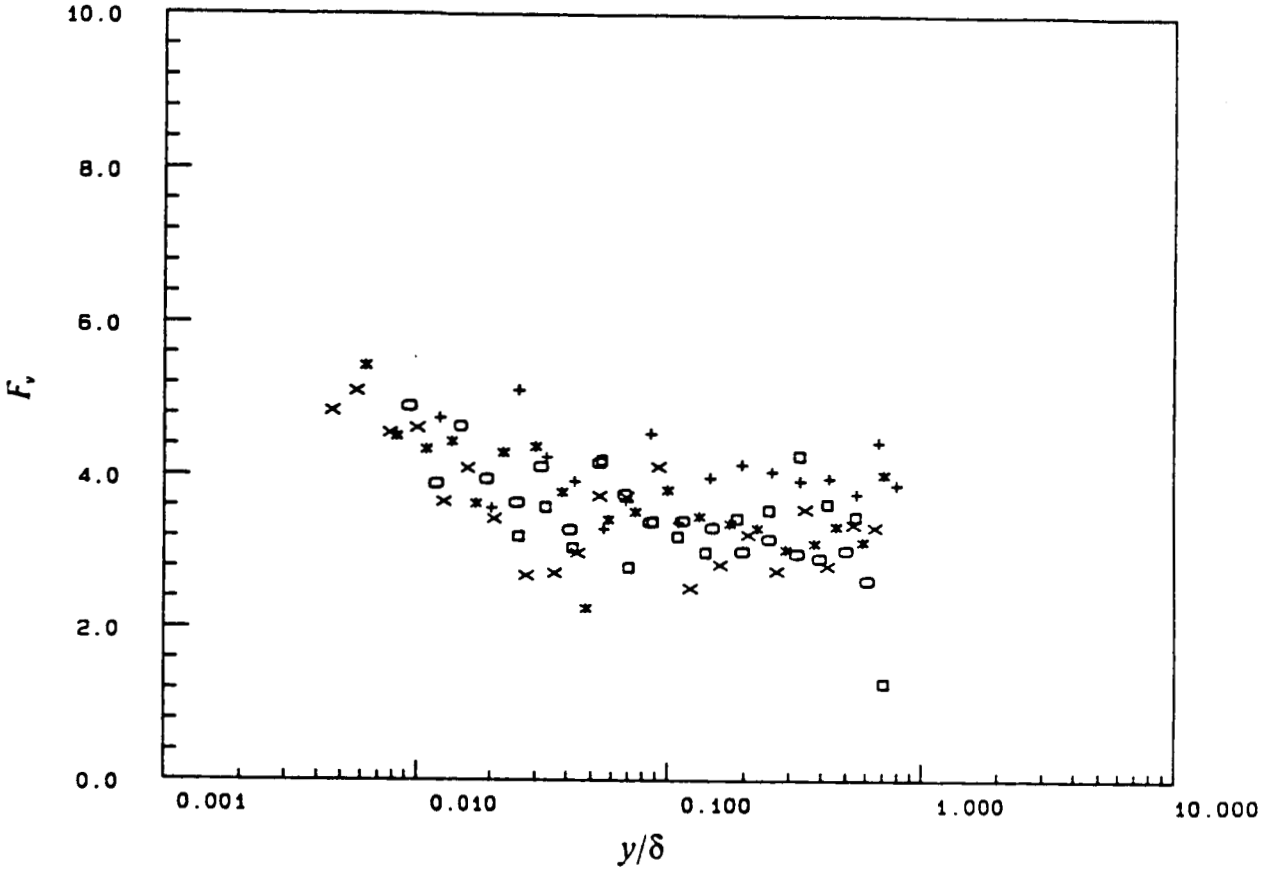

Figure 44 . Flatness factor, F_v for flow C without roughness element. " □ " 3.45m; " + " 3.96m; " ✱ " 4.47m; " O " 4.88m; " × " 5.77m.

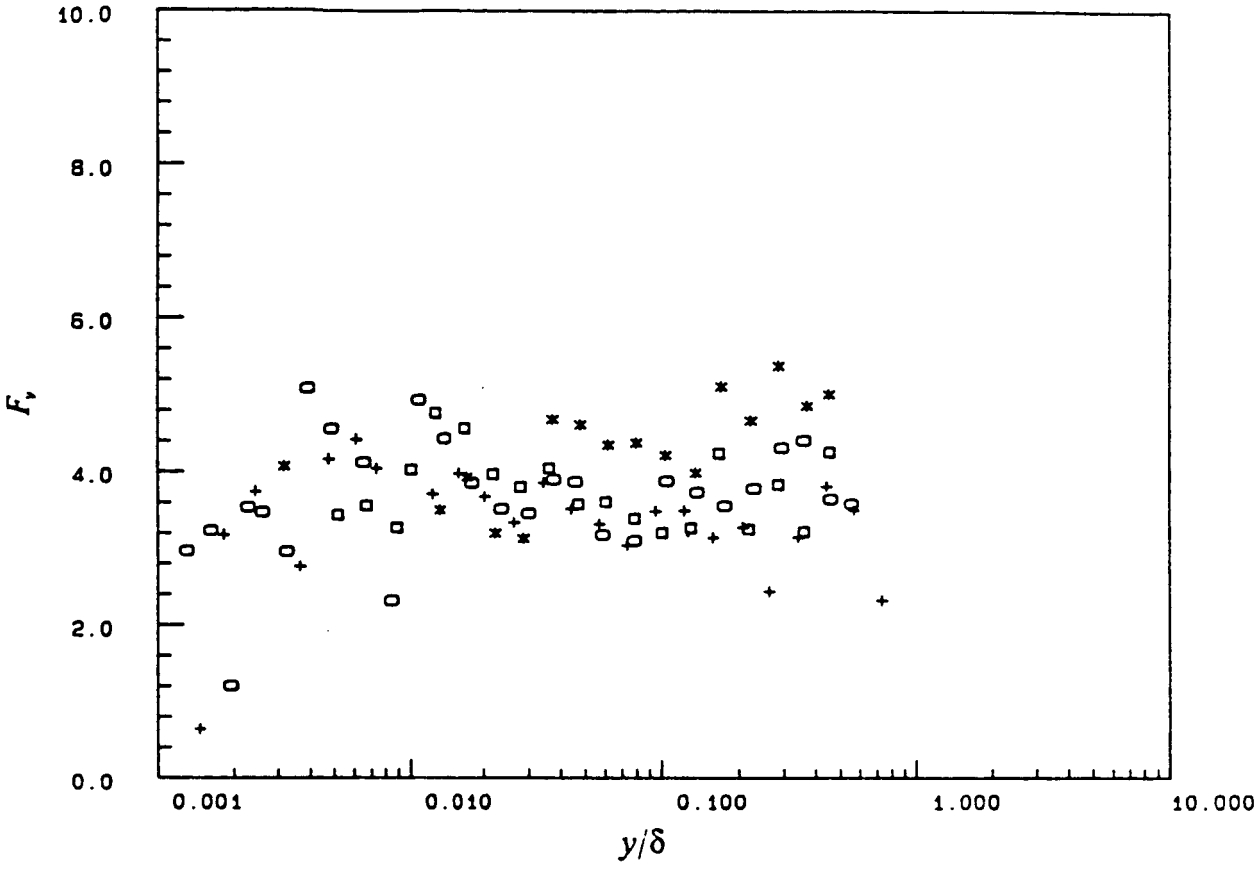

Figure 45 . Flatness factor, F_v for flow D with roughness element. " □ " 3.20m; " + " 3.45m; " ✱ " 3.96m; " O " 4.47m.

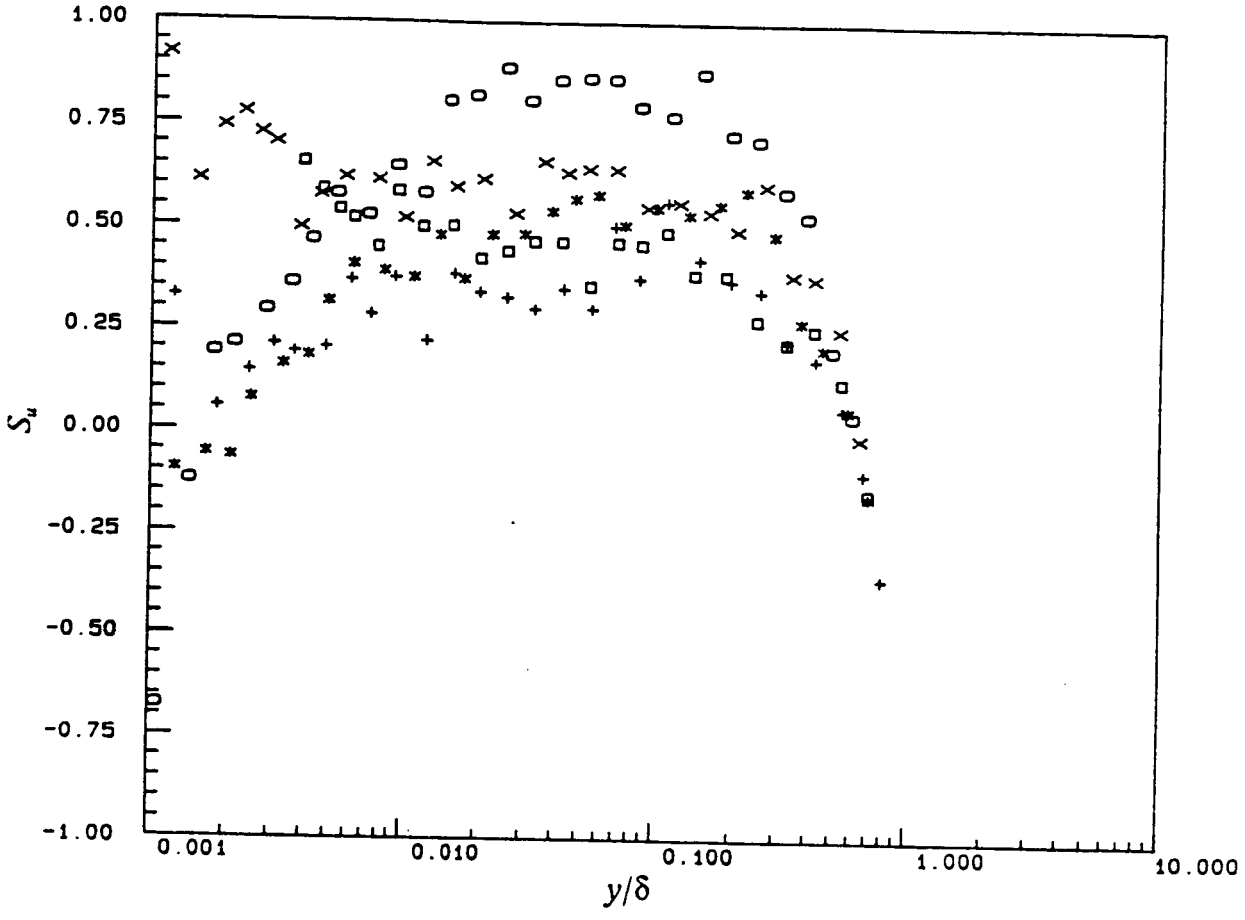

Figure 46 . Skewness factor, S_u for flow C without roughness element downstream of intermittent detachment. " □ " 3.45m; " + " 3.96m; " ✱ " 4.47m; " O " 4.88m; " × " 5.77m.

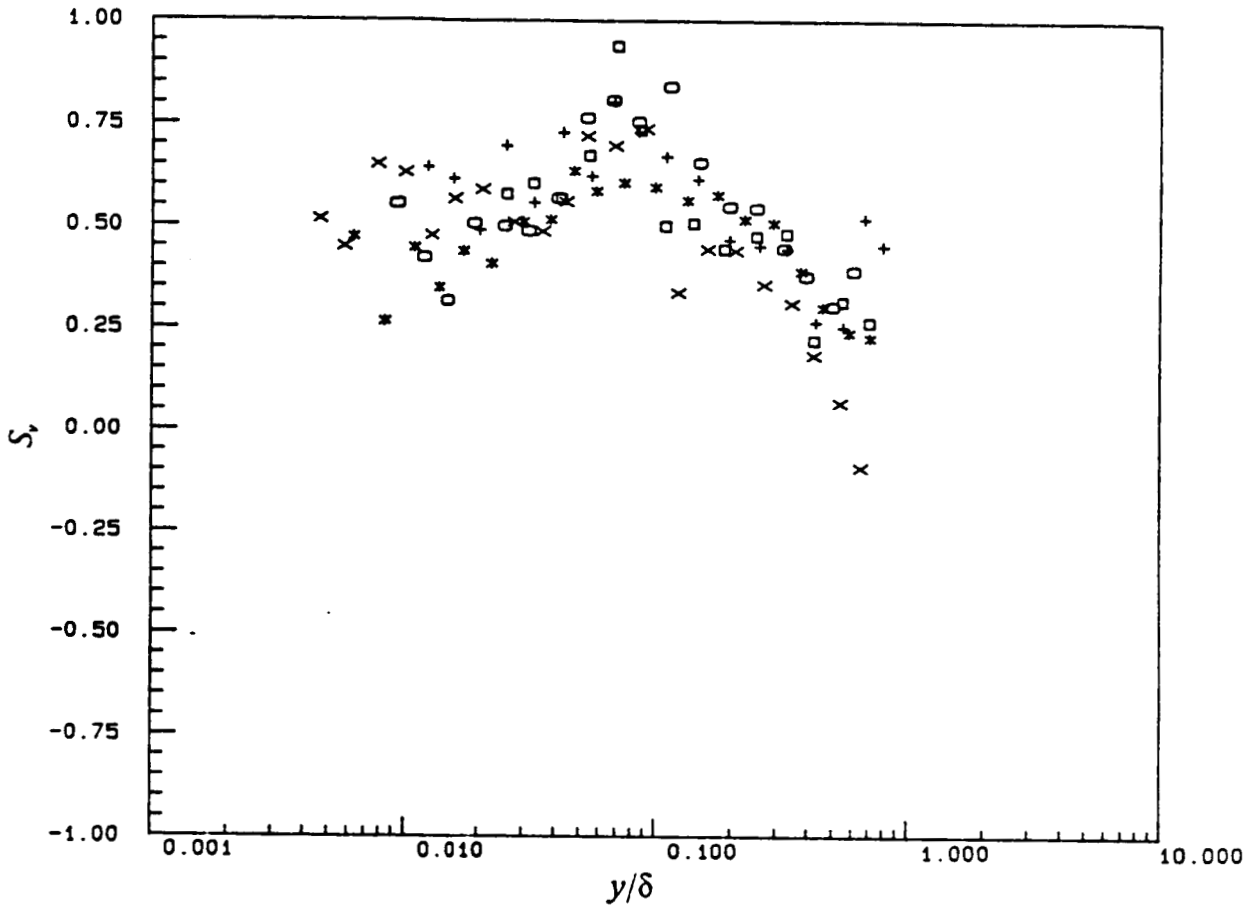

Figure 47 . Skewness factor, S_v for flow C without roughness element downstream of intermittent detachment. " □ " 3.45m; " + " 3.96m; " ✱ " 4.47m; " O" 4.88m; " ✕ " 5.77m.

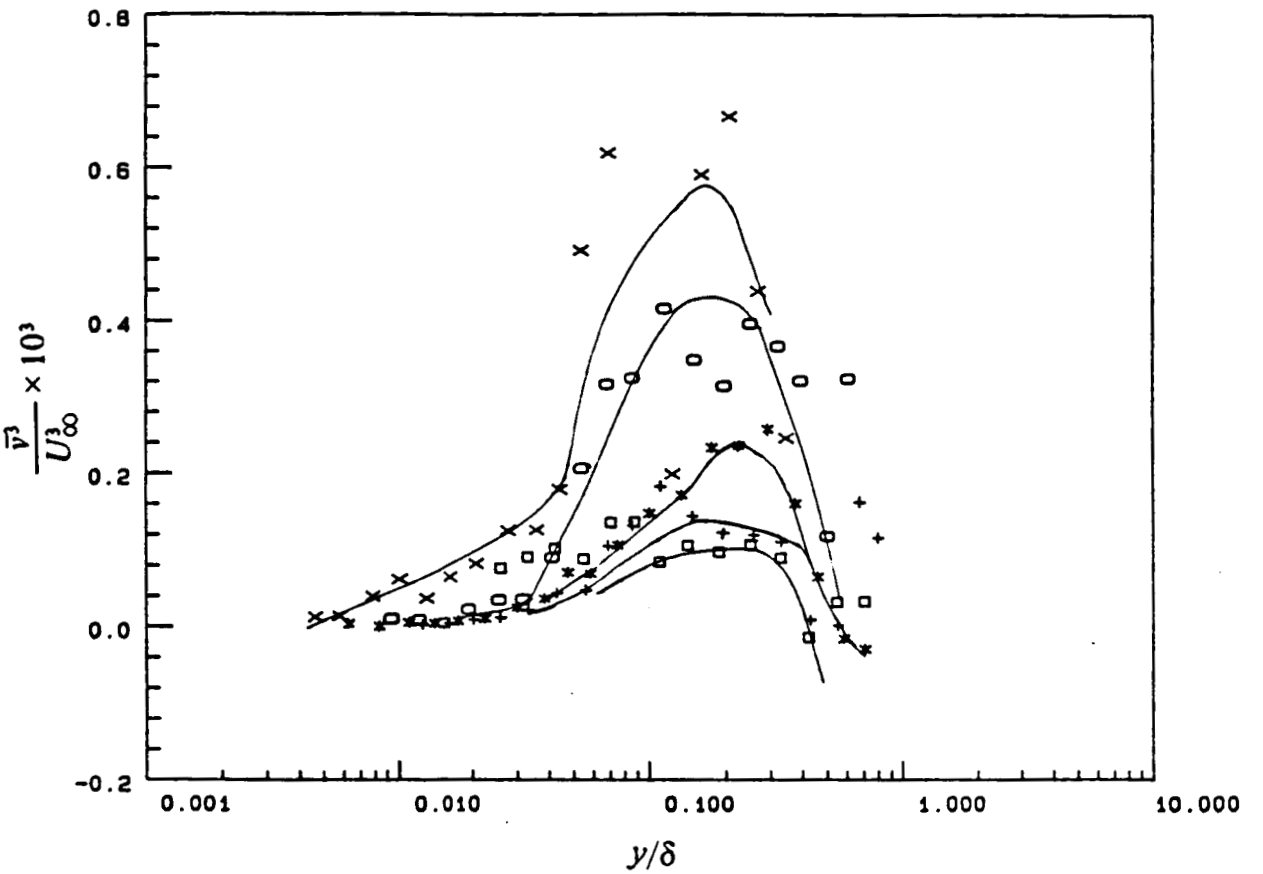

Figure 48 . Higher order fluctuating velocity component $\overline{v^3}/\ U_\infty^3$ vs. y/δ for flow C without roughness element. Solid lines are for visual aid only. " □ " 3.45m; " + " 3.96m; " ✱ " 4.47m; " ○ " 4.88m; " × " 5.77m.

C-2

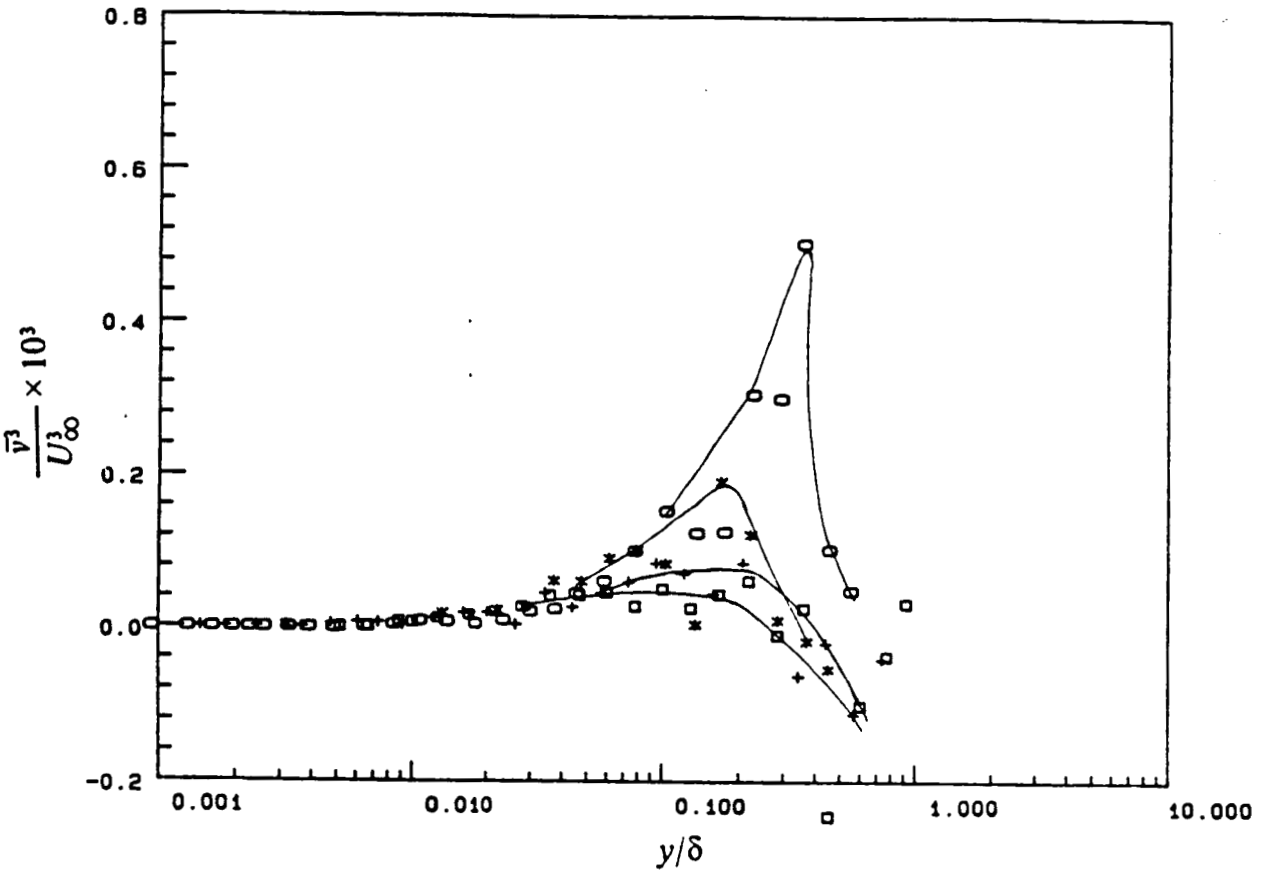

Figure 49 . Higher order fluctuating velocity component $\overline{v^3}/\ U_\infty^3$ vs. y/δ for flow D with roughness element. Solid lines are for visual aid only. " □ " 3.20m; " + " 3.45m; " ✱ " 3.96m; " O " 4.47m.

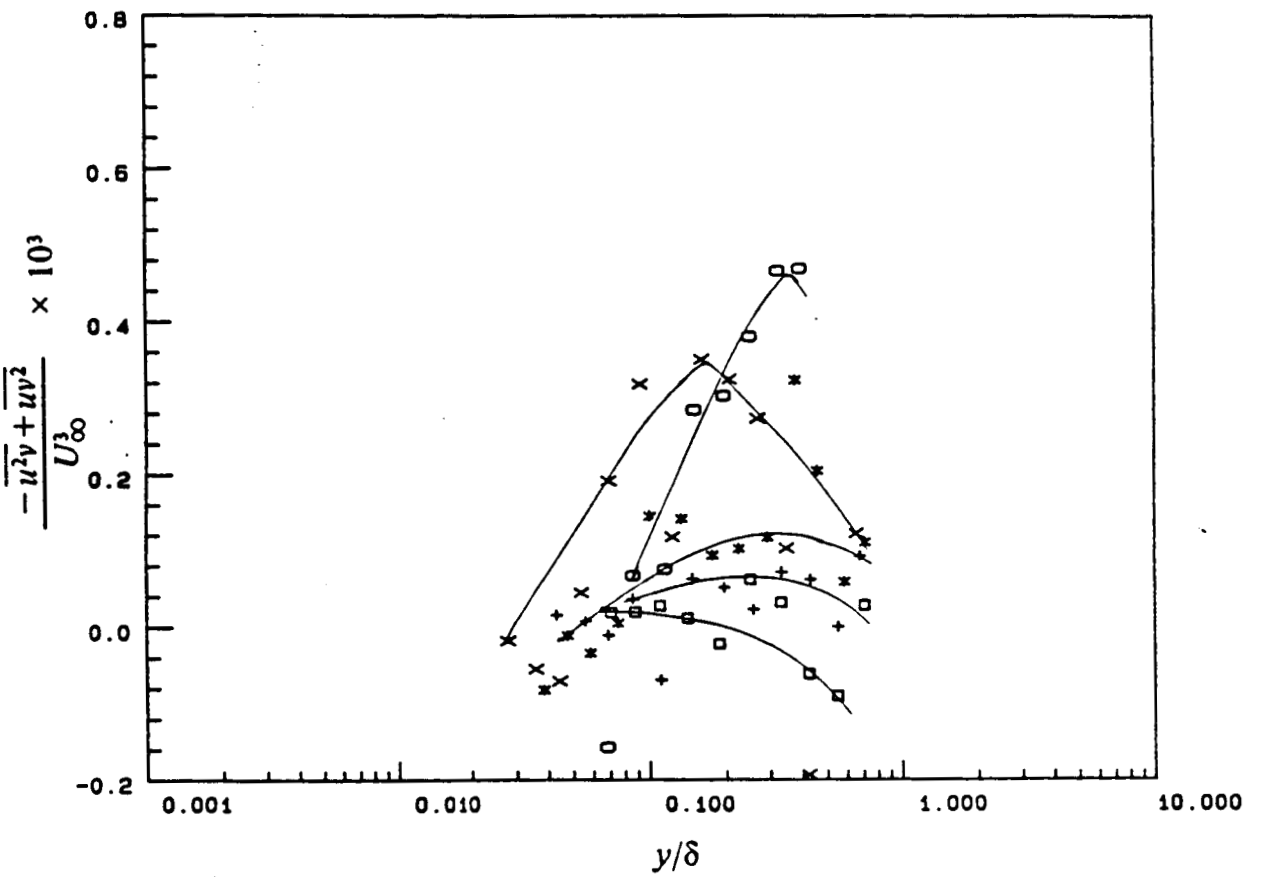

Figure 50 . Triple product $-\overline{u^2v}+\overline{uv^2}$ vs. y/δ for flow C without roughness element. Solid lines are for visual aid only. " □ " 3.45m; " + " 3.96m; " * " 4.47m; " O" 4.88m; " × " 5.77m.

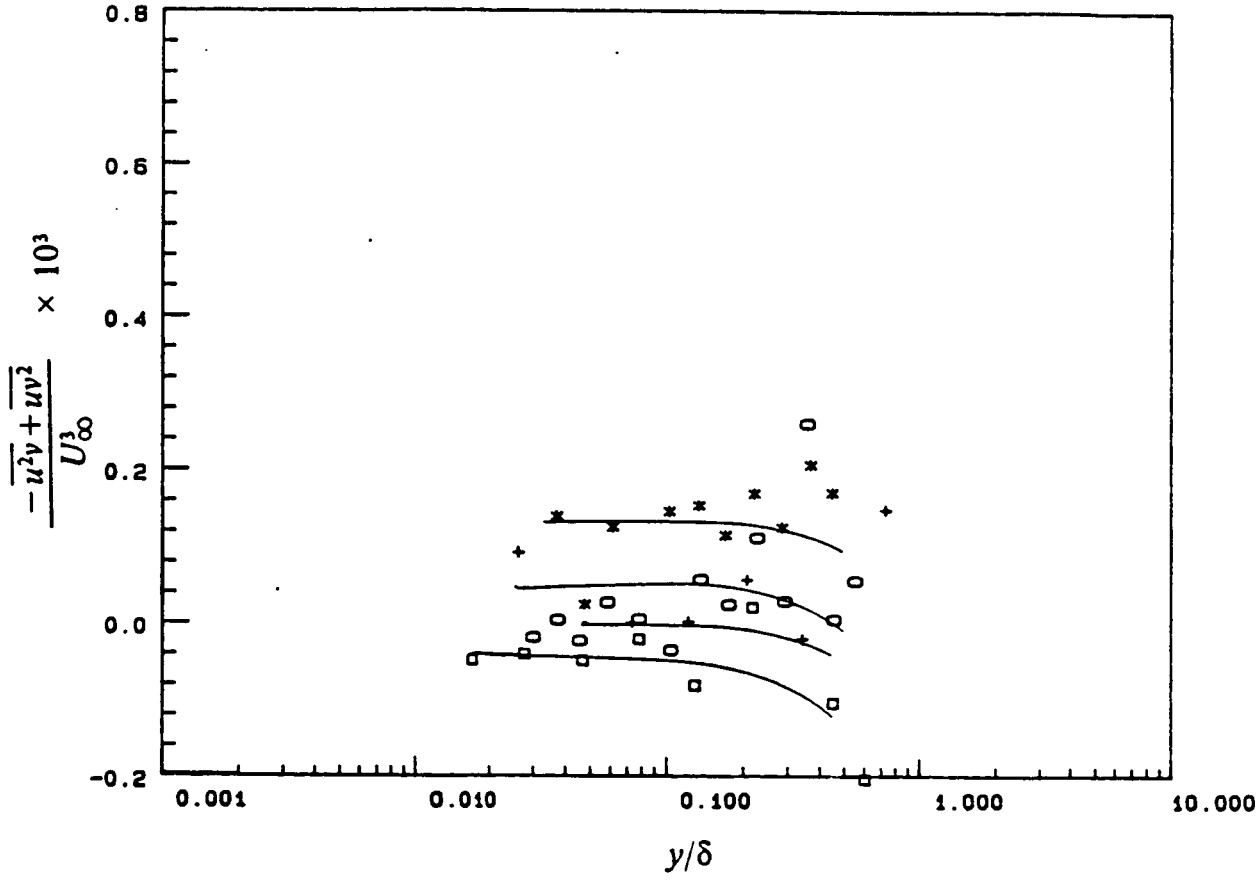

Figure 51 . Triple product $-\overline{u^2v}+\overline{uv^2}$ vs. y/δ for flow D with roughness element. Solid lines are for visual aid only. " □ " 3.20m; " + " 3.45m; " ✱ " 3.96m; " ○ " 4.47m.

APPENDIX I

Laser Anemometer Data X = 136in. or 3.46m Flow C

y (inch)	U (m/s)	γ_{pu}	$\bar{u}^2$ $(m/s)^2$	$\bar{u}^3$ $(m/s)^3$	$\bar{u}^4$ $(m/s)^4$	$\bar{v}^2$ $(m/s)^2$	$\bar{v}^3$ $(m/s)^3$	$\bar{v}^4$ $(m/s)^4$	$\overline{(u-v)}^2$ $(m/s)^2$	$\overline{(u-v)}^3$ $(m/s)^3$	$\overline{(u-v)}^4$ $(m/s)^4$
0.0250	1.9390	0.8970	2.8000	1.8910	23.0900						
0.0300	2.0900	0.9030	2.8490	1.6200	27.3400						
0.0350	2.2980	0.9290	3.0350	1.5220	30.4400						
0.0400	2.2870	0.9360	3.2940	1.5960	30.6900						
0.0500	2.4780	0.9256	3.4060	1.2420	36.2200						
0.0600	2.6100	0.9383	3.3630	2.0580	34.8100						
0.0750	2.8190	0.9409	3.6910	1.7460	41.3800						
0.1000	2.9500	0.9500	3.7050	1.7830	42.2900						
0.1300	3.2260	0.9568	3.8610	1.2940	45.1600						
0.1650	3.3660	0.9710	3.5000	1.2360	35.7100	1.7300	0.7414	9.5800			
0.2100	3.5670	0.9750	3.8850	1.6250	45.3900	1.8460	0.8824	12.2300			
0.2700	3.8630	0.9780	4.2990	1.8900	54.7100	2.1520	0.9920	14.1400			
0.3500	4.0830	0.9795	4.2140	0.9087	52.5900	1.6150	0.8601	10.9700			
0.4500	4.2910	0.9836	4.4790	2.0050	57.0000	1.5500	1.3255	6.7180	3.2820	1.2450	30.2800
0.5600	4.6680	0.9900	4.7010	2.1040	62.0300	1.9690	1.3330	13.2030	3.7520	1.3590	40.3000
0.7000	5.0350	0.9936	4.9040	2.5830	72.5500	2.2280	0.8280	15.9100	4.0240	2.5830	72.5500
0.9000	5.5300	0.9930	5.3850	1.6900	83.1500	2.5360	1.0320	19.2600	4.5000	1.0040	51.6700
1.2000	6.4500	0.9990	5.6320	1.7810	86.4100	2.8970	0.9504	28.9300	4.8490	0.1914	60.1000
1.6000	7.6550	0.9991	6.3100	0.3770	114.3000	2.7740	1.0360	27.3700	5.2900	1.1820	71.6500
2.1000	9.3560	1.0000	6.5470	-0.5351	123.1000	2.4360	0.8762	25.3100	5.7330	-0.4563	82.1700
2.7000	11.4000	1.0000	6.2880	0.0182	89.9600	2.7210	-0.1337	26.9200	6.0980	-1.6390	80.2900
3.5000	14.4000	1.0000	6.0480	-1.8840	116.0500	2.8660	0.3139	28.5100	5.9140	-4.8280	75.6900
4.5000	17.5500	1.0000	6.0230	-5.8730	76.0500	8.0110	0.3206	81.6800	3.1900	-5.3520	53.4500

Laser Anemometer Data X = 156in. or 3.96m Flow C

0.0100	-0.0117	0.3367	0.1771	0.0058	0.1160						
0.0150	-0.1480	0.3594	0.2721	-0.0275	0.3161						
0.0200	-0.1869	0.3760	0.4900	-0.0359	0.5989						
0.0250	-0.1731	0.4150	1.2900	-0.0590	4.8050						
0.0300	-0.2098	0.4190	1.7070	-0.1323	10.7900						
0.0400	-0.2147	0.4413	2.2100	-0.1546	12.3000						
0.0500	-0.1803	0.4260	2.6940	0.5182	30.0100						
0.0600	-0.3113	0.4250	3.4820	0.2153	38.9000						
0.0750	-0.3255	0.4438	3.4290	0.7879	32.2900						
0.1000	-0.2628	0.4533	3.7050	-0.2222	49.5700	0.1299	0.0183	0.0801			
0.1300	-0.3000	0.4390	4.0780	1.0960	60.1700	0.2276	0.0393	0.6105			
0.1650	-0.3533	0.4280	4.3000	0.7892	48.2400	0.4846	0.0802	0.8393			
0.2100	-0.3249	0.4280	4.1700	0.6430	54.1900	0.3754	0.1020	0.7208			
0.2700	-0.3533	0.4250	4.3000	0.4282	54.2400	0.7220	0.1873	2.2090			
0.3500	-0.1815	0.4500	4.6960	0.9974	58.2600	0.8590	0.3786	2.8950	3.1510	1.0340	30.1300
0.4550	-0.0248	0.4600	5.2450	0.5984	75.9500	1.0760	0.4117	3.8250	3.5270	0.3943	32.7300
0.5600	-0.0930	0.4702	4.9870	2.7970	82.8200	1.3980	0.9091	7.1900	3.7050	1.6230	42.0800
0.7000	0.6170	0.4887	5.5330	1.6150	92.6100	1.7870	1.1390	14.5400	4.3680	1.4410	61.4700
0.9000	0.6550	0.5887	6.0070	4.5800	142.8000	2.4240	1.5758	19.9200	0.0000	1.2200	37.4800
1.2000	1.1390	0.6456	6.3710	2.7500	148.1000	2.2780	1.2440	20.6500	5.2370	3.1590	80.8100
1.6000	1.7690	0.7354	7.2400	2.3160	161.4000	2.8860	1.0520	34.5900	6.2500	2.6150	106.7000
2.1000	3.1870	0.8687	8.0330	2.1250	210.4000	2.9830	1.0300	36.1100	6.8880	1.6980	125.6000
2.7000	4.6210	0.9333	8.7920	-0.7377	221.9000	2.9130	0.9570	33.4100	6.9940	0.1975	129.3000
3.5000	6.6080	0.9857	9.0580	-1.9690	234.2000	3.0910	0.0777	37.9700	7.5540	-0.4200	158.0000
4.5000	9.3930	0.9973	9.2490	-5.4520	264.6000	3.1390	0.0116	37.1300	8.1960	-5.4520	152.4000
5.5000	12.1700	0.9991	7.8620	-7.7090	188.2000	3.0150	1.4000	40.4100	7.2320	-6.6890	115.7000
6.5000	14.9100	1.0000	5.7350	-8.3420	117.3000	2.9190	1.0000	33.1200	5.4170	12.3800	147.9000

Laser Anemometer Data X = 176in. or 4.47m Flow C

y (inch)	U (m/s)	γ_{pu}	$\bar{u}^2$ $(m/s)^2$	$\bar{u}^3$ $(m/s)^3$	$\bar{u}^4$ $(m/s)^4$	$\bar{v}^2$ $(m/s)^2$	$\bar{v}^3$ $(m/s)^3$	$\bar{v}^4$ $(m/s)^4$	$\overline{(u-v)}^2$ $(m/s)^2$	$\overline{(u-v)}^3$ $(m/s)^3$	$\overline{(u-v)}^4$ $(m/s)^4$
0.0100	-0.3260	0.1400	0.2520	-0.1772	0.7065						
0.0150	-0.7040	0.1800	0.7780	-0.2378	2.6610						
0.0200	-0.8600	0.1785	1.0760	-0.3425	4.3250						
0.0250	-1.0160	0.1904	1.4790	-0.5660	7.6720						
0.0300	-1.1500	0.1726	1.6350	-0.3597	8.4240						
0.0400	-1.3510	0.1700	2.1430	-0.2817	13.9200						
0.0500	-1.5630	0.1818	2.8640	-0.3272	26.9600						
0.0600	-1.5910	0.1679	3.0530	0.3447	31.4600						
0.0750	-1.7650	0.1638	3.3740	0.9602	36.1800	0.2548	0.0286	0.3526			
0.1000	-1.9160	0.1446	3.6950	0.9974	40.6100	0.3093	0.0026	0.4314			
0.1300	-1.8450	0.1690	3.8430	0.9359	44.0100	0.3473	0.0400	0.5235			
0.1650	-1.9600	0.1554	3.8280	1.6990	49.9400	0.4723	0.0318	0.9899			
0.2100	-1.9510	0.1620	3.8060	0.8971	43.7100	0.4533	0.0574	0.7466			
0.2700	-1.9960	0.1600	3.8890	1.7540	45.6400	0.6417	0.0806	1.7700			
0.3600	-1.9050	0.1672	3.9470	1.8090	45.8800	0.8010	0.1863	2.8090			
0.4600	-1.8630	0.1780	4.2950	2.5550	63.0000	1.0240	0.2737	3.9690	2.6860	1.3450	23.2600
0.5700	-2.0260	0.1772	4.0330	2.5760	51.8800	1.2500	0.5338	3.5240	2.7290	1.9230	27.5200
0.7000	-1.8580	0.1831	4.2670	2.8970	54.0800	1.3520	0.5237	6.2700	2.7860	1.9880	24.8200
0.9000	-1.6840	0.2143	4.6760	2.5830	62.9700	1.7300	0.8056	10.5800	3.0940	1.8430	29.2000
1.2000	-1.5540	0.2386	4.9090	3.2390	71.1700	2.1970	1.1190	18.4400	3.7650	3.7920	45.4100
1.6000	-1.1980	0.3050	5.8270	3.9610	94.8800	2.5870	1.2970	23.2400	4.7610	4.2970	68.0100
2.1150	-0.4914	0.3993	6.7910	5.4140	127.4000	3.0880	1.7610	32.2400	5.7590	4.7410	90.5800
2.7000	0.0676	0.4960	7.8000	7.3800	244.7000	3.5560	1.7820	41.9700	6.8050	6.7850	130.6000
3.5000	1.0290	0.6104	9.2700	6.5560	271.7000	3.8560	1.9420	45.1400	8.0440	5.9710	179.9000
4.5000	2.9930	0.8074	10.4800	0.6880	305.5000	4.2270	1.2110	55.7100	9.2270	3.1610	244.0000
5.5000	5.0810	0.9280	11.1700	-1.6440	342.3000	4.5500	0.4932	69.2500	9.8200	0.2060	261.4000
7.0000	8.1660	0.9886	11.6100	-7.6920	399.2000	4.7840	-0.1155	71.8100	9.7970	-6.8900	264.1000
8.5000	11.5400	0.9989	10.6000	-13.9900	352.9000	4.5390	-0.2204	82.9700	8.2630	-12.4900	219.9000

Laser Anemometer Data X = 196in. or 4.88m Flow C

0.0150	-0.4657	0.2940	0.4860	-0.3135	0.9342						
0.0200	-1.0470	0.1360	1.0850	-0.4212	4.3190						
0.0250	-1.2390	0.1370	1.3480	-0.0921	6.2420						
0.0300	-1.4320	0.1369	1.6500	-0.0815	8.1850						
0.0400	-1.7830	0.1180	2.3180	0.1522	16.9100						
0.0500	-1.8770	0.1060	2.5270	0.4391	22.3800						
0.0600	-1.9330	0.1240	2.6450	0.9241	23.3700						
0.0750	-2.0360	0.1160	3.0070	1.7050	32.7500						
0.1000	-2.1230	0.1080	3.0880	1.4950	32.4600						
0.1300	-2.1760	0.1070	3.1500	2.2130	35.4100	0.3436	0.0611	0.5789			
0.1660	-2.2980	0.1097	3.3220	1.9940	36.3700	0.4490	0.0515	0.7835			
0.2100	-2.3040	0.0980	3.0900	3.0230	37.4100	0.5645	0.0279	1.4787			
0.2700	-2.1970	0.1284	3.7220	4.0950	49.4200	0.6560	0.1354	1.7020			
0.3550	-2.2530	0.1200	3.8280	4.7750	55.9500	0.8880	0.2082	2.8750			
0.4400	-2.2460	0.1177	3.8690	4.2480	53.6600	0.9400	0.2158	3.6390			
0.5750	-2.1120	0.1600	4.0190	4.9060	62.5400	1.4290	0.5407	6.7240			
0.7500	-1.6970	0.1501	4.1210	5.1410	59.8200	1.8030	1.2380	13.5600			
0.9500	-1.9860	0.1514	4.2990	5.4570	65.1800	2.2720	1.8980	19.4300	2.2270	0.7400	13.1700
1.2000	-1.8680	0.1700	4.3230	4.9000	61.7100	2.4650	1.9450	20.6500	2.4030	1.7300	20.2400
1.6000	-1.6680	0.1970	4.6110	5.1660	71.6700	2.6120	2.4870	23.3000	2.5560	1.2980	22.1100
2.1000	-1.1560	0.2700	5.9760	9.1780	115.6000	2.9910	2.0870	29.7500	2.8810	1.9890	28.0400
2.7500	-0.5450	0.3730	7.2840	9.3780	149.6000	3.4300	1.8830	35.4300	3.5330	2.0650	37.9900
3.5000	0.4410	0.4963	8.8250	12.1400	213.8000	4.0370	2.3720	51.7500	4.0880	2.9570	50.1700
4.5000	1.9240	0.6790	11.1700	12.5800	508.0000	5.0220	2.1960	75.1900	4.9680	2.0400	66.9100
5.5000	3.5020	0.8260	12.0800	11.6200	414.6000	6.1270	1.9230	109.6000	5.5930	1.3030	88.3200
7.0000	5.6690	0.9351	13.5200	-2.4410	509.3000	5.6020	0.7081	94.9100	6.3020	1.7130	110.9000
8.5000	8.8290	0.9844	14.4900	-11.5300	558.7000	5.7640	1.9380	87.2200	7.3280	-1.9780	121.0000

Laser Anemometer Data X = 227in. or 5.77m Flow C

y (inch)	U (m/s)	γ_{pu}	$\bar{u}^2$ $(m/s)^2$	$\bar{u}^3$ $(m/s)^3$	$\bar{u}^4$ $(m/s)^4$	$\bar{v}^2$ $(m/s)^2$	$\bar{v}^3$ $(m/s)^3$	$\bar{v}^4$ $(m/s)^4$	$\overline{(u-v)}^2$ $(m/s)^2$	$\overline{(u-v)}^3$ $(m/s)^3$	$\overline{(u-v)}^4$ $(m/s)^4$
0.0150	1.0560	0.8855	0.9639	0.6316	3.0520						
0.0200	1.3890	0.8844	1.4980	0.6628	6.7560						
0.0250	1.4600	0.9048	1.4440	0.8524	6.2700						
0.0300	1.6280	0.8978	2.1350	1.6370	17.2300						
0.0350	1.7720	0.8920	2.5080	1.8860	24.1600						
0.0400	1.8590	0.8900	2.6850	1.9910	27.0900						
0.0500	2.0570	0.9197	2.6070	1.0260	23.0300						
0.0600	2.3370	0.9275	2.9450	1.6390	28.1600	0.2664	0.0365	0.3436			
0.0750	2.3360	0.9290	3.0680	1.9750	23.3500	0.3507	0.0411	0.6274			
0.1020	2.5700	0.9390	3.3490	2.2190	37.0100	0.4396	0.1162	0.8798			
0.1300	2.5900	0.9331	3.2480	1.5690	37.6700	0.6120	0.1812	1.7300			
0.1660	2.7760	0.9450	3.5610	2.7250	47.2700	0.6100	0.1077	1.3580			
0.2100	2.7460	0.9448	3.2140	1.9850	36.1600	0.7160	0.1904	2.0990			
0.2700	2.9520	0.9610	3.3280	2.2100	38.1900	0.8010	0.2414	2.2050			
0.3600	3.0770	0.9611	3.3840	1.7430	35.8300	1.2640	0.3679	4.2890	2.4230	1.2210	18.9800
0.4650	3.0750	0.9660	3.2650	2.4100	36.3000	1.3510	0.3698	4.9600	2.7270	1.5590	23.6300
0.5750	3.1510	0.9630	3.5660	2.5720	42.2300	1.4300	0.5255	6.1050	2.9050	1.4260	25.6700
0.7000	3.2520	0.9670	3.7240	2.8160	45.2500	2.1170	1.4380	16.7700	3.2100	1.7800	29.8400
0.9000	3.3660	0.9780	3.4440	2.4950	37.6300	2.5520	1.8080	24.2700	3.4820	2.3760	39.3900
1.2000	3.4420	0.9750	3.7560	2.1700	44.4000	3.1970	2.7720	42.1400	4.0430	2.1880	48.0500
1.6000	3.7620	0.9730	4.2760	2.7370	59.0300	3.6120	0.5847	32.8900	4.6680	3.1990	62.4400
2.1000	3.9990	0.9798	4.4520	2.6900	61.4600	4.3210	1.7260	52.9200	5.6710	4.0330	97.4400
2.7000	4.2700	0.9790	5.2210	2.9010	75.3300	4.7340	1.9480	72.5100	6.6520	3.7980	119.8000
3.5000	4.6970	0.9789	6.5500	5.8930	138.4000	5.2890	1.2830	76.9800	8.0960	7.0100	181.4000
4.5000	5.5990	0.9860	7.3210	2.6530	145.9000	5.2580	0.7216	98.6400	8.7150	2.8490	194.3000
5.5000	6.6240	0.9940	8.0050	2.8590	175.2000	5.6950	-0.9032	91.4300	9.6450	2.0640	239.9000
7.0000	8.6730	0.9985	8.8090	0.0111	235.7000	5.5860	-2.4190	105.1000	10.0300	-5.5070	273.2000
8.5000	10.5800	0.9998	8.0960	-6.0600	186.6000	5.0680	-3.8980	85.4700	9.0750	-1.0780	250.7000

Laser Anemometer Data X = 126in. or 3.20m Flow D

y (inch)	U (m/s)	$\bar{u}^2$ $(m/s)^2$	$\bar{u}^3$ $(m/s)^3$	$\bar{u}^4$ $(m/s)^4$	$\bar{v}^2$ $(m/s)^2$	$\bar{v}^3$ $(m/s)^3$	$\bar{v}^4$ $(m/s)^4$	$-\overline{uv}$ $(m/s)^2$	$\overline{(u-v)^3}$ $(m/s)^3$	$\overline{(u-v)^4}$ $(m/s)^4$
0.0310	2.7780	1.7291	0.7821	9.0000	0.0398	0.0021	0.0054			
0.0400	3.0740	1.9430	1.0610	11.7000	0.0755	0.0044	0.0202			
0.0530	3.2300	2.0090	1.0420	12.4700	0.1916	0.0244	0.1200			
0.0600	3.3820	2.0030	0.9017	12.2800	0.2373	0.0208	0.2266			
0.0750	3.5120	2.0980	0.9076	13.5700	0.2905	0.0364	0.4018			
0.1000	3.7960	2.1980	0.8325	14.5300	0.3590	0.0478	0.5881	0.2430	0.3631	6.8400
0.1000	3.7960	2.1980	0.8325	14.5300	0.3590	0.0478	0.5881			
0.1300	3.8760	2.3760	1.1100	16.9200	0.4179	0.0627	0.6929			
0.1660	4.0420	2.3200	0.9921	15.9700	0.4885	0.0808	0.9079	0.2580	0.5607	8.8450
0.1660	4.0420	2.3200	0.9921	15.9700	0.4885	0.0808	0.9079			
0.2150	4.2820	2.5210	1.1500	18.9700	0.5815	0.1228	1.3690			
0.2800	4.4680	2.6800	1.1260	21.3200	0.6616	0.1230	1.5690	0.4040	0.5776	13.1800
0.2800	4.4680	2.6800	1.1260	21.3200	0.6616	0.1230	1.5690			
0.3600	4.7600	2.7940	1.2710	23.2400	0.7604	0.1342	2.0890			
0.4670	5.1780	3.0900	1.1830	27.6400	0.8645	0.0819	2.5360	0.4990	0.9204	17.7000
0.4670	5.1780	3.0900	1.1830	27.6400	0.8645	0.0819	2.5360			
0.6000	5.5620	3.2890	1.2510	31.0700	0.9855	0.1483	3.1150			
0.7750	6.0740	3.4960	1.2660	34.9200	1.0460	0.0765	3.5780	0.5200	0.4883	21.6000
0.7750	6.0740	3.4960	1.2660	34.9200	1.0460	0.0765	3.5780			
1.0000	6.7730	3.5940	0.5521	36.1400	1.0110	0.1283	4.3300			
1.3050	7.7250	3.9050	-0.1176	40.8500	1.1680	0.1806	4.4380	0.6230	-0.1176	40.8500
1.3050	7.7250	3.9050	-0.1176	40.8500	1.1680	0.1806	4.4380			
1.7000	8.9060	3.7830	-1.1240	40.2600	1.1230	-0.0253	4.8380			
2.1500	10.2300	3.5090	-2.0910	36.0900	1.1910	0.0759	4.5730	0.4190	-4.8490	84.1600
2.1500	10.2300	3.5090	-2.0910	36.0900	1.1910	0.0759	4.5730			
2.7000	11.0100	2.9340	-1.7560	30.2700	0.9032	-0.7012	3.4740	0.4660	-1.9550	21.5700
2.7000	11.0100	2.9340	-1.7560	30.2700	0.9032	-0.7012	3.4740			
3.6000	12.6600	1.7130	-0.5285	14.7000	0.5754	-0.2899	4.8500	0.2770	-1.9890	22.3200
3.6000	12.6600	1.7130	-0.5285	14.7000	0.5754	-0.2899	4.8500			
4.6000	13.5600	1.6660	2.9610	78.2500	0.6361	-0.1048	11.1300	0.2080	-0.8475	13.1600
4.6000	13.5600	1.6660	2.9610	78.2500	0.6361	-0.1048	11.1300			
5.5000	13.9200	1.5260	1.9680	65.8000	0.2174	0.0945	11.3500	0.0340	-0.4054	11.0200

Laser Anemometer Data X = 136in. or 3.46m Flow D

0.0120	0.8750	0.9100	0.2953	2.5410	0.0189	0.0005	0.0002			
0.0150	0.7730	0.7710	0.2526	2.6680	0.0229	0.0005	0.0017			
0.0200	0.7700	0.9430	0.2852	2.6540	0.0343	0.0018	0.0044			
0.0300	0.8520	1.2320	0.1872	4.8720	0.0510	0.0001	0.0072			
0.0390	1.2530	1.4960	0.5519	8.3100	0.0856	0.0121	0.0305			
0.0500	1.2670	1.7030	0.4949	9.3340	0.1160	0.0178	0.0594			
0.0600	1.3420	1.8700	0.2364	10.0100	0.1470	0.0162	0.0871			
0.0750	1.3540	1.9190	0.5906	11.4400	0.1630	0.0074	0.9912			
0.1000	1.4690	2.0930	0.3411	14.0900	0.2166	0.0317	0.1739			
0.1300	1.5970	2.0810	0.3710	12.8700	0.2580	0.0493	0.2648			
0.1650	1.6080	2.1180	-0.0428	12.8900	0.3110	0.0509	0.3558			
0.2150	1.8240	2.1380	-0.0597	13.7000	0.3640	0.0109	0.4425	0.2680	0.5319	15.8200
0.2150	1.8240	2.1380	-0.0597	13.7000	0.3640	0.0109	0.4425			
0.2800	1.9380	2.2100	0.3375	14.3300	0.5170	0.1159	1.0320			
0.3600	1.9390	2.2980	0.4016	15.6800	0.5422	0.0691	1.0350			
0.4650	2.1770	2.5380	0.1306	19.9700	0.6910	0.1173	1.5860			
0.6000	2.5900	2.5370	0.4590	19.9300	0.7550	0.1537	1.7350	0.4050	0.3062	12.3000
0.6000	2.5900	2.5370	0.4590	19.9300	0.7550	0.1537	1.7350			
0.7750	2.8870	2.7390	0.6739	22.6200	1.0740	0.2166	4.0290			
1.0000	3.1380	2.2320	0.6535	23.6600	1.2120	0.1816	5.1360	0.3700	0.4869	19.4200
1.0000	3.1380	2.2320	0.6535	23.6600	1.2120	0.1816	5.1360			
1.3000	3.8150	3.1740	0.8193	29.7100	1.3100	0.1138	5.3920			
1.7000	4.4970	3.6840	0.4875	40.7500	1.3870	0.2171	6.3140	0.5580	0.7036	27.2200
1.7000	4.4970	3.6840	0.4875	40.7500	1.3870	0.2171	6.3140			
2.1500	5.4630	3.6300	-0.7409	35.5500	1.5350	0.8232	5.7460			
2.8000	6.9680	4.0110	-0.8069	44.6500	1.5060	-0.1572	7.1480	0.5740	-0.8069	29.7900
2.8000	6.9680	4.0110	-0.8069	44.6500	1.5060	-0.1572	7.1480			
3.6000	8.4290	4.4140	-1.6390	41.0400	1.3080	-0.0488	6.5280			
4.6500	10.5500	3.0950	-2.3850	34.1700	1.1150	-0.2830	4.3520			
6.0000	12.8300	3.3620	-1.7060	51.1700	0.8210	-0.1016	1.5640	0.1810	-0.4869	33.0900

Laser Anemometer Data X = 156in. or 3.96m Flow D

y (inch)	U (m/s)	$\bar{u}^2$ $(m/s)^2$	$\bar{u}^3$ $(m/s)^3$	$\bar{u}^4$ $(m/s)^4$	$\bar{v}^2$ $(m/s)^2$	$\bar{v}^3$ $(m/s)^3$	$\bar{v}^4$ $(m/s)^4$	$-\overline{uv}$ $(m/s)^2$	$\overline{(u-v)}^3$ $(m/s)^3$	$\overline{(u-v)}^4$ $(m/s)^4$
0.0400	-0.2056	1.1350	0.1496	5.6020	0.0682	0.0060	0.0189			
0.1650	-0.2871	1.5110	0.3184	6.9870	0.2653	0.0443	0.2467			
0.2150	-0.2587	1.6860	0.4888	8.9490	0.2822	0.0361	0.3130			
0.2800	-0.2115	1.7080	0.2419	9.0280	0.3527	0.0535	0.3985			
0.3600	-0.2299	1.6830	0.4825	8.4020	0.4580	0.0642	0.6573			
0.4680	-0.1340	2.0340	0.4594	11.6100	0.4440	0.1425	0.9234	0.1290	0.9796	39.4900
0.4680	-0.1340	2.0340	0.4594	11.6100	0.4440	0.1425	0.9234			
0.6015	-0.1213	2.1090	0.7094	11.7800	0.5212	0.1408	1.2530	0.0370	0.3586	13.2300
0.6015	-0.1213	2.1090	0.7094	11.7800	0.5212	0.1408	1.2530			
0.7760	-0.0031	2.2850	0.8620	12.4700	0.6434	0.2110	1.8020	0.2630	1.0890	13.5400
0.7760	-0.0031	2.2850	0.8620	12.4700	0.6434	0.2110	1.8020			
1.0000	0.1115	2.5820	1.1980	23.1800	0.7227	0.2369	2.2870			
1.3000	0.4250	2.8850	1.1430	26.9300	0.9994	0.1956	4.2100	0.1610	1.1540	16.7600
1.3000	0.4250	2.8850	1.1430	26.9300	0.9994	0.1956	4.2100			
1.7000	0.8620	3.0600	1.5810	28.4300	1.1310	0.0114	5.1000	0.3570	1.5130	19.0000
1.7000	0.8620	3.0600	1.5810	28.4300	1.1310	0.0114	5.1000			
2.1500	1.3760	3.5000	1.7590	39.9700	1.2270	0.4427	7.6900	0.5330	1.3280	23.8800
2.1500	1.3760	3.5000	1.7590	39.9700	1.2270	0.4427	7.6900			
2.8000	2.2460	4.1780	1.5720	51.5700	1.3650	0.2846	8.6940	0.5800	1.3730	33.7400
2.8000	2.2460	4.1780	1.5720	51.5700	1.3650	0.2846	8.6940			
3.6000	3.2260	4.9830	1.0230	71.2700	1.5430	0.0253	12.8100	0.6240	0.3447	42.2000
3.6000	3.2260	4.9830	1.0230	71.2700	1.5430	0.0253	12.8100			
4.6500	5.1690	5.1990	-1.1770	81.0400	1.5480	-0.0380	11.6500	0.7725	-1.3030	49.5900
4.6500	5.1690	5.1990	-1.1770	81.0400	1.5480	-0.0380	11.6500			
5.6650	6.9570	4.9860	-2.3260	70.3300	1.5470	-0.1218	12.0000	0.5000	-2.7000	42.3400

Laser Anemometer Data X = 176in. or 4.47m Flow D

0.0145	-0.1926	0.2777	0.3028	-0.0153	0.2463	0.0030	-0.0001	0.0001			
0.0200	-0.4056	0.1689	0.2880	-0.0105	0.3126	0.0050	-0.0001	0.0001			
0.0250	-0.5867	0.1439	0.4396	-0.0302	0.6878	0.0062	0.0000	0.0001			
0.0300	-0.6791	0.1549	0.6952	-0.0145	1.2445	0.0135	0.0000	0.0002			
0.0350	-0.8051	0.1447	0.7600	-0.0467	2.1410	0.0177	0.0002	0.0011			
0.0400	-0.9245	0.1325	0.8666	-0.0455	2.8000	0.0226	0.0001	0.0018			
0.0500	-0.8807	0.1377	0.9443	-0.0244	3.5800	0.0394	0.0002	0.0046			
0.0600	-0.9953	0.1374	1.0460	-0.0405	4.1390	0.0499	0.0001	0.0127			
0.0750	-1.1320	0.1201	1.1420	-0.1103	4.6730	0.0480	-0.0010	0.0105			
0.1000	-1.2050	0.1226	1.1710	0.0648	4.5570	0.0703	0.0020	0.0203			
0.1300	-1.2690	0.1297	1.2450	0.2779	4.7030	0.1771	0.0081	0.0725			
0.1650	-1.3250	0.1179	1.3470	0.1829	5.5400	0.1219	0.0160	0.0733			
0.2100	-1.3790	0.1034	1.2710	0.1563	4.5910	0.1464	0.0141	0.0949			
0.2750	-1.4190	0.1087	1.3730	0.3987	5.4140	0.1820	0.0094	0.1277			
0.3600	-1.5010	0.1131	1.3850	0.4978	5.7890	0.1880	0.0180	0.1244			
0.4600	-1.4420	0.1213	1.4270	0.5444	6.3860	0.2190	0.0387	0.1660	0.8850	0.4054	2.9310
0.5750	-1.4960	0.1137	1.5500	0.4821	6.5740	0.2760	0.0450	0.2972	1.0960	0.4583	4.0430
0.7000	-1.5020	0.1330	1.7170	0.8008	9.4650	0.3580	0.0827	0.4967	1.1890	0.5936	5.1790
0.9000	-1.5690	0.1250	1.8400	0.6719	11.3400	0.4250	0.1100	0.5746	1.2540	0.7073	6.3230
1.2000	-1.4090	0.1543	1.9620	0.9227	13.0000	0.5450	0.1803	0.9223	1.4270	0.7712	5.9840
1.6000	-1.3110	0.1903	2.1990	1.6320	15.5300	0.7650	0.2732	2.2720	1.7290	1.1700	10.4400
2.1000	-1.0110	0.2414	2.4310	1.2830	12.1100	0.8830	0.2228	2.9120	1.9680	1.3680	18.3800
2.7000	-0.6090	0.3416	2.9070	1.8070	27.3900	1.0800	0.2256	4.1500	2.3310	1.7130	16.6700
3.5000	-0.1652	0.4396	3.4570	1.8730	35.0900	1.3010	0.5440	6.4000	2.8590	1.9250	22.1400
4.5000	0.5846	0.5990	4.0710	1.8310	45.4700	1.8010	0.5349	13.9900	3.5860	1.4500	32.9600
5.5000	1.6020	0.7545	4.7640	1.1960	61.0300	2.2400	0.8930	22.1200	4.3660	1.6870	45.0700
7.0000	3.0900	0.9017	5.4390	0.3260	81.0600	2.3530	0.1849	20.2000	4.6900	0.1671	52.6200
8.5000	4.7300	0.9737	5.3930	-1.4320	81.1100	2.4150	0.0882	20.9200	4.3990	-1.2250	46.0500

X-Wire Anemometer Data X = 87in. or 2.21m Flow C

y (inch)	U (m/s)	$\overline{u}^2$ $(m/s)^2$	$\overline{v}^2$ $(m/s)^2$	$-\overline{uv}$ $(m/s)^2$
0.0500	16.0837	4.7556	1.2013	1.0214
0.0600	16.6944	4.8011	1.1738	1.0495
0.0750	17.2043	4.7322	1.1775	1.0879
0.0900	18.0976	4.9904	1.2659	1.1571
0.1100	18.6613	4.9128	1.2750	1.1364
0.1350	18.9769	4.8433	1.2784	1.1874
0.1600	19.6457	4.9412	1.3210	1.2451
0.1900	19.9045	4.5988	1.3197	1.1237
0.2250	20.6142	4.5283	1.3703	1.1504
0.2650	21.6121	4.5738	1.4447	1.1332
0.3100	21.5539	4.1214	1.3190	1.0368
0.3550	22.1758	4.0092	1.3731	1.0090
0.4000	22.6182	3.7818	1.2934	0.9702
0.4500	23.7945	3.7722	1.2727	0.9021
0.5100	24.7538	3.4802	1.2066	0.8614
0.5800	24.6406	2.9565	1.0571	0.7388
0.6500	24.6413	2.5777	0.8983	0.6746
0.7500	25.7688	2.1259	0.7210	0.5087
0.8750	26.7440	1.4734	0.5284	0.3189
1.0250	27.8875	0.8163	0.3205	0.1464
1.2000	28.5129	0.2522	0.1388	0.0419
1.4000	28.7824	0.1229	0.0455	0.0232
1.7000	28.9920	0.1117	0.0110	0.0204
2.0000	29.1320	0.2877	0.0539	0.0781
2.5000	29.2658	0.3132	0.0321	0.0850
2.9500	29.4530	0.4812	0.0535	0.1424

X-Wire Anemometer Data X = 112in. or 2.85m Flow C

0.0550	9.2619	3.7497	0.6524	0.4650
0.0650	9.6703	3.6180	0.6929	0.4736
0.0800	9.6508	3.6022	0.7230	0.5263
0.0950	9.9934	3.7728	0.8062	0.5903
0.1100	10.2751	3.8197	0.8796	0.6530
0.1250	10.3192	3.7846	0.8877	0.6526
0.1500	10.5023	3.7531	0.9526	0.6897
0.1750	10.9319	3.9240	1.0603	0.7552
0.2000	11.2128	4.0248	1.1232	0.7616
0.2300	11.8329	4.2579	1.2765	0.8856
0.2650	12.1809	4.2277	1.3138	0.8863
0.3000	12.3482	4.4126	1.3643	0.9574
0.3400	12.6947	4.4257	1.4199	0.9783
0.3900	13.2644	4.4717	1.4789	0.9971
0.4500	13.8802	4.6996	1.6005	1.0988
0.5100	14.5942	4.7600	1.6662	1.0923
0.6000	15.5678	4.8976	1.7102	1.1437
0.7000	15.8709	4.5670	1.6242	1.1203
0.8500	17.1084	4.3618	1.5497	1.0306
1.0000	18.1676	3.8876	1.3765	0.9095
1.2000	19.6260	3.2429	1.1858	0.7646
1.4000	20.9430	2.2803	0.9454	0.4929
1.7000	22.3751	1.4109	0.5398	0.2527
2.0000	23.1426	0.2639	0.1937	0.0296
2.5000	24.1075	0.0494	0.0263	-0.0000
2.9300	24.3018	0.0928	0.0501	0.0175
3.5000	23.9520	0.1156	0.0396	0.0036

X-Wire Anemometer Data X = 136in. or 3.46m Flow C

y (inch)	U (m/s)	$\overline{u}^2$ $(m/s)^2$	$\overline{v}^2$ $(m/s)^2$	$-\overline{uv}$ $(m/s)^2$
0.2500	3.6390	2.3004	0.4337	-0.0221
0.5000	3.9890	2.7009	0.6786	0.0752
0.7500	4.8054	3.4155	1.0338	0.1906
1.0000	5.5324	4.0742	1.2997	0.2919
1.5000	7.1179	5.1086	1.7578	0.4908
2.0000	8.3606	5.9457	1.9875	0.7320
2.5000	10.6967	6.3334	2.2557	0.9488
3.0000	12.6125	5.9158	2.2035	1.0263
3.5000	16.3218	5.5974	2.1326	1.0370
4.0000	18.4448	3.9605	1.5302	0.6152
4.5000	19.2952	1.4508	0.7060	0.2450
5.0000	19.7964	0.2455	0.2727	0.0483
5.5000	19.3653	0.1428	0.1082	0.0429
6.0000	19.2303	0.0772	0.0762	0.0331

X-Wire Anemometer Data X = 156in. or 3.96m Flow C

0.5000	2.9838	1.6654	0.3068	-0.0376
0.7500	3.0836	1.8838	0.3990	0.0039
1.0000	3.3447	2.1084	0.5063	0.0294
1.5000	3.7657	2.6796	0.6796	0.0942
2.0000	4.0521	3.1547	0.8538	0.1941
2.5000	4.8183	4.2153	1.2119	0.3136
2.9800	5.7100	5.5114	1.6063	0.4820
3.5000	6.8663	6.7307	2.2238	0.5531
4.0000	7.8617	7.8556	2.5785	0.7519
4.5000	9.1056	8.1946	2.8939	0.8589
5.0000	10.7399	8.7830	3.2224	1.1018
5.5000	12.3935	8.6596	3.1842	1.2451
6.0000	14.3067	9.0588	3.1613	1.2835
7.0000	17.5550	6.2678	2.2287	0.8311
8.0000	19.5323	1.6613	0.9794	0.3448
9.0000	19.8701	0.2179	0.2757	0.0283
10.0000	19.6806	0.1381	0.1291	0.0102
11.0000	19.7214	0.2632	0.1871	0.1264
12.0000	19.8177	0.0640	0.1258	0.0316
13.0000	19.7490	0.0196	0.1636	0.0158

X-Wire Anemometer Data X = 176in. or 4.47m Flow C

0.4924	3.1604	1.5206	0.3646	-0.2432
0.7386	3.2446	1.5930	0.4482	-0.2105
0.9848	3.2671	1.7563	0.4894	-0.2078
1.2310	3.2479	1.7891	0.5107	-0.2473
1.4772	3.4544	2.1535	0.6038	-0.2608
1.7234	3.6660	2.3532	0.6820	-0.1613
1.9696	3.8518	2.6073	0.7329	-0.1856
2.4620	4.2487	3.2474	0.9219	-0.1550
2.9544	4.6218	3.8466	1.0466	-0.1099
3.4468	5.2150	4.8841	1.4360	0.1563
3.9392	5.6640	5.4794	1.6659	0.2135
4.4316	6.1091	6.2982	2.0248	0.4003
4.9240	7.2763	7.4067	2.5780	0.7310
5.4164	7.7202	8.0213	2.8261	0.8091
5.9088	8.6243	8.9803	3.1293	0.9592
6.8937	10.1052	9.5812	3.6539	1.1571
7.8785	11.9285	9.6659	3.7863	1.4091
8.8633	13.8725	8.3794	3.6654	1.3976
9.8481	15.8858	7.4260	3.0582	1.1685
10.8329	17.8637	3.8620	2.0135	0.6997
11.8177	18.9086	1.6472	1.2026	0.3540
12.8025	19.0509	0.5889	0.6102	0.0748
13.7873	19.1932	0.5554	0.4426	0.0088
15.7569	19.0986	0.3180	0.2113	-0.1290

X-Wire Anemometer Data X = 196in. or 4.88m Flow C

y (inch)	U (m/s)	$\overline{u}^2$ $(m/s)^2$	$\overline{v}^2$ $(m/s)^2$	$-\overline{uv}$ $(m/s)^2$
1.4772	3.4882	1.9037	0.6108	-0.2252
1.9696	3.8358	2.4896	0.7745	-0.2707
2.4620	3.8837	2.5075	0.7502	-0.2177
2.9544	4.1272	3.1073	0.9204	-0.1619
3.4468	4.0521	2.9817	0.8705	-0.1728
3.9392	4.4217	3.4408	1.0831	-0.0973
4.4316	4.7086	4.0534	1.2163	0.0861
4.9240	5.3612	4.7996	1.5478	0.1212
5.4164	5.8382	5.6858	1.8317	0.4057
5.9088	6.1655	6.1676	2.0423	0.5342
6.4013	6.6871	6.4277	2.3118	0.7037
6.8937	7.5016	7.3573	2.8631	1.0390
7.3861	8.1768	7.6507	3.1954	1.2182
7.8785	8.6163	7.7492	3.4162	1.4043
8.8633	9.8009	7.9723	3.8348	1.7664
9.8481	11.2089	8.2488	4.4101	2.1216
10.8329	12.8831	7.8994	4.0572	1.9130
11.8177	14.1429	6.5467	3.7675	1.6541
13.7873	16.7117	3.0878	2.2018	0.8060
15.7569	17.5341	1.1178	0.8525	0.2581
17.7265	17.6293	0.3183	0.2715	0.0575
19.6962	17.0204	0.2593	0.1637	0.0433

X-Wire Anemometer Data X = 227in. or 5.57m Flow C

0.2500	3.8104	3.5941	0.2979	-0.0786
0.5000	4.2427	3.2986	0.4952	-0.0976
0.7500	4.5201	3.9043	0.6882	0.1166
1.0000	4.3486	3.1493	0.8165	0.1175
1.2500	4.8952	3.7087	1.0743	0.2547
1.5000	5.2245	3.9555	1.4011	0.3660
2.0000	5.6355	4.1944	1.7281	0.5212
2.5000	5.8366	4.5932	1.9355	0.7342
3.0000	5.8111	4.5553	2.1293	0.8355
3.5000	6.0522	4.5997	2.2738	1.0074
4.0000	6.4218	4.9727	2.5585	1.1483
4.5000	6.9855	5.3602	2.7587	1.2203
5.0000	7.7464	6.0344	3.4935	1.6523
5.5000	7.9086	6.2725	3.4957	1.8848
6.0000	8.5739	6.5100	3.8050	2.0348
7.0000	9.2782	6.6318	3.9039	2.1577
8.0000	10.6204	6.5228	4.3427	2.2291
9.0000	11.7950	5.9030	4.0158	2.0564
10.0000	12.8169	4.7428	3.8438	1.6391
12.0000	14.6859	2.9170	2.9246	0.9560
14.0000	15.8498	1.1502	1.4880	0.2856
16.0000	16.0706	0.5789	0.6140	0.1570
18.0000	16.2732	0.3569	0.3254	0.0880
20.0000	15.6064	1.2574	0.3548	0.0028

X-Wire Anemometer Data X = 87in. or 2.21m Flow D

y (inch)	U (m/s)	$\overline{u}^2$ $(m/s)^2$	$\overline{v}^2$ $(m/s)^2$	$-\overline{uv}$ $(m/s)^2$
0.0500	12.3526	3.3142	0.7233	0.6166
0.0550	12.1035	2.9192	0.6698	0.5869
0.0600	12.8870	3.0969	0.7333	0.6429
0.0700	13.5237	3.3528	0.7491	0.6769
0.0800	13.5631	3.1545	0.7549	0.6755
0.0950	14.0225	3.1986	0.7532	0.6642
0.1100	14.3696	3.2872	0.7837	0.7087
0.1310	14.9595	3.2343	0.8038	0.7260
0.1500	14.7334	3.0935	0.7831	0.6789
0.1750	14.7471	3.0547	0.7498	0.6578
0.2000	14.9340	2.9331	0.7636	0.6503
0.2300	14.8506	2.7079	0.7300	0.6347
0.2700	15.4194	2.7364	0.7228	0.6009
0.3100	15.5327	2.6536	0.7077	0.5707
0.3500	16.0812	2.5489	0.7196	0.5817
0.4000	17.0413	2.7899	0.7094	0.5819
0.5000	17.2438	2.4211	0.6583	0.5179
0.6000	17.5554	2.0185	0.5674	0.4357
0.7000	17.7000	1.7367	0.4973	0.3569
0.9000	18.1711	1.2765	0.4301	0.2615
1.1000	18.4643	1.0043	0.3535	0.1947

X-Wire Anemometer Data X = 112in. or 2.85m Flow D

0.0500	5.6806	2.0830	0.2836	0.2070
0.0600	6.1012	2.1624	0.3061	0.2364
0.0700	6.1762	2.0829	0.3271	0.2419
0.0800	6.5729	2.3151	0.3842	0.2805
0.0950	6.9137	2.5120	0.4475	0.3196
0.1100	7.0350	2.4504	0.4722	0.3472
0.1300	7.1050	2.3192	0.4987	0.3496
0.1500	7.4689	2.6086	0.5565	0.3826
0.1750	7.5484	2.6547	0.6166	0.4092
0.2000	7.9486	2.8044	0.6458	0.4275
0.2400	8.4300	2.9301	0.7323	0.4779
0.2900	8.2222	2.7209	0.7169	0.4803
0.3500	9.0782	3.0997	0.8207	0.5586
0.4100	8.9064	2.8161	0.8178	0.5201
0.4800	9.3029	2.9366	0.8512	0.5589
0.5600	9.3717	2.8046	0.8585	0.5597
0.6500	10.0390	3.1141	0.8902	0.6141
0.7500	10.5930	3.0099	0.9092	0.5951
0.9500	11.1312	2.9958	0.8960	0.6066
1.1000	11.6022	2.7455	0.7943	0.5423
1.3000	12.3538	2.5476	0.7485	0.5066
1.5000	13.5370	2.4243	0.7181	0.4349
1.8000	14.4607	1.9151	0.5824	0.3268
2.1000	15.0146	1.4831	0.4701	0.2558
2.4000	15.3107	1.0136	0.3406	0.1587

X-Wire Anemometer Data X = 136in. or 3.46m Flow D

y (inch)	U (m/s)	$\overline{u}^2$ $(m/s)^2$	$\overline{v}^2$ $(m/s)^2$	$-\overline{uv}$ $(m/s)^2$
3.9392	10.0528	3.0654	1.0775	0.5578
4.1854	10.6145	2.8184	1.0081	0.4881
4.4316	10.8496	2.7490	0.8887	0.3869
4.6778	11.3215	2.1166	0.7952	0.3687
4.9240	11.6486	2.1389	0.7879	0.3776
5.4164	12.5556	1.5661	0.6054	0.2763
5.9088	12.9029	0.9405	0.4011	0.1576
6.4013	13.3200	0.5770	0.2566	0.0856
6.8937	13.3563	0.4201	0.2007	0.0656
7.8785	13.8768	0.2097	0.1038	0.0161
8.8633	14.0198	0.0974	0.0571	0.0096
9.8481	13.9212	0.0553	0.0246	0.0069

X-Wire Anemometer Data X = 156in. or 3.96m Flow D

4.9240	7.0651	3.2912	1.2705	0.5199
5.9088	8.0005	3.1396	1.2111	0.4794
6.8937	9.9384	2.9165	1.0809	0.4544
7.8785	11.3620	1.6987	0.7010	0.2944
8.8633	12.4117	0.8878	0.4451	0.1558
9.8481	13.1974	0.3487	0.2100	0.0562
10.8329	14.0186	0.0004	0.0000	0.0000
11.8177	13.5543	0.0002	0.0001	0.0000
13.7873	13.9924	0.0003	0.0003	-0.0003
15.7569	13.8094	0.0004	0.0000	0.0000

X-Wire Anemometer Data X = 176in. or 4.47m Flow D

0.2462	1.6718	0.3394	0.0687	-0.0740
0.4924	1.5920	0.3434	0.0812	-0.0596
0.7386	1.7107	0.3602	0.0988	-0.0630
0.9848	1.8708	0.4102	0.1100	-0.0653
1.2310	1.9280	0.4275	0.1273	-0.0651
1.4772	1.9692	0.4579	0.1322	-0.0629
1.9696	1.9932	0.5652	0.1672	-0.0743
2.4620	2.2003	0.6456	0.1979	-0.0467
2.9544	2.1815	0.6939	0.2064	-0.0597
2.9544	2.2204	0.8026	0.2326	-0.0442
3.4468	2.3588	0.8020	0.2588	-0.0493
3.9392	2.7586	1.1887	0.3602	-0.0320
4.4316	3.2538	1.4459	0.5067	0.0270
4.9240	3.5525	1.6830	0.5627	0.0224
5.4164	3.9421	1.8210	0.6797	0.0502
5.9088	4.3615	2.0974	0.8135	0.1933
6.4013	4.8188	2.1754	0.8555	0.1637
6.8937	5.3014	2.3793	1.0123	0.2589
7.3861	6.0799	2.7282	1.1318	0.3363
7.8785	6.3830	2.7082	1.1668	0.3966
8.8633	7.6812	2.6297	1.1796	0.4385
9.8481	8.8618	2.3479	1.0466	0.3761
10.8329	9.4903	1.7836	0.8248	0.3110
11.8177	10.6408	1.0691	0.5630	0.1860
12.8025	11.2920	0.5265	0.3270	0.1034
13.7873	11.6033	0.2175	0.1817	0.0326

Single Wire Anemometer Data X = 64in. or 1.63m Flow C

y (inch)	U (m/s)	$\overline{u}^2$ $(m/s)^2$
0.0120	17.2880	5.0711
0.0140	17.3389	4.9738
0.0160	17.7079	4.9723
0.0180	17.9333	4.9298
0.0200	18.2223	5.0001
0.0230	18.5643	5.0140
0.0260	18.6664	4.8309
0.0290	18.9224	4.8269
0.0320	19.3295	4.9647
0.0350	19.6279	4.9578
0.0400	19.9534	4.9549
0.0450	20.3305	5.0454
0.0500	20.3435	4.9095
0.0600	21.0506	5.0013
0.0750	21.6972	5.0182
0.0900	22.2790	4.8634
0.1100	22.9651	4.8383
0.1500	23.6542	4.3837
0.2000	24.8365	4.0186
0.2750	26.0894	3.4213
0.3750	27.3699	2.6636
0.4500	28.3753	2.1320
0.6000	30.0015	1.2469
0.8000	31.0498	0.3741
1.0000	31.3637	0.0678
1.2500	31.4259	0.0473
1.5000	31.4723	0.0966

Single Wire Anemometer Data X = 87in. or 2.21m Flow C

0.0120	12.8042	5.1553
0.0140	12.9072	5.1165
0.0160	13.2946	5.1225
0.0180	13.9056	5.0214
0.0200	13.9908	4.7978
0.0230	14.1627	4.5685
0.0260	14.4936	4.5073
0.0290	14.5936	4.4627
0.0320	14.8922	4.4966
0.0350	14.9530	4.4085
0.0400	15.1974	4.3625
0.0450	15.5248	4.3721
0.0500	16.0054	4.4640
0.0600	16.4195	4.5819
0.0750	16.9295	4.5813
0.0900	17.4319	4.6254
0.1100	18.0805	4.7127
0.1500	18.8011	4.5719
0.2000	19.4933	4.3441
0.2750	20.5866	4.1504
0.3750	21.9824	3.8321
0.4500	22.8266	3.5444
0.6250	24.5839	2.7174
0.8000	26.6737	1.9219
1.0000	28.4822	0.9488
1.2500	28.8440	0.1711
1.5000	29.1442	0.0438
2.0000	29.2994	0.0834
2.5000	28.7573	0.0821

Single Wire Anemometer Data X = 112in. or 2.85m Flow C

y (inch)	U (m/s)	$\bar{u}^2$ $(m/s)^2$
0.0120	6.9879	3.7673
0.0140	7.2568	3.8198
0.0160	7.5643	3.8551
0.0180	7.8050	3.8596
0.0200	8.1265	3.9111
0.0230	8.3893	3.8721
0.0260	8.5841	3.8058
0.0290	8.5487	3.7029
0.0320	8.6174	3.6655
0.0350	8.7478	3.6812
0.0400	9.0074	3.7257
0.0450	9.1851	3.7150
0.0500	9.3864	3.7427
0.0600	9.6131	3.7820
0.0750	9.8872	3.8906
0.0900	10.3033	4.0914
0.1100	10.7441	4.2621
0.1500	11.1889	4.3778
0.2000	11.5634	4.4272
0.2750	12.3898	4.6969
0.3750	13.4218	4.9383
0.4500	14.2017	5.0038
0.6000	15.2868	4.9383
0.8000	16.9814	4.6733
1.0000	18.5816	4.1590
1.2500	20.5109	3.2966
1.5000	22.2033	2.2210
2.0000	24.2451	0.3315
2.5000	24.5143	0.0515
3.0000	24.5537	0.0668
4.0000	24.4613	0.0858

Single Wire Anemometer Data X = 136in. or 3.46m Flow C

0.0120	1.3832	0.7552
0.0140	1.3959	0.8512
0.0160	1.4238	0.8827
0.0180	1.4407	0.9775
0.0200	1.6037	1.0460
0.0230	1.7668	1.1651
0.0260	1.7856	1.2151
0.0290	1.8045	1.2417
0.0320	1.8852	1.3242
0.0350	1.9741	1.4044
0.0400	1.9719	1.3949
0.0450	2.0961	1.5502
0.0500	2.0842	1.5058
0.0600	2.1365	1.6468
0.0750	2.2648	1.6663
0.0900	2.4197	1.8917
0.1100	2.4243	1.8653
0.1500	2.5617	2.0515
0.2000	2.7025	2.0750
0.2750	3.1317	2.4666
0.3750	3.3927	2.9848
0.4500	3.6908	3.1380
0.6000	4.3071	4.0116
0.8000	4.8659	4.8287
1.0000	5.5083	5.1165
1.2500	6.6363	5.9948
1.5000	8.1492	6.8879
2.0000	10.5804	7.6054
2.5000	13.4089	7.3932
3.0000	16.0128	6.3497
4.0000	20.3027	2.2609
5.0000	21.4569	0.1301
5.7500	21.8702	0.0517
6.5000	21.9977	0.0325
7.5000	21.9636	0.0002

Single Wire Anemometer Data X = 227in. or 5.77m Flow C

y (*inch*)	U (*m/s*)	$\bar{u}^2$ $(m/s)^2$
0.0230	1.3870	0.6341
0.0260	1.4813	0.7376
0.0290	1.5229	0.8509
0.0340	1.5685	0.8572
0.0370	1.5119	0.7878
0.0400	1.5279	0.7629
0.0450	1.5099	0.7658
0.0500	1.5069	0.7349
0.0600	1.5536	0.7536
0.0750	1.4753	0.6680
0.0900	1.5767	0.7681
0.1100	1.5671	0.7577
0.1500	1.6184	0.7819
0.2000	1.6810	0.8279
0.2750	1.7247	0.8247
0.3750	1.7958	0.8775
0.4500	1.9276	1.0681
0.6000	1.9809	1.0454
0.8000	2.0774	1.1640
1.0000	2.1225	1.2854
1.2500	2.7097	2.1434
1.5000	3.0651	2.6059
2.2500	3.4480	3.0707
2.5000	4.0540	4.2412
3.0000	3.9062	4.0346
4.0000	4.9018	5.4835
5.0000	6.0688	6.9482
6.0000	7.4733	8.1865
7.0000	8.4918	8.6003
8.0000	10.2138	9.2640
9.5000	12.5525	8.6499
11.0000	14.8275	6.8442
12.5000	16.4404	3.6151
14.0000	17.5776	1.2649
15.5000	17.4087	0.4404
17.0000	17.5089	0.2481

Single Wire Anemometer Data X = 64in. or 1.63m Flow D

0.0120	11.3357	3.8801
0.0140	11.6351	3.7802
0.0160	11.8223	3.6996
0.0180	12.4498	3.7923
0.0200	12.6424	3.6172
0.0230	13.0111	3.5597
0.0260	13.2139	3.4277
0.0290	13.3396	3.3977
0.0320	13.5499	3.5279
0.0350	13.8226	3.3958
0.0400	14.2014	3.3532
0.0450	14.5211	3.3596
0.0500	14.7350	3.2437
0.0600	14.9324	3.3043
0.0750	15.6540	3.3082
0.0900	16.2169	3.3515
0.1100	16.6175	3.2990
0.1500	17.5304	3.2187
0.2000	18.3964	2.9741
0.2750	19.0824	2.6374
0.3750	19.7181	2.1684
0.4500	20.1493	1.9122
0.6000	20.6450	1.4644
0.8000	20.8554	1.0553
1.0000	21.3016	0.8686
1.2500	21.4457	0.7240

Single Wire Anemometer Data X = 87in. or 2.21m Flow D

y (*Inch*)	U (m/s)	$\bar{u}^2$ $(m/s)^2$
0.0120	9.1166	3.5148
0.0140	9.3218	3.4138
0.0160	9.5720	3.3864
0.0180	9.8025	3.3721
0.0200	10.0497	3.2653
0.0230	10.1808	3.1792
0.0260	10.5156	3.1995
0.0290	10.7700	3.1063
0.0320	10.9944	3.1078
0.0350	11.0694	2.9843
0.0400	11.2799	2.9582
0.0450	11.4955	3.0021
0.0500	11.6935	2.9386
0.0600	11.9914	2.8518
0.0750	12.1917	2.8937
0.0900	12.5627	2.9410
0.1100	12.9800	2.9277
0.1500	13.5680	2.9863
0.2000	14.2186	3.0132
0.2750	14.8772	2.7948
0.3750	15.5931	2.6265
0.4500	16.3378	2.5228
0.6000	16.9642	2.1315
0.8000	17.6862	1.6246
1.0000	18.5918	1.2687
1.2500	19.0696	0.9050
1.5000	19.1690	0.6641
2.0000	19.4085	0.4449
2.5000	19.5049	0.3193
3.0000	20.0664	0.2224
4.0000	20.1488	0.0688
5.0000	20.3377	0.0285
7.0000	20.3277	0.0835

Single Wire Anemometer Data X = 112in. or 2.85m Flow D

0.0120	3.9247	1.9279
0.0140	4.1958	2.0148
0.0160	4.4246	2.0931
0.0180	4.6339	2.1353
0.0200	4.8146	2.1386
0.0230	4.9912	2.1222
0.0260	5.0662	2.1137
0.0290	5.1670	2.1760
0.0320	5.2925	2.1325
0.0350	5.3662	2.1333
0.0400	5.5236	2.0918
0.0500	5.7342	2.1277
0.0600	5.9353	2.1641
0.0750	6.2178	2.2684
0.0900	6.3704	2.2941
0.1100	6.5867	2.3060
0.1500	7.0559	2.5198
0.2000	7.4776	2.6352
0.2750	7.8669	2.8704
0.3750	8.4507	2.9086
0.4500	8.8041	3.0928
0.6000	9.5862	3.0791
0.8000	10.6588	3.1038
1.0000	11.3465	2.9289
1.2500	12.3393	2.5175
1.5000	13.1374	2.1110
2.0000	14.3717	1.2997
2.5000	14.9770	0.7519
3.0000	15.3909	0.5508
4.0000	15.7357	0.2813
5.0000	15.8293	0.1161
7.0000	16.0523	0.0407
9.0000	16.0521	0.0588

Single Wire Anemometer Data X = 136in. or 3.46m Flow D

y (*Inch*)	U (*m/s*)	$\bar{u}^2$ $(m/s)^2$
0.0140	0.8040	0.1705
0.0160	0.8755	0.2253
0.0180	0.8558	0.2271
0.0200	0.9656	0.2961
0.0230	1.0759	0.3694
0.0260	1.1122	0.4031
0.0290	1.2388	0.4757
0.0320	1.2395	0.4509
0.0350	1.2474	0.4880
0.0400	1.3333	0.5574
0.0450	1.3346	0.5667
0.0500	1.3442	0.5347
0.0600	1.4319	0.6177
0.0750	1.5353	0.7135
0.0900	1.6026	0.6722
0.1100	1.7048	0.7534
0.1500	1.7738	0.8068
0.2000	1.7889	0.8213
0.2750	2.1344	1.0710
0.3750	2.2840	1.0977
0.4500	2.3617	1.2219
0.6000	2.6914	1.5208
0.8000	3.1290	1.6570
1.0000	3.3429	2.0117
1.2500	3.8509	2.2816
1.5000	4.3111	2.6818
2.0000	5.6749	3.2766
2.5000	7.1404	3.7444
3.0000	8.1663	3.8387
3.5000	8.9818	3.2279
4.0000	10.2641	2.9709
4.5000	11.1596	2.2720
5.0000	12.0801	1.7718
5.5000	12.8677	1.1644
6.0000	13.1858	0.6423
6.5000	13.6843	0.4403
7.0000	13.8724	0.3244
7.5000	14.2955	0.2364
8.0000	14.1528	0.1652

Single Wire Anemometer Data X = 156in. or 3.96m Flow C

y (*inch*)	U (m/s)	$\bar{u}^2$ (m/s)^2
0.0200	0.8490	0.1544
0.0230	0.8067	0.1613
0.0260	0.8174	0.1398
0.0290	0.8357	0.1417
0.0320	0.8850	0.1622
0.0350	0.8551	0.1512
0.0400	0.9044	0.1925
0.0450	0.8920	0.1588
0.0500	0.8919	0.1689
0.0600	0.9407	0.1874
0.0750	1.0047	0.1973
0.0900	0.9514	0.1906
0.1100	1.0229	0.2375
0.1500	1.0923	0.2355
0.2000	1.1042	0.2783
0.2750	1.1643	0.2776
0.3750	1.2229	0.3095
0.4500	1.2909	0.3258
0.6000	1.2603	0.3638
0.8000	1.3704	0.4097
1.0000	1.5162	0.5657
1.2500	1.6238	0.6282
1.5000	1.8183	0.7432
2.0000	1.8832	0.8603
2.5000	2.3159	1.2675
3.0000	3.0184	1.7105
3.5000	3.4557	2.0984
4.0000	4.2384	2.6645
4.5000	5.0052	3.2855
5.0000	5.7364	3.2968
5.5000	6.7471	3.4401
6.0000	7.3882	3.4739
6.5000	8.2874	3.3036
7.0000	9.2803	2.9188
8.0000	10.8226	2.0837
9.0000	11.8160	1.1015
10.0000	12.5455	0.4752
12.0000	13.0347	0.1012
14.0000	13.0088	0.0605

1 Report No	2 Government Accession No	3 Recipient's Catalog No

4 Title and Subtitle

Experimental Study of Two Separating Turbulent Boundary Layers

5 Report Date

May 1987

6 Performing Organization Code

7 Author(s)

K.A. Nagabushana, R.L. Simpson and N.K. Agarwal

8 Performing Organization Report No

10 Work Unit No

9 Performing Organization Name and Address

Aerospace and Ocean Engineering Department
Virginia Polytechnic Institute and State University
BLACKSBURG, VA 24061

11 Contract or Grant No.

1-446

13 Type of Report and Period Covered

Contractor Report

12 Sponsoring Agency Name and Address

National Aeronautics and Space Administration
WASHINGTON, DC 20546-5225

14 Sponsoring Agency Code

505-61-51-06

15 Supplementary Notes

Langley Technical Monitor: Thomas F. Brooks

16 Abstract

A detailed study of two strong adverse pressure gradient flows, one with free-stream velocity of 33 m/sec., at throat (producing a Re_θ of 27000 at detachment) and another with free-stream velocity of 22 m/sec., at throat (producing a Re_θ of 19000 at detachment) is presented here.

In these flows flow separates slowly and reattaches very rapidly over a very short distance in streamwise direction. In backflow region, there appears to be a semi-logarithmically flat region in the streamwise fluctuating velocity component, u', which spreads over a definite range of y/δ.

In power spectra, the flow variables $\varphi_{uu}(k_1\delta)/-\overline{uv}_{max}$ vs. $k_1\delta$ forms a unique set of scaling parameters for adverse pressure gradient flows.

The experimental results presented here is compared with previous studies which shows good agreement.

17 Key Words (Suggested by Author(s))	18 Distribution Statement
Turbulence Boundary Layers Adverse Pressure Gradient Power Spectra	Unclassified - Unlimited Subject Category 71

19. Security Classif. (of this report)	20. Security Classif. (of this page)	21. No. of pages	22. Price*
Unclassified	Unclassified	118	A07

*For sale by the National Technical Information Service, Springfield, Virginia 22161